②

AD-A232 867

TECHNICAL REPORT BRL-TR-3197

BRL

CLASSICAL DYNAMICS STUDIES OF UNIMOLECULAR DECOMPOSITION OF NITROMETHANE

BETSY M. RICE
DONALD L. THOMPSON

DTIC
ELECTE
MAR 21 1991
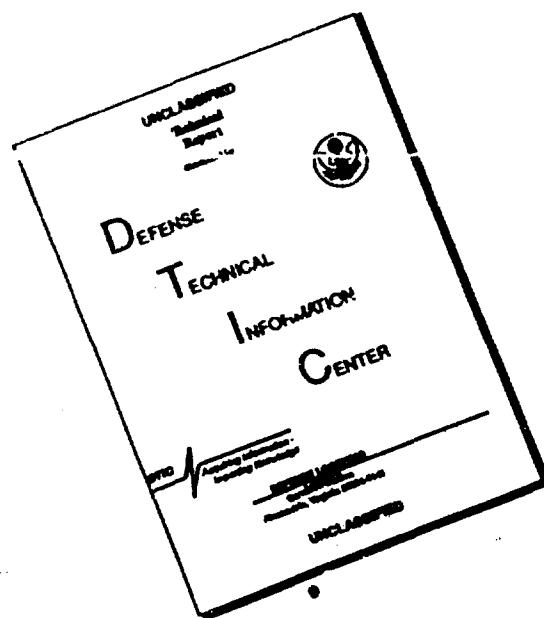**S** **E** **D**

FEBRUARY 1991

U.S. ARMY LABORATORY COMMAND

BALLISTIC RESEARCH LABORATORY
ABERDEEN PROVING GROUND, MARYLAND

91 3 12 036

DISCLAIMER NOTICE

THIS DOCUMENT IS BEST QUALITY AVAILABLE. THE COPY FURNISHED TO DTIC CONTAINED A SIGNIFICANT NUMBER OF PAGES WHICH DO NOT REPRODUCE LEGIBLY.

NOTICES

UNCLASSIFIED

REPORT DOCUMENTATION PAGE	Form Approved OMB No. 0704-0188

Public reporting burden for this collection of information is estimated to average 1 hour per response, including the time for reviewing instructions, searching existing data sources, gathering and maintaining the data needed, and completing and reviewing the collection of information. Send comments regarding this burden estimate or any other aspect of this collection of information, including suggestions for reducing this burden, to Washington Headquarters Services, Directorate for Information Operations and Reports, 1215 Jefferson Davis Highway, Suite 1204, Arlington, VA 22202-4302, and to the Office of Management and Budget, Paperwork Reduction Project (0704-0188), Washington, DC 20503.

1. AGENCY USE ONLY (Leave blank)	2. REPORT DATE February 1991	3. REPORT TYPE AND DATES COVERED Final, Dec 88 - Jan 90	

4. TITLE AND SUBTITLE Classical Dynamics Studies of Unimolecular Decomposition of Nitromethane	5. FUNDING NUMBERS 1L161102AH43

6. AUTHOR(S) Betsy M. Rice Donald L. Thompson	

7. PERFORMING ORGANIZATION NAME(S) AND ADDRESS(ES)	8. PERFORMING ORGANIZATION REPORT NUMBER

9. SPONSORING/MONITORING AGENCY NAME(S) AND ADDRESS(ES) US Army Ballistic Research Laboratory ATTN: SLCBR-DD-T Aberdeen Proving Ground, MD 21005-5066	10. SPONSORING/MONITORING AGENCY REPORT NUMBER BRL-TR-3197

11. SUPPLEMENTARY NOTES

Donald L. Thompson works for the Department of Chemistry at Oklahoma State University, Stillwater, OK 74078.

12a. DISTRIBUTION/AVAILABILITY STATEMENT Approved for public release; distribution unlimited.	12b. DISTRIBUTION CODE

13. ABSTRACT (Maximum 200 words)

Classical trajectories are used to investigate the unimolecular decomposition of nitromethane on three model potential energy surfaces. The surfaces differ mainly in the barrier height for the isomerization of nitromethane to methyl nitrite (216.4, 55.1, and 47.6 kcal/mol). In addition to the two primary reactions observed by Wodtke, Hintsa, and Lee (1986), a third reaction was observed: $CH_3NO_2 \rightarrow CH_3ONO^\dagger \rightarrow CH_3 + NO_2$. The dynamics results also show that there are two mechanisms for isomerization of nitromethane to methyl nitrite: (a) a two-step process of dissociation of nitromethane of $CH_3 + NO_2$ and subsequent recombination of these radicals to form methyl nitrite and (b) a one-step process of concerted C-N bond breaking and C-O bond formation. Product energy distributions indicate that the products formed from C-N bond scission in nitromethane and C-O bond scission in methyl nitrite are indistinguishable. The branching ratio for the potential energy surface with the barrier height of 47.6 kcal/mol is close to the experimentally determined value near the threshold energy of the reactions, while the branching ratio for the potential energy surface with a barrier of 55.1 kcal/mol is an order of magnitude smaller than the experimental value.

14. SUBJECT TERMS Decomposition; Nitromethane; Unimolecular Decomposition; Molecular Dynamics	15. NUMBER OF PAGES 100
	16. PRICE CODE SAR

17. SECURITY CLASSIFICATION OF REPORT UNCLASSIFIED	18. SECURITY CLASSIFICATION OF THIS PAGE UNCLASSIFIED	19. SECURITY CLASSIFICATION OF ABSTRACT UNCLASSIFIED	20. LIMITATION OF ABSTRACT

NSN 7540-01-280-5500

UNCLASSIFIED

Standard Form 298 (Rev 2-89)
Prescribed by ANSI Std Z39-18
298-102

INTENTIONALLY LEFT BLANK.

TABLE OF CONTENTS

Dist   Avail and/or
        Special

A-1

Codes

INTENTIONALLY LEFT BLANK.

LIST OF FIGURES

LIST OF TABLES

INTENTIONALLY LEFT BLANK.

ACKNOWLEDGMENTS

INTENTIONALLY LEFT BLANK.

1. INTRODUCTION

Organo-nitro compounds exhibit complex chemical behavior, and resolution of the mechanistic details of the reactions of these compounds at a molecular level is an experimental and a theoretical challenge. The chemistry of the simplest organo-nitro compound, nitromethane, is not completely understood, despite several experimental[1-13] and theoretical[14-20] studies done on the system. Even seemingly direct studies of the unimolecular decomposition of gas-phase nitromethane have indicated complexities in the mechanism of decomposition.[2,3]

The infrared multiphoton dissociation (IRMPD) experiments of Wodtke, Hintsa, and Lee[2] indicate that isomerization of nitromethane to methyl nitrite competes with scission of the C-N bond. Assuming an isomerization channel and using RRKM theory to fit the experimental results, Wodtke et al. predict a 55.5 kcal/mol barrier to isomerization which is slightly lower than the C-N bond dissociation energy (59.5 kcal/mol). They conclude that unimolecular decay of nitromethane can occur in either of two competing reactions:

[I] $$CH_3NO_2 \rightarrow CH_3NO_2^\dagger \rightarrow CH_3 + NO_2 \quad ;$$

[II] $$CH_3NO_2^\dagger \rightarrow CH_3ONO^\dagger \rightarrow CH_3O + NO.$$

They also determined the branching ratio of Reaction II to Reaction I to be 0.6.

Determination of the location and energy of the transition state for isomerization of nitromethane to methyl nitrite has been a focus of several ab initio calculations;[14-19] however, the multi-configurational nature of the ground state of nitromethane is a formidable problem in electronic structure studies. Good quality ab initio calculations performed on this system predict that the transition state structure is "tight" (the C-O and C-N bond lengths are approximately 2.0 Å), and the energy of this structure is approximately 76 kcal/mol above that of equilibrium nitromethane.[14,15,17] It has been suggested that another transition state exists that is more of a van der Waals complex, with longer C-N and C-O bonds (approximately 4.0 Å).[18,19] The exact nature of the transition state can be determined only by performing large active space CASSCF plus CI calculations using extended basis sets. Such multi-configurational quantum mechanical studies are often limited to systems with only a

1

few degrees of freedom because the computational requirements for these problems are immense and existing computer resources are limited.

In addition to the problems associated with calculating points on the potential energy surface, quantum mechanical dynamics calculations on a system such as this are not computationally feasible. Classical mechanical methods do not require the computer resources that quantum mechanical calculations do; therefore, classical trajectory or molecular mechanics calculations are often employed to study the dynamics of systems with many degrees of freedom. We present the results of a classical dynamics calculation of the unimolecular decomposition of nitromethane in order to further understand the dynamics of a system with many degrees of freedom and complex reaction behavior.

We have constructed three model potential energy surfaces to describe unimolecular processes in nitromethane and have performed a series of classical trajectory studies of the unimolecular decomposition of nitromethane. Because the energy and the geometry of the transition state is not established, we have attempted to determine the effect of different barrier heights on the reaction scheme suggested by Wodtke et al.[2] An interesting result of this dynamics study is that all three surfaces predict that the unimolecular decay of nitromethane occurs not just through Reaction I and II but also by the reaction

[III]
$$CH_3NO_2^\dagger \rightarrow CH_3ONO^\dagger \rightarrow CH_3 + NO_2.$$

This reaction has a strong energy dependence and occurs more readily at higher total energies. At all energies, it makes a significant contribution to the number of isomerizing trajectories. The branching ratio calculated by Wodtke et al.[2] was determined from the number density of NO and NO_2 appearing as NO^+ in the time-of-flight spectra. We assume that the experiment did not distinguish between the NO_2 formed in Reaction I from that which might be formed in Reaction III. In order to compare our results with the experiment, we define the branching ratio to be the ratio of the number of NO formed to that of the number of NO_2 formed, i.e., Reaction II/(Reaction I + Reaction III).

The first potential energy surface (PES 1) has a very high barrier to isomerization (216.4 kcal/mol) whereas C-N bond rupture can occur with 60 kcal/mol. One might predict intuitively that isomerization to methyl nitrite would not occur on this surface. However, the results of trajectories indicate that isomerization can occur on this surface through a mechanism of "dissociation" to

2

$CH_3 + NO_2$ followed by recombination of these particles to form methyl nitrite. Because an individual trajectory represents a single isolated molecule in a vacuum, the calculations indicate that this mechanism is feasible even in a "collision-free" environment. However, isomerization on this surface is rare (between 1 to 40 isomerizations in every 1,000 reactive trajectories over the range of energies studied) and does not reproduce the experimentally determined branching ratio.[2] The branching ratios, as defined above, are between 0.001 and 0.025 over the energies studied for this potential energy surface (69.2 to 161.4 kcal/mol above the zero point energy of nitromethane).

The second potential energy surface (PES 2) has an isomerization barrier height of 55.1 kcal/mol, the value suggested by Wodtke et al.[2] The third potential energy surface (PES 3) has an isomerization barrier height of 47.6 kcal/mol, the value predicted from the MINDO/3 calculations of Dewar and Ritchie.[16] The isomerization of nitromethane to methyl nitrite on these surfaces does not occur through a dissociation-recombination mechanism but rather occurs through a concerted C-N bond-breaking C-O bond-forming process. Although PES 2 and PES 3 differ by only a few kcal/mol in the barrier heights, the dynamics results are dramatically different. The branching ratio, as defined above, for PES 2 at the threshold energy of C-N bond dissociation is 0.032, whereas the branching ratio for PES 3 at the same energy is 0.79. The branching ratios for PES 2 increase slightly with increasing energy to a maximum value of 0.065, whereas the branching ratios for PES 3 decrease with increasing energy to a minimum value of 0.12. Additionally, the probability of Reaction III increases with increasing energy for both PES 2 and PES 3, but the probability of Reaction II decreases with increasing energy for PES 3. Conversely, the probability of Reaction II is approximately constant as a function of energy for PES 2. These potential energy surfaces properly describe the fundamental vibrational frequencies and geometries for reactants and products and the correct thermochemistry for the reaction channels shown above. The main differences in the surfaces are in the transition state region.

In addition to providing mechanistic details of the unimolecular decomposition of nitromethane, we present a new approach to construction of an empirical potential energy surface which describes a many-body system which can undergo more than one type of reaction.

2. POTENTIAL ENERGY SURFACE

A limitation of a classical trajectory calculation, aside from the inability to describe important quantum mechanical effects, is that an approximate potential energy surface must be used. A complete and accurate multidimensional potential energy surface can be constructed only by ab initio quantum mechanical calculations; however, they are not computationally possible at this time for large molecular systems. Therefore, the potential energy surfaces used in classical mechanics calculations are usually empirical in nature and are based only in part on theoretical calculations. Most of the potential energy surfaces used in classical trajectory simulations have an analytic form (to allow rapid calculation of the forces), with the parameters of the potential function fit to spectroscopic, kinetic, and thermodynamic data. Additionally, selected points calculated by ab initio methods are sometimes incorporated into the fit. Usually, most of the experimental data correspond to the equilibrium state of the reactant or product species and the transition state.

In our approach to constructing a potential energy surface, we have assumed that the potential energy is the sum of terms which correctly describe the equilibrium properties of each stable species in the system, weighted by functions which are dependent on geometric considerations. The form of the overall potential is:

$$V_{Total} = \sum V_i S_i \, , \tag{1}$$

where i denotes all the reactant and decomposition products. The V_i describes the stable species i at equilibrium and is made up of terms which describe stretching and bending motions. The parameters of the functions in V_i are fit to the known data of the species near equilibrium. The S_i is a weighting function which is dependent on critical geometries of the species. This function increases or decreases the contribution of the V_i to the overall potential depending on the molecular geometry.

An advantage to using this form of potential is that the weighting functions can be monitored throughout a trajectory to characterize the system at any time. As will be illustrated in this paper, following the weighting functions in time provides an easy way to determine a reaction mechanism in a complex system without having to rely on plots of individual internal coordinates as functions of time. Another advantage to using this type of potential is that it is "modular"; the different V_i developed can be used in other dynamics studies which use a potential energy surface of the form in Equation 1. If other channels need to be added, all that is necessary is that the new $V_i S_i$ be added to

4

Equation 1, and the existing weighting functions modified accordingly. We attempted to adjust the surface features by modifying the S_i only and leaving the V_i unchanged, thus developing V_i potential terms that can be used in studies of other related systems.

Using the form of the potential energy surface given in Equation 1, the total potential energy function to describe the nitromethane/methyl nitrite system is:

$$V_{Total} = V_{CH_3NO_2} S_{CH_3NO_2} + V_{CH_3ONO'} S_{CH_3ONO'} + V_{CH_3O'NO} S_{CH_3O'NO}$$
$$+ V_{CH_3+NO_2} S_{CH_3+NO_2} + V_{CH_3O+NO'} S_{CH_3O+NO'} + V_{CH_3O'+NO} S_{CH_3O'+NO} \qquad (2)$$

Note that there are two terms to describe the methyl nitrite species and two terms to describe the product fragments CH_3O and NO. The terms differ only in the labeling of the oxygens, which are labelled O and O'. These are chemically equivalent species and in reality cannot be distinguished. A dynamics study must allow unbiased formation of methyl nitrite and the product fragments with either O or O' bound to the carbon atom. Therefore, it is necessary, according to the formulation of the potential energy surface given in Equation 1, to have terms which explicitly describe the species in which either O or O' is bound to the carbon atom.

The functions which make up the V_i are:

(a) morse functions to describe bond stretching motion,

$$V^{stretch} = D_e\{1-exp(-\alpha[R-R_e])\}^2 - D_e; \qquad (3)$$

(b) harmonic oscillator functions to describe bending motion,

$$V^{bend} = k(\theta - \theta_e)^2 ; \qquad (4)$$

(c) and truncated cosine series to describe torsional motion, where applicable,

$$V_T(\tau) = \Sigma A_n cos(n\tau). \qquad (5)$$

Where necessary, these standard functions have been modified as described below.

Because the S_i is a weighting function for the contribution of the V_i to the overall potential, it must be a smoothly varying function between 0 and 1. Additionally, its first derivatives must be continuous. Although there is substantial information about the geometry and intramolecular interactions of each reactant or product species near its equilibrium, little, if anything, is known about the regions of the potential between the limits of the reactant and product species. Therefore, we have little information to guide us in choosing the functional form of the S_i to describe the regions between the asymptotic limits of reactants and products.

The function which makes up the S_i is:

$$F'(Q) = exp[-G(Q-Q_{eq})^N],$$

(6)

where Q defines some internal coordinate and N is an even integer greater than or equal to 2. Figures 1a and 1b show F' for different N and G, respectively. A modified form of F' used in constructing the S_i is:

$$F(Q) = \begin{cases} 1, & Q < Q_{eq} \\ F'(Q), & Q \geq Q_{eq} \end{cases}$$

(7)

and is illustrated in Figure 1c.

The description of the details of V_{Total} will be as follows: each reactant or product fragment will be discussed in separate sections, and the V_i and S_i will be detailed, along with the experimental data and theoretical information about the fragment which are used in fitting the parameters. The functions F' and F will be denoted with subscripts, for use in referencing the parameters given in Table 1.

2.1 Nitromethane.

2.1.1 Form of the Potential. The term which describes equilibrium nitromethane is:

$$V_{CH_3NO_2} = \Sigma V_{CH}^{Stretch} + V_{CN}^{Stretch} + \Sigma V_{NO}^{Stretch}$$
$$+ \Sigma V_{HCH}^{Bend} + V_{ONO}^{Bend} + \left[\Sigma V_{HCN}^{Bend} + \Sigma V_{CNO}^{Bend} \right] F_a(R_{CN}),$$

(8)

Table 1. Parameters for Weighting Functions

Function Index	G PES 1	G PES 2	G PES 3	Q PES 1	Q PES 2	Q PES 3	N PES 1	N PES 2	N PES 3
1	$1.5\ \text{Å}^{-4}$	$0.0015\ \text{Å}^{-20}$	$0.0015\ \text{Å}^{-20}$	$1.479\ \text{Å}$	$1.479\ \text{Å}$	$1.479\ \text{Å}$	4	20	20
2	$1.5\ \text{Å}^{-4}$	$0.5\ \text{Å}^{-10}$	$0.5\ \text{Å}^{-10}$	$1.421\ \text{Å}$	$1.421\ \text{Å}$	$1.421\ \text{Å}$	4	10	10
3	$1.5\ \text{Å}^{-4}$	$1.5\ \text{Å}^{-4}$	$1.5\ \text{Å}^{-4}$	$1.326\ \text{Å}$	$1.326\ \text{Å}$	$1.326\ \text{Å}$	4	4	4
4	$6.0\ \text{Å}^{-2}$	$2.85\ \text{Å}^{-2}$	$4.5\ \text{Å}^{-2}$	$1.479\ \text{Å}$	$1.479\ \text{Å}$	$1.479\ \text{Å}$	2	2	2
5	$4.0\ \text{Å}^{-2}$	$2.85\ \text{Å}^{-2}$	$4.5\ \text{Å}^{-2}$	$1.421\ \text{Å}$	$1.421\ \text{Å}$	$1.421\ \text{Å}$	2	2	2
7	$4.0\ \text{Å}^{-2}$	$2.85\ \text{Å}^{-2}$	$4.5\ \text{Å}^{-2}$	$1.326\ \text{Å}$	$1.326\ \text{Å}$	$1.326\ \text{Å}$	2	2	2
8	12.0	1.5	1.5	117.1°	117.1°	117.1°	8	20	20
9	12.0	—	—	32.4°	—	—	8	—	—
16	$10.0\ \text{Å}^{-12}$	$0.5\ \text{Å}^{-12}$	$0.5\ \text{Å}^{-12}$	$1.421\ \text{Å}$	$1.421\ \text{Å}$	$1.421\ \text{Å}$	12	12	12

where all of the functions have been defined in Equations 3–7. The form of the function which determines the contribution of $V_{CH_3NO_2}$ to the overall potential is a function of R_{CN} and the two C-N-O angles, θ_{CNO} and $\theta_{CNO'}$:

$$S_{CH_3NO_2} = F_1(R_{CN})F_8(\theta_{CNO})F_8(\theta_{CNO'}).$$ (9)

This function attenuates $V_{CH_3NO_2}$ as the molecule approaches decomposition to $CH_3 + NO_2$ or isomerization to either CH_3ONO' or $CH_3O'NO$. The parameters for the F_i functions are given in Table 1.

2.1.2 Experimental Data and Theoretical Information Used for Parameter Fitting.

(1) Structure. Gas phase electron diffraction and microwave spectra of CH_3NO_2 have been used by several groups[4-8] to determine the structural parameters of CH_3NO_2 and to study the internal rotations of the methyl group relative to the NO_2 group in nitromethane. While the interest of the early microwave studies focused on determination of the barrier height to internal rotation,[4-6] Cox and Waring[7] provide an experimental structure for nitromethane (see Table 2). The analysis of the experimental results is based on assumptions about the methyl top. Although the heavy atom bond lengths were accurately determined in this experiment, the C-H bond length was not determined but was assumed to be 1.089 Å. A later microwave spectral study of CH_3NO_2 was performed by Cox and co-workers[8] to determine the structure of the methyl group. The study shows that $R_{CH} = 1.0979 \pm 0.0009$ Å, and $\theta_{HCN} = 107.61 \pm 0.15°$.

Electronic structure calculations[14,15] show a dependence of geometric parameters on orientation of the methyl group with respect to the NO_2 group. Changes in bond lengths and the degree to which the methyl and NO_2 rotors tilt off the C-N bond axis as the nitromethane molecule undergoes internal rotation are predicted by the ab initio calculations. McKean and Watt,[9] in an interpretation of infrared (IR) spectra of nitromethane, predict changes in the C-H bond lengths of up to 0.006 Å during internal rotation, affirming the effects predicted by first principles calculations. The barrier to rotation of the methyl group about the C-N bond axis is 0.006 kcal/mol,[6] causing it to be a free rotor at room temperature. Because we are specifically interested in high energy processes in nitromethane (unimolecular decomposition) and the geometric changes due to the rotation are small, we have chosen not to include terms in Equation 8 which are dependent on internal rotation. These effects, however, could easily be incorporated into the potential by using the form of the potential suggested by McKean and Watt,[9] which is a function of torsional angle.

8

Table 2. Structural Parameters of Nitromethane

Internal Coordinate[a]	Expt'l.[b]	PES 1[c]	PES 2[c]	PES 3[c]
R(CH)	1.088	1.076	1.076	1.076
R(CN)	1.489	1.479	1.479	1.479
R(NO)	1.224	1.221	1.221	1.221
$\angle$(HCN)	107.2	107.40	107.40	107.40
$\angle$(ONO)	125.3	125.80	125.87	125.87

[a] Units are: R in Å, $\angle$ in degrees
[b] Cox and Waring, Ref. 7
[c] G. F. Adams, unpublished results.

(2) Vibrational Analyses. Nitromethane has 14 fundamental vibrational modes and one internal rotational degree of freedom (torsional mode). Assignments of frequencies from infrared (IR) spectra are provided by several groups[9-13] and shown in Table 3.

(3) Bond Dissociation Energies. The dissociation energy of the C-N bond in nitromethane has been measured to be 58 to 60 kcal/mol,[21] while the C-H and N-O bond dissociation energies are not firmly established. The C-H bond energy in nitromethane has been measured at 107.5 kcal/mol,[22] but McKee[15] predicts a substantially lower bond dissociation energy of 88 kcal/mol based on MP2/6-31G* + ZPC level and MCSCF/6-31G + CI level calculations. We have assumed a C-H bond dissociation energy of 102 kcal/mol as a reasonable approximation. The N-O bond dissociation energy in CH_3NO_2 has been estimated to be 93.5 kcal/mol.[23]

2.1.3 Results of the Fit. The parameters of the potential energy function described in Equations 8–9 were fitted to the geometric parameters predicted by SCF calculations of Adams,[14] except for the slight differences due to internal rotation. His calculated results are in good agreement with the experiment, except for the C-N bond distances. The internal coordinates of CH_3NO_2 at equilibrium predicted by the three potential energy surfaces are listed in Table 2.

9

Table 3. Normal Mode Frequencies[a] for Nitromethane

Mode	Reference 10	Reference 11	Reference 12	Reference 13	Reference 9	PES 1	PES 2	PES 3
ν_9	3048	3065	3080.4	3065	3080	3091.15	3091.15	3091.15
	—	—	2984	3045	3044	3088.56	3088.56	3088.56
ν_1	2965	2972	2964.3	2967	2973.9	2956.76	2956.76	2956.76
ν_7	1582	1586	1583.3	1561	1583.8	1582.10	1582.10	1582.10
ν_{10}	1488	1482	1438.0	1426	—	1557.92	1557.92	1557.92
	1449	1443	—	1426	—	1413.76	1413.76	1413.76
ν_2	—	1397	1397	1402	1397.4	1380.88	1380.88	1380.88
ν_3	1384	1377	1378.8	1379	1380.4	1374.50	1374.50	1374.50
ν_{11}	1153	1100	1146	1103	1119	1106.41	1106.41	1106.41
	1097	1087	1091	1103	1099	1077.51	1077.51	1077.51
ν_4	921	918	917.1	917	917.9	836.81	836.81	836.81
ν_5	647	658	656	655	657.4	647.02	647.02	647.02
ν_6	599	605	—	607	602.5	—	—	—
ν_8	476	477	—	480	475.2	473.85	473.85	473.85

[a] Frequencies are in cm^{-1}

10

Assuming the bond dissociation energies listed above, all other parameters in Equations 8–9 were fitted to the experimental frequencies shown in Table 3. The three surfaces predict 13 vibrational modes, shown for comparison with experimental values in Table 3. No torsional mode exists as this motion was not explicitly described in Equations 8–9, as explained above. Additionally, the NO_2 out-of-plane rock is not present. The calculated frequencies are in reasonable agreement with the experiment, except for vibrational modes υ_{10} and υ_4. The best fit parameters are given in Table 4.

2.2 Methyl Nitrite.

2.2.1 Form of the Potential.

The term which describes a methyl nitrite molecule at equilibrium is considerably more complex than that of the nitromethane molecule. Two geometric isomers of methyl nitrite exist—The "cis" and "trans" species. The force constants and geometries differ in these isomers. Also, there is evidence that forces and geometries change upon internal rotation of the methyl group in methyl nitrite. Using the available information, we have incorporated the effects of internal rotation in the potential energy function. The symbol τ' will be used to denote the CONO dihedral angle, and τ_i, i = 1, 2, or 3, will denote the $H_{(i)}$CON dihedral angles. Without loss of generality, we will use the $V_{CH_3ONO}\cdot S_{CH_3ONO}\cdot$ term to describe the methyl nitrite potential; the $V_{CH_3ONO}S_{CH_3ONO}$ term has the same form, except for the position of the oxygen atoms. Additionally, a few terms differ between PES 1 and PES 2 and 3. The difference occurs only in use of attenuation functions and the parameters of the attenuation functions. The differences will be specified below.

The forms of the potential describing methyl nitrite at equilibrium are:

<u>PES 1</u>

$$
\begin{aligned}
V_{CH_3ONO'} =\ & \Sigma V_{CH}^{Stretch}(\tau',\tau_i) + V_{CO}^{Stretch}(\tau') + V_{ON}^{Stretch}(\tau') \\
& + V_{N=O'}^{Stretch}(\tau') + \{ V_{H_{(1)}CH_{(2)}}^{Bend}(\tau',\tau_i) + V_{H_{(2)}CH_{(3)}}^{Bend}(\tau',\tau_i) \\
& + V_{H_{(1)}CH_{(3)}}^{Bend}(\tau',\tau_i) + \Sigma V_{H_{(i)}CO}^{Bend}(\tau',\tau_i) \\
& + [V_{ONO}^{Bend}(\tau',\tau_1,\tau_2,\tau_3) + V_{CON}^{Bend}(\tau',\tau_1,\tau_2,\tau_3) \\
& + V_T(\tau')] F_7(R_{ON}) F_5(R_{CO}).
\end{aligned}
\tag{10a}
$$

11

Table 4. Potential Energy Parameters, Nitromethane Term

Morse Parameters			
Bond	D_e (eV)	α (Å^{-1})	R_{eq} (Å)
CH	4.423174	1.89	1.076
CN	2.601867	2.085	1.479
NO	4.045904	2.377	1.221
Harmonic Oscillator Parameters			
Angle	k (eV/rad^2)		θ_{eq} (degrees)
HCH	1.375		111.46
HCN	2.45		107.40
CNO	3.20		117.10
ONO	9.35		125.80

PES 2 and 3

$$V_{CH_3ONO^-} = \Sigma V_{CH}^{Stretch}(\tau';\tau_j) + V_{CO}^{Stretch}(\tau') + V_{ON}^{Stretch}(\tau')$$

$$+ V_{N=O}^{Stretch}(\tau') + V_{H_{(1)}CH_{(2)}}^{Bend\,(\tau';\tau_j)} + V_{H_{(2)}CH_{(3)}}^{Bend\,(\tau';\tau_j)}$$

$$+ V_{H_{(1)}CH_{(3)}}^{Bend\,(\tau';\tau_j)} + \{ \Sigma\, V_{H_{(i)}CO}^{Bend\,(\tau';\tau_j)}$$

$$+ [V_{ONO^-}^{Bend}(\tau';\tau_1,\tau_2,\tau_3) + V_{CON}^{Bend}\tau';\tau_1,\tau_2,\tau_3)$$

$$+ V_T(\tau')]F_7(R_{ON}) \}F_5(R_{CO}). \qquad (10b)$$

12

We have indicated the dependence of each term on the torsion angles. These terms are, of course, dependent on other internal coordinates. Those dependencies are not explicitly shown. Note that the only difference between Equation 10a and Equation 10b is that the HCH bending terms described in Equation 10a are not attenuated by the function $F_5(R_{CO})$.

The modified Morse function which describes the C-H stretching motion is:

$$V_{CH_{(i)}}^{Stretch}(\tau', \tau_i) = D_{CH} \{1.0 - \exp(-\alpha_{CH}[R_{CH_{(i)}} - R_{eq}^{CH}])\}^2 - D_{CH}, \tag{11}$$

where α_{CH} is a function of τ', and τ_i and has the form:

$$\alpha_{CH} = A_1^{CH} + B_1^{CH} + A_2^{CH}[1.0 - \cos(\tau')]$$

$$+ \{C_1^{CH} + C_2^{CH}[1.0 - \cos(\tau')]\}\cos^2(\tau_i). \tag{12}$$

The modified Morse function which describes the C-O stretching motion is

$$V_{CO}^{Stretch}(\tau') = D_{CO} \{1.0 - \exp(-\alpha_{CO}[R_{CO} - R_{eq}^{CO}])\}^2 - D_{CO}, \tag{13}$$

where α_{CO} is a function of τ',

$$\alpha_{CO} = B_1^{CO} + B_2^{CO}[1.0 - \cos(\tau')]. \tag{14}$$

The O-N bond is described by a modified Morse function,

$$V_{ON}^{Stretch}(\tau') = D_{ON} \{1.0 - \exp(-\alpha_{ON}[R_{ON} - R_{eq}^{ON}])\}^2 - D_{ON}, \tag{15}$$

where α_{ON} is a function of τ',

$$\alpha_{ON} = B_1^{ON} + B_2^{ON}[1.0 - \cos(\tau')]. \tag{16}$$

13

The terminal N=O bond is described by a modified Morse function,

$$V_{N=O}^{Stretch}(\tau') = D_{N=O}\{1.0-\exp(-\alpha_{N=O}[R_{N=O}-R_{eq}^{N=O}])\}^2-D_{N=O}, \qquad (17)$$

where $\alpha_{N=O}$ is a function of τ',

$$\alpha_{N=O} = B_1^{N=O}+B_2^{N=O}[1.0-\cos(\tau')]. \qquad (18)$$

The potential term describing motion of $H_{(1)}CH_{(2)}$ angle is

$$V_{H_{(1)}CH_{(2)}}^{Bend}(\tau',\tau_2) = k_{HCH}[\theta_{H_{(1)}CH_{(2)}}-\theta_o]^2, \qquad (19)$$

where θ_0 is a function of internal rotations and has the form

$$\begin{aligned}
\theta_o = {} & T_o^{HCH}+A_1^{HCH}[1.0-\cos(\tau')] \\
& + \{B_1^{HCH}+B_2^{HCH}[1.0-\cos(\tau')]\}\cos(\tau_2) \\
& + \{C_1^{HCH}+C_2^{HCH}[1.0-\cos(\tau')]\}\cos^2(\tau_2). \qquad (20)
\end{aligned}$$

The terms describing the motion of the $H_{(2)}CH_{(3)}$ and the $H_{(1)}CH_{(3)}$ angles, respectively, have the same form as Equations 19 and 20, except for θ_o for the $H_{(2)}CH_{(3)}$ angle is a function of τ_1 and θ_o for the $H_{(1)}CH_{(3)}$ angle is a function of τ_3.

The ONO bending potential term has the form

$$V_{ONO}^{Bend}(\tau',\tau_1,\tau_2,\tau_3) = k_{ONO}[\theta_{ONO}-\theta_o]^2, \qquad (21)$$

where

$$k_{ONO} = k_o^{ONO}+ C_1^{ONO}[1.0-\cos(\tau')], \qquad (22)$$

14

and

$$\theta_o^{ONO} = T_o^{ONO} + A_1^{ONO}[1.0 - \cos(\tau')]$$

$$+ \{B_1^{ONO}[1.0 - \cos(\tau')]\} \prod_{i=1}^{3} [1.0 - \cos(\tau_i)]. \tag{23}$$

The CON bending potential has the form

$$V_{CON}^{Bend}(\tau'; \tau_1, \tau_2, \tau_3) = k_{CON}[\theta_{CON} - \theta_o]^2, \tag{24}$$

where

$$k_{CON} = k_o^{CON} + A_1^{CON}[1.0 - \cos(\tau')], \tag{25}$$

and

$$\theta_o = T_o^{CON} + \{B_1^{CON} \prod_{i=1}^{3} [1.0 - \cos(\tau_i)] + D_1^{CON} \prod_{i=1}^{3} [1.0 + \cos(\tau_i)]\}$$

$$X [1.0 - \cos(\tau')] + \{C_1^{CON} \prod_{i=1}^{3} [1.0 + \cos(\tau_i)]\} [1.0 + \cos(\tau')]. \tag{26}$$

The potential term which describes the $H_{(i)}CO$ angle bending potential is

$$V_{H_{(i)}CO}^{Bend}(\tau'; \tau_i) = k_{H_{(i)}CO}[\theta_{H_{(i)}CO} - \theta_o]^2, \tag{27}$$

where

$$k_{H_{(i)}CO} = D_1^{HCO} + A_1^{HCO} + A_2^{HCO}[1.0 - \cos(\tau')]$$

$$+ \{C_1^{HCO} + C_2^{HCO}[1.0 - \cos(\tau')]\} \cos(\tau_i), \tag{28}$$

15

and

$$\theta_o = T_o^{HCO} + A_3^{HCO} + A_4^{HCO} [1.0-\cos(\tau')]$$

$$+ \{B_1^{HCO} + B_2^{HCO} [1.0-\cos(\tau')]\} \cos(\tau_i)$$

$$+ \{C_3^{HCO} + C_4^{HCO} [1.0-\cos(\tau')]\} \cos^2(\tau_i) \quad . \tag{29}$$

The potential which describes the internal rotation of the CONO group is that given by Darsey and Thompson[24] and has the form given in Equation 5.

The weighting function $S_{CH_3ONO'}$ is a function of R_{CO}, R_{ON}, $R_{CO''}$ and θ_{CNO} and has the following forms for the three surfaces:

PES 1

$$S_{CH_3 ONO'} = F_2(R_{CO}) F_3(R_{ON}) F'_9(\theta_{CNO}) [1.0-F_{16}(R_{CO'})]. \tag{30a}$$

PES 2 and 3

$$S_{CH_3 ONO'} = F_2(R_{CO}) F_3(R_{ON}) [1.0-F_8(\theta_{CNO})][1.0-F_{16}(R_{CO'})] . \tag{30b}$$

This function attenuates $V_{CH_3ONO'}$ as the molecule approaches decomposition to $CH_3 + NO_2$ or $CH_3O + NO'$, or when the system is in a geometry consistent with nitromethane. The weighting function $S_{CH_3O'NO}$ has a similar form as Equation 30:

PES 1

$$S_{CH_3 O'NO} = F_2(R_{CO'}) F_3(R_{O'N}) F'_9(\theta_{CNO'}) [1.0-F_{16} (R_{CO})] . \tag{31a}$$

PES 2 AND 3

$$S_{CH_3 O'NO} = F_2(R_{CO'}) F_3(R_{O'N}) [1.0-F_8(\theta_{CNO'})] [1.0-F_{16}(R_{CO})] . \tag{31b}$$

16

Parameters of the weighting functions F_i are given in Table 1.

2.2.2 Experimental Data and Theoretical Information Used for Parameter Fitting.

(1) Structure. Accurate structures of both cis and trans isomers of methyl nitrite have been derived from microwave spectral studies[25,26] as well as barrier heights to internal rotation.[25,26] The experimental results show decreases in the CON and ONO bond angles upon cis-trans isomerization as well as changes in the bond lengths and the tilt of the methyl group. The methyl tilt is defined as the angle between the C-O bond and the perpendicular from the carbon atom to the basal plane of the CH_3 pyramid. Turner et al.[25] determined the methyl tilt to be 5.4° ±1.5° away from the nitrosyl oxygen atom in the cis isomer; the structure and conformation of the methyl group for trans-CH_3ONO was not determined. The decreases in the CON and ONO bond angles upon conversion from the cis to trans isomer is thought to be due to reduced steric interaction in the trans conformation. The experimentally determined structural parameters of both cis- and trans-methyl nitrite are given in Table 5. Ab initio calculations of methyl nitrite predict changes in bond lengths and valence angles upon internal rotations.[15,27] McKee[15] provides calculated changes in the methyl tilt upon internal rotation and discusses these in the context of conformational stabilities within methyl nitrite. Ha, Meyer, Ghosh, Bauder, and Günthard[27] examined the structural relaxation of the cis conformer upon the internal rotation of the methyl group and its effect on the rotational constants upon torsional excitation. These changes in geometric parameters upon internal rotation are shown in Table 5.

(2) Vibrational Analyses. Methyl nitrite has 15 vibrational degrees of freedom. The IR gas phase spectrum of cis- and trans-methyl nitrite recorded over the range 4,000-300 cm^{-1} is reported by Ghosh and Günthard,[28] and they provide assignments of the vibrational frequencies for both the cis and trans isomers. These assignments are given in Tables 6 and 7.

(3) Bond Dissociation Energies. Because the C-H bond dissociation energy is not well established, we have assumed a value of 102 kcal/mol, the same value assumed for nitromethane. The O-N bond energy has been measured to be 39 to 41 kcal/mol;[21] we used 41.2 kcal/mol. Based on heats of formation calculated by Melius,[17] we assume the bond dissociation energy of the terminal N=O bond is 151.8 kcal/mol and that of the C-O bond is 58 kcal/mol.

Table 5. Structural Parameters of Cis- and Trans-Methyl Nitrite

Int.[a] Coord.	Expt.[b]	Theor.[c]	PES 1	PES 2	PES 3	Theor.[c]	PES 1	PES 2	PES 3
Cis-Methyl Nitrite									
		Staggered				Eclipsed			
O=N	1.182	1.162	1.162	1.168	1.168	1.160	1.162	1.166	1.166
N-O	1.398	1.326	1.326	1.348	1.349	1.331	1.326	1.338	1.338
O-C	1.437	1.421	1.421	1.435	1.435	1.425	1.421	1.429	1.429
C-H_i	1.09	1.078	1.080	1.080	1.080	1.075	1.080	1.080	1.080
C-H_o	1.102	1.080	1.080	1.080	1.080	1.080	1.080	1.080	1.080
∠ONO	114.8	115.2	115.2	118.0	118.0	116.4	116.4	118.0	118.0
∠NOC	114.7	117.6	117.6	122.6	122.6	120.7	120.7	123.7	123.7
∠OCH_i	101.8	104.4	104.4	104.7	104.7	111.7	111.7	111.3	111.3
∠OCH_o	109.9	110.8	110.8	110.6	110.6	107.2	107.2	107.4	107.4
∠H_oCH_o	108.1	—	108.1	107.7	107.7	—	111.6	112.3	112.3
H_iCH_o	—	—	111.3	111.6	111.6	—	109.6	109.1	109.1
Trans-Methyl Nitrite									
O=N	1.164	1.156	1.162	1.160	1.160	1.155	1.162	1.160	1.160
N-O	1.415	1.339	1.326	1.326	1.326	1.339	1.326	1.326	1.326
O-C	1.436	1.415	1.421	1.421	1.421	1.416	1.421	1.421	1.421
C-H_i	1.09	1.078	1.080	1.080	1.080	1.081	1.080	1.080	1.080
C-H_o	1.09	1.082	1.080	1.080	1.080	1.080	1.080	1.080	1.080
∠ONO	111.8	111.5	111.5	111.5	111.5	111.6	111.5	111.5	111.5
∠NOC	109.9	111.3	111.3	111.3	111.3	112.6	112.6	112.6	112.6
∠OCH_i	109.5	105.6	105.6	105.6	105.6	110.1	110.1	110.1	110.1
∠OCH_o	109.5	110.7	110.7	110.7	110.7	108.4	108.4	108.4	108.4
∠H_oCH_o	109.5	—	108.2	108.2	108.2	—	110.5	110.5	110.5
∠H_iCH_o	109.5	—	110.8	110.8	110.8	—	109.7	109.7	109.7

[a] Units are: R in Å, ∠ in degrees. H_i designates the hydrogen atom in the plane of the molecule and H_o designates the hydrogen atom out of the plane of the molecule.
[b] Turner, Corkill, and Cox, Reference 25.
[c] McKee, Reference 15.

Table 6. Normal Mode Frequencies[a] for Cis-Methyl Nitrite

Mode	Expt.[b]	PES 1	PES 2	PES 3	PES 1	PES 2	PES 3
		Staggered			Eclipsed		
ν_1	3038	3051.7	3069.1	3069.1	3044.9	3051.1	3051.1
ν_{11}	2993	3020.2	3018.8	3018.8	3027.2	3027.9	3027.9
ν_2	2956	2913.9	2914.7	2914.7	2912.8	2914.7	2914.7
ν_3	1620	1616.4	1683.9	1682.6	1616.5	1621.1	1620.8
ν_4	1458.5	1472.8	1550.2	1549.0	1483.4	1534.5	1533.9
ν_{12}	1444.7	1437.5	1444.9	1444.4	1453.7	1451.5	1451.5
ν_5	1410	1408.1	1393.2	1393.2	1441.5	1448.1	1448.1
ν_6	1240	1270.3	1236.2	1236.1	1253.2	1243.4	1242.9
ν_{13}	1003.5	975.2	1182.1	1179.7	1027.3	1040.4	1040.0
ν_7	990.5	937.9	956.4	955.8	849.2	977.6	977.5
ν_8	841	708.0	878.1	877.0	756.5	843.6	843.3
ν_9	628	629.9	653.5	653.3	631.0	687.3	687.3
ν_{10}	346.2	356.3	619.1	619.0	375.3	636.6	636.6
τ (CONO)	—	347.3	313.3	313.1	353.0	376.1	376.0
τ (HCON)	—	—	176.0 i	175.9 i	—	126.7	126.7

[a] Frequencies are in cm^{-1}.
[b] Ghosh and Günthard, Ref. 28

19

Table 7. Normal Mode Frequencies[a] for Trans-Methyl Nitrite

Mode	Expt.[b]	PES 1	PES 2	PES 3	PES 1	PES 2	PES 3
		Staggered			Eclipsed		
ν_1	2921	2933.5	2933.5	2933.5	2933.7	2933.7	2933.7
ν_{11}	2887	2891.9	2891.9	2891.9	2896.2	2896.2	2896.2
ν_2	2829	2795.8	2795.8	2795.7	2794.6	2794.6	2794.6
ν_3	1677.5	1669.2	1669.3	1669.2	1671.0	1671.0	1671.0
ν_4	1463	1478.2	1478.3	1478.1	1491.7	1491.8	1491.7
ν_{12}	1451.2	1446.8	1447.0	1446.6	1450.6	1451.0	1450.4
ν_5	1429	1418.2	1418.2	1418.2	1439.1	1439.1	1439.1
ν_6	1190	1178.2	1178.6	1178.1	1209.7	1210.0	1209.5
ν_7	1046	1069.8	1070.4	1069.6	1052.4	1053.0	1052.1
ν_{13}	1031	870.4	870.4	870.4	911.7	911.7	911.7
ν_8	812.2	818.8	818.8	818.8	817.2	817.2	817.2
ν_9	564.2	594.5	594.9	594.3	588.2	588.6	588.0
ν_{10}	379	356.5	356.5	356.5	341.0	341.1	341.1
τ (CONO)	—	176.8	176.8	176.8	177.0	177.0	177.0
τ (HCON)	—	—	—	—	—	—	—

[a] Frequencies are in cm⁻¹.
[b] Ghosh and Günthard, Ref. 28.

2.2.3 Results of the Fit. Because McKee[15] provided the most detailed information about geometric changes in methyl nitrite upon internal rotation, we have fitted the parameters of the functions in Equations 10–31 to his ab initio values.

Using the bond dissociation energies discussed above, all other parameters were fitted to give agreement with the experimental vibrational frequencies shown in Tables 6 and 7. Vibrational frequencies calculated from a normal mode analysis using these three surfaces are provided for comparison with experiment in Tables 6 and 7.

PES 1 predicts 14 vibrational modes, including the torsional mode of the CONO dihedral angle. The frequency of this motion has not been observed experimentally for either the cis or trans isomer. Agreement with experiment is good with the exception of mode υ_8 for the cis isomer and mode υ_{13} for the trans isomer.

PES 2 and PES 3 predict 15 vibrational modes for cis-methyl nitrite and 14 vibrational modes for trans-methyl nitrite. The normal frequencies for cis-methyl nitrite differ from those calculated using PES 1, particularly for modes υ_4, υ_{13}, υ_8, and υ_{10} for the cis-staggered species, and υ_4, υ_7, υ_8, and υ_{10} for the cis-eclipsed species. Because the cis-staggered methyl nitrite has an imaginary frequency for the torsional motion of the methyl group about the C-O bond, this indicates it is a transition state species on PES 2 and PES 3. The eclipsed cis-methyl nitrite, however, has no imaginary frequencies and therefore is a stable configuration on all three surfaces. Vibrational frequencies of equilibrium trans-methyl nitrite are the same for all three potential energy surfaces. Agreement with experiment is good, except for υ_{13}. The best fit parameters for the V_i are given in Table 8.

2.3 Product Fragments Methyl and Nitrogen Dioxide Radicals.

2.3.1 Form of the Potential.

The $V_{CH_3 + NO_2}$ term is written as:

$$V_{CH_3 \cdot NO_2} = V_{CH_3} + V_{NO_2}.$$

(32)

Table 8. Potential Energy Parameters, Methyl Nitrite Team

α (Å⁻¹)		k (eV/rad²)		θ$_{eq}$ (degrees)	
A_1^{CH}	-0.023930	k_{HCH}	1.585558	T_o^{HCH}	108.11
A_2^{CH}	-0.041760	k_o^{ONO}	8.533768	A_1^{HCH}	2.522218
B_1^{CH}	1.870784	C_1^{ONO}	0.805765	A_2^{HCH}	-0.038579
C_1^{CH}	0.023930	k_o^{CON}	5.355633	B_1^{HCH}	1.777910
C_2^{CH}	0.007841	A_1^{CON}	-1.081012	B_2^{HCH}	-0.316682
B_1^{CO}	2.704537	D_1^{HCO}	1.789699	C_1^{HCH}	-0.758857
B_2^{CO}	0.033294	A_1^{HCO}	-1.405667	C_2^{HCH}	-0.212692
B_1^{ON}	3.355830	A_2^{HCO}	0.355721	T_o^{ONO}	116.4
B_2^{ON}	-0.428253	C_1^{HCO}	1.405667	A_1^{ONO}	-2.45
$B_1^{N=O}$	2.225035	C_2^{HCO}	-0.384331	B_1^{ONO}	-1.20
$B_2^{N=O}$	0.060037			T_o^{CON}	117.6
				B_1^{CON}	-6.30
				D_1^{CON}	-5.0
				C_1^{CON}	3.10
				T_o^{HCO}	104.4
				A_3^{HCO}	4.915147
				A_4^{HCO}	0.401516
				B_1^{HCO}	3.636363
				B_2^{HCO}	-0.686364
				C_3^{HCO}	-1.260600
				C_4^{HCO}	-0.506062

The function used to describe the methyl radical is:

$$V_{CH_3} = \Sigma V_{CH}^{Stretch} + \Sigma \{ V_{HCH}^{Bend} [1.0 - F_5(R_{CO})][1.0 - F_5(R_{CO'})] \}, \tag{33}$$

where all the terms are defined in Equations 3–7. Several others have fit analytic functions that reproduce experimental frequencies for CH_3.[29] Some of these functions have included terms which explicitly describe the out-of-plane large amplitude (OPLA) motion of the methyl radical. Because we think addition of this term probably will not affect the dynamics of the reactions of CH_3NO_2, we have opted to leave it out. However, a few groups [29a,e,f] provide terms which describe this motion that could easily be incorporated into this potential.

The form of the term used to describe NO_2 is:

$$V_{NO_2} = \Sigma V_{NO}^{Stretch} + V_{ONO}^{Bend} [1.0 - F_5(R_{CO})][1.0 - F_5(R_{CO'})]. \tag{34}$$

where all the terms are defined in Equations 3–7. The weighting function for V_{CH_3} + $_{NO_2}$ has the form:

$$S_{CH_3 + NO_2} = [1.0 - F_1(R_{CN})][1.0 - F_2(R_{CO})][1.0 - F_2(R_{CO'})]F_3(R_{NO})F_3(R_{NO'}). \tag{36}$$

Parameters for the weighting functions F_i are given in Table 1.

2.3.2 Experimental Data and Theoretical Information Used for Parameter Fitting.

(1) Structure. The structure of the methyl radical in the ground state was established by Herzberg;[30] it is planar with D_{3h} symmetry. Experimentally determined values of the structural parameters are given in Table 9. The structural parameters of ground state NO_2 were determined from microwave spectra[31] and are also given in Table 9.

23

Table 9. Structural Parameters of CH₃ + NO₂

Internal Coordinate[a]	Expt'l.[b,c]	PES 1	PES 2	PES 3
Methyl radical				
R(CH)	1.079	1.080	1.080	1.080
∠HCH	120.0	120.0	120.0	120.0
Nitrogen Dioxide radical				
R(NO)	1.1934	1.1934	1.1934	1.1934
∠ONO	134.07	134.4	134.5	134.5

[a] Units are: R in Å, ∠ in Degrees
[b] Methyl radical: Herzberg, Ref. 30
[c] Nitrogen Dioxide radical: Bird et al., Ref. 31.

(2) **Vibrational Analyses.** Although most of the experimental studies of the vibrational spectrum of CH_3 have focused on the OPLA motion,[32] Jacox[33] has provided a compendium of vibrational data for the ground state methyl radical, which are listed in Table 10. The fundamental vibrational frequencies of NO_2 have been determined by Bird et al.[31a] and by Sams and Lafferty;[34] they are listed in Table 10.

(3) **Bond Dissociation Energies.** Although the bond dissociation energies of the product fragments have not been firmly established, the thermochemistry of the unimolecular dissociation of nitromethane to CH_3 + NO_2 has been determined.[35] Experiments indicate that nitromethane is approximately 60 kcal/mol more stable than the product fragments; using this information and Melius' calculated values[17] for N-O bond energies in NO_2, we must use a C-H bond dissociation energy of 116.2 kcal/mol to obtain the correct thermochemistry. This is not an unreasonable value for a C-H bond.

2.3.3 Results of the Fit. The internal coordinates at equilibrium of the methyl and nitrogen dioxide radicals predicted from the three potential energy surfaces are shown in Table 9. Assuming the bond dissociation energies given above, all other parameters were fitted to give agreement with the experimentally observed spectroscopic data. Normal mode analysis of the product fragments gives the fundamental frequencies shown in Table 10. The three surfaces predict five fundamental frequencies

24

Table 10. Normal Mode Frequencies[a] for $CH_3 + NO_2$

Mode	Expt.[b]	PES 1	PES 2	PES 3
Methyl radical				
$\upsilon(CH)$	3160.821	3176.0	3176.0	3176.0
$\upsilon(CH)$	3004.8	2988.6	2988.6	2988.6
$\delta(CH_3)$	1396[c]	1404.2	1404.2	1404.2
OPLA	606.4[d]	—	—	—
Nitrogen Dioxide radical				
Mode	Expt.[e]	Expt.[f]	PES 1	PES 2	PES 3
$\upsilon(NO)$	1665.5	1616.8	1620.3	1620.3	1620.3
$\upsilon(NO)$	1357.8	1319	1220.3	1220.3	1220.2
$\delta(ONO)$	756.8	749.6	766.4	766.4	766.4

[a] Frequencies are in cm.$^{-1}$
[b] Jacox, Ref. 33
[c] CH_3 in rare gas matrix
[d] Out-of-Plane Large Amplitude Motion; see text
[e] Bird et al., Ref. 31
[f] Sams and Lafferty, Ref. 34.

for CH_3 rather than six because, as discussed above, a term which explicitly describes the OPLA motion was left out. Agreement with experiment for the other frequencies is good to within 20 cm^{-1}.

Fundamental frequencies of nitrogen dioxide calculated from these potentials are also shown in Table 10. Agreement with experiment is good except for the symmetric stretch, which differs substantially from the experimental value. The calculated equilibrium geometry and fundamental frequencies do not differ among the three potential energy surfaces. The best fit parameters for the V_i are given in Table 11.

2.4 Product Fragments Methoxy and Nitrogen Oxide Radicals.

2.4.1 Form of the Potential. As in the description of the methyl nitrite potential, we choose, without loss of generality, to describe the methoxy and nitrogen oxide potentials using the term

Table 11. Potential Energy Parameters, $CH_3 + NO_2$ Term

Morse Parameters			
Bond	D_e (eV)	α (Å^{-1})	R_{eq} (Å)
CH	5.038950	1.8125	1.080
NO	3.122241	2.90	1.1934
Harmonic Oscillator Parameters			
Angle	—	k (eV/rad^2)	θ_{eq} (degrees)
HCH	—	1.282	120.0
ONO	—	6.25	134.4

V_{CH_3O} + NO·,

$$V_{CH_3O+NO\cdot} = V_{CH_3O} + V_{NO\cdot} .$$ (36)

The potential describing the methoxy radical is

$$V_{CH_3O} = \Sigma \ V_{CH}^{Stretch} + V_{CO}^{Stretch} + \Sigma \ \{ V_{HCH}^{Bend} + V_{HCO}^{Bend} \},$$ (37)

where the terms in this equation are defined in Equations 3–7. The term describing the nitrogen oxide species is simply:

$$V_{NO} = V_{NO}^{Stretch},$$ (38)

which is defined in Equation 3.

2.4.2 Experimental Data and Theoretical Information Used for Parameter Fitting.

(1) Structure. The structure of the methoxy radical was determined by microwave spectral studies of Endo, Saito, and Hirota;[36] the structural parameters are given in Table 12. Several ab initio calculations have been done that predict the equilibrium structure of methoxy radical;[37-40] however, we have used the experimental values for the equilibrium structure. The structure of the NO radical was taken from Herzberg[41] and is also given in Table 12.

26

Table 12. Structural Parameters of CH₃O + NO

Internal Coordinate[a]	Expt'l.[b,c]	PES 1	PES 2	PES 3
Methoxy Radical				
R(CO)	1.376	1.376	1.376	1.376
R(CH)	1.0937	1.080	1.080	1.080
∠HCO	108.25	108.25	108.25	108.25
∠HCH	—	110.66	110.66	110.66
Nitrogen Monoxide Radical				
R(NO)	1.1508	1.1508	1.1526	1.1526

[a] Units are: R in Å, ∠ in degrees.
[b] Methoxy radical: Endo, Saito, and Hirota, Ref. 36.
[c] Nitrogen Monoxide radical: Herzberg, Ref. 41.

(2) **Vibrational Analyses.** The methoxy radical has nine vibrational degrees of freedom. Assignments of the fundamentals from infrared spectral studies compiled by Jacox[33] are given in Table 13. The fundamental frequency of nitrogen oxide is 1,904.03 cm⁻¹.[41]

(3) **Bond Dissociation Energies.** As with the product fragments CH_3 and NO_2, the bond dissociation energies have not been firmly established for the methoxy radical, but the thermochemistry of the dissociation of methyl nitrite has been determined.[21] Therefore, we have assumed as reasonable bond dissociation energies 175.6 kcal/mol and 61.0 kcal/mol for C-O and C-H bonds, respectively, and assumed a bond dissociation energy of 151 kcal/mol for N-O to give the correct thermochemistry.

2.4.3 Results of the Fit. The internal coordinates of the methoxy and nitrogen oxide fragments predicted by these potential energy functions are shown for comparison with the experimental values in Table 12. Assuming the bond dissociation energies given above, all other parameters were fit to give agreement with the spectroscopic data. Calculated fundamental frequencies for the three potentials are given in Table 13 along with the experimental values. The equilibrium geometries and fundamental vibrational frequencies do not differ among the three potential energy surfaces. The calculated frequencies agree well with the experimental values except for the $\delta(CH_3)$ mode at 1,362 cm⁻¹ (the experimental value). The three potential energy surfaces predict a higher value for this mode (1,431.8 cm⁻¹). The best fit parameters for the V_i are given in Table 14.

27

Table 13. Normal Mode Frequencies[a] for CH₃O + NO

Mode	Expt.[b,c]	PES 1	PES 2	PES 3
Methoxy Radical				
υ(CH)	2840	2873.6	2873.6	2873.6
υ(CH)	2774	2758.7	2758.7	2758.7
δ(HCH)	1487	1486.8	1486.8	1486.8
δ(CH₃)	1362	1431.9	1431.8	1431.8
υ(CO)	1047	1005.3	1005.3	1005.3
δ(HCO)	653	654.7	654.7	654.7
Nitrogen Monoxide Radical				
υ(NO)	1904.03	1905.9	1905.9	1905.9

[a] Frequencies are in cm⁻¹.
[b] Methoxy radical: Jacox, Ref. 33.
[c] Nitrogen Monoxide radical: Herzberg, Ref. 41.

Table 14. Potential Energy Parameters for CH₃O + NO Term

Morse Parameters			
Bond	D_e (eV)	α (Å⁻¹)	R_{eq} (Å)
CH	2.645232	2.275	1.080
CO	7.614798	1.705	1.376
NO	6.548033	2.76	1.1508
Harmonic Oscillator Parameters			
Angle	k (eV/rad²)		θ_{eq}(degrees)
$\angle$HCH	1.725		110.66
$\angle$HCO	0.805		108.25

28

3. FEATURES OF THE POTENTIAL ENERGY SURFACE

Table 15 gives the relative energies of all reactant and product species of interest in this study. In addition to giving reasonable values for the equilibrium properties of all stable species of interest, the three surfaces correctly describe the thermochemistry of the reactions. The values of the relative energies calculated from the three potential energy surfaces described above agree well with experiment and with each other except for the transition state. Also, the often dramatic changes in structure of the species upon reaction are also described. For example, as nitromethane undergoes bond scission to form $CH_3 + NO_2$, the methyl group "flattens" from a tetrahedral geometry to a planar one as the asymptote is approached. Similarly, the ONO angle opens up. These changes are apparent in Figure 2, which illustrates C-N bond scission in nitromethane. For each point generated at a C-N bond distance, all other internal coordinates are relaxed to an equilibrium position (a point at which the gradient in these coordinates disappears). Figures 2a, 2c, and 2e are the potential energy as a function of the C-N bond distance in nitromethane calculated from PES 1, PES 2, and PES 3, respectively. Figures 2b, 2d, and 2f show the corresponding change in HCH and ONO angles as a function of R(C-N) (solid and dashed lines, respectively). In agreement with experiment,[2] there is no barrier to back reaction of bond scission of nitromethane. The parameters in $S_{CH_3NO_2}$ and $S_{CH_3 + NO_2}$ were adjusted such that there is no back reaction barrier for these surfaces. The potential energy curves shown in Figures 2c and 2e are not as smooth as the curve in Figure 2a. The bumps in the curves are artifacts due to the choice of parameters for the weighting functions for PES 2 and PES 3 and are sufficiently small that they should not affect the dynamics results.

Figures 3 and 4 show simple C-O bond rupture of cis- and trans-methyl nitrite, respectively, for the three potential energy surfaces. As in Figure 2, all internal coordinates are allowed to relax to an equilibrium position for each C-O value in the figures. Figures 3a, 3c, and 3e, and 4a, 4c, and 4e are the potential energy curves vs. R(C-O) for cis- and trans-methyl nitrite, respectively. The potential energy curve calculated from PES 1 (Figures 3a and 4a) have no barrier to back reaction; however, the potential curves calculated from PES 2 and PES 3 have small barriers. The barrier heights for the back reaction for cis and trans conformers on PES 2 are 1.5 and 1.0 kcal/mol, respectively (Figures 3b and 4b). The barriers to back reaction for the cis- and trans- conformers on PES 3 are 0.75 and 0.76 kcal/mol, respectively (Figures 3c and 4c). This is a result of the choice of parameter values that give the desired transition state energies. Because these exit channel barriers are so small, and enormous difficulty was encountered in obtaining the desired transition state energies for PES 2 and PES 3, we

Table 15. Relative Energies[a] of Species on the CH_3NO_2 Potential Energy Surface

Molecule	PES 1	PES 2	PES 3	Expt'l.
CH_3NO_2	0.0	0.0	0.0	0.0
cis-CH_3ONO	2.30	3.04	3.04	2.3[b]
trans-CH_3ONO	3.36	3.36	3.36	3.1[c]
CH_3O + NO	43.0	43.0	43.0	43.5[d]
CH_3 + NO_2	60.0	60.0	60.0	59.5[b,d]
T.S.[e]	216.4	55.1	47.6	55.5[f]

[a] Energies in kcal/mol.
[b] S. W. Benson, Thermochemical Kinetics (Wiley, New York, 1976).
[c] Gwinn, Anderson, and Stelman, Ref. 26.
[d] Batt and Robinson, Ref. 21.
[e] Transition state for isomerization of CH_3NO_2 to CH_3ONO.
[f] Wodtke, Hintsa, and Lee, Ref. 2.

opted to use these parameter values. Figures 3b, 3d, 3f, 4b, 4d, and 4f show the changes in the HCH and ONO angles (solid and dashed lines, respectively) as C-O bond rupture occurs.

Figures 5 and 6 show simple O-N bond rupture of cis- and trans-methyl nitrite, respectively. Although all three surfaces do not have barriers to the back reaction, PES 2 and PES 3 show a sharp change in the potential energy curve at approximately 1.7 Å which is, as discussed above, attributed to the choice for parameter values used to fit the isomerization barrier. This is the point at which the contribution of the methyl nitrite potential energy term rapidly approaches zero, and the contribution of the CH_3O + NO term becomes the dominant term in the potential energy surface. The switch from the domination of the methyl nitrite term in the potential to that of the CH_3O + NO term is more gradual and takes place over a longer O-N bond range on PES 1. Figures 5b, 5d, and 5f, and 6b, 6d, and 6f show the changes in the HCH and HCO angles (solid and dashed lines, respectively) as the O-N bond becomes large for cis- and trans-methyl nitrite, respectively. Although the changes in these geometries show discontinuities, note that the changes are small compared to those for the formation of CH_3 + NO_2. This is because the methyl group remains in a tetrahedral arrangement as the methoxy radical is formed.

The transition state for isomerization of nitromethane to methyl nitrite has been located on each of the three potential energy surfaces. The internal coordinates of the transition state on each potential energy surface are given in Table 16. The energy of the transition state on PES 1 is 216.4 kcal/mol. PES 2 has a transition state energy of 55.1 kcal/mol, the value suggested by Wodtke et al.[2] The energy value of the transition state on PES 3 is 47.6 kcal/mol, which is the value predicted from the MINDO/3 calculations of Dewar and Ritchie.[16] The geometries of the transition states are similar, except that the CN and CO bonds are from 0.3 to 0.7 Å longer for PES 2 and PES 3 than for PES 1. The frequencies of the vibrational modes of the transition states are given in Table 17; a substantially larger frequency for the transition state occurs for PES 1 compared to those of PES 2 and PES 3.

Figures 7, 8, and 9 are contour plots of the potential energy as a function of the CNO angle and the C-N bond distance for PES 1, PES 2, and PES 3, respectively. For each grid point (i.e., C-N bond distance and CNO angle) in these plots, all other internal coordinates are allowed to relax to the equilibrium position. Regions which energetically describe the species CH_3NO_2, CH_3ONO, and $CH_3 + NO_2$ are all shown on these plots: The portion of the figures which describes nitromethane is the well in the lower right-hand corner; this well corresponds to the equilibrium C-N bond distance in nitromethane of 1.479 Å and $\theta_{CNO} = 117.1°$. The lowest relative energy value of the system is located at this grid point, and has the value of 0.0 kcal/mol for all three surfaces. The region of the figure that describes CH_3ONO is located at the lower left-hand corner, corresponding to a C-N bond distance of approximately 2.3 Å and $\theta_{CNO} = 32°$, the equilibrium C-N bond distance and CNO angle in methyl nitrite. The value of the lowest energy point in the methyl nitrite well is 3.4 kcal/mol for all three surfaces, indicating that this is the trans conformer. The flat region which runs across the upper portion of the contour plots at a constant value of 60.0 kcal/mol corresponds to the $CH_3 + NO_2$ region of the surfaces.

On PES 1 (Figure 7), the barrier to isomerization from nitromethane to methyl nitrite is located at a CNO angle of approximately 75° and a C-N bond distance of 1.567 Å, and has a value of 216.4 kcal/mol. At the energies considered in this study (190 kcal/mol is the highest total energy of the system and includes the zero-point energy of nitromethane), isomerization to methyl nitrite from nitromethane cannot occur on PES 1 via the transition state, but it can occur if a trajectory undergoes C-N bond scission and leaves the nitromethane well, passes through the flat region of the potential (the $CH_3 + NO_2$ region), and then moves inward to the methyl nitrite well. For this surface, isomerization is a two-step process: bond scission to $CH_3 + NO_2$ followed by recombination to methyl nitrite. For

31

Table 16. Structural Parameters of the Transition State

Internal Coordinate[a]	PES 1	PES 2	PES 3
R(CN)	1.567	2.276	2.196
R(CO)	1.713	2.022	1.950
R(ON)	1.236	1.256	1.260
R(N=O)	1.185	1.189	1.187
R(CH)[b]	1.078	1.078	1.078
$\angle$(ONO)	119.19	122.22	122.45
$\angle$(CNO)	74.30	62.17	61.90
$\angle$(CNO′)[c]	129.78	131.25	137.69
$\angle$(H$_o$CH$_i$)[d]	97.5	107.7	107.8
$\angle$(H$_o$CH$_o$)	98.8	109.1	109.3
$\angle$(H$_o$CO)[d]	114.9	112.12	112.02
$\angle$(H$_i$CO)	122.6	118.8	118.3
τ(CONO′)	122.3	118.5	118.0
τ(H$_i$CON)	70.46	86.39	87.70
τ(H$_o$CON)[d]	127.18	123.27	130.84
	179.10	178.86	178.77
	92.70	70.66	69.74
	267.29	288.66	289.48

[a] Units are: R in Å, $\angle$ in degrees. H$_i$ designates the hydrogen atom in the plane of the molecule, and H$_o$ designates the hydrogen atom out of the plane of the molecule.

[b] Does not differ for in-plane and out-of-plane hydrogen atoms.

[c] O′ denotes the terminal oxygen.

[d] The transition state structures do not have symmetry; therefore, the H$_o$CH$_i$ and H$_o$CO angles differ depending on relative orientation to the CONO frame. Thus, two values are reported for both angles involving the two H$_o$ atoms.

Table 17. Vibrational Frequencies[a] at the Transition State

PES 1	PES 2	PES 3
2477.25	3013.62	3008.79
2451.46	3005.18	2997.59
2389.64	2888.21	2880.76
1209.32	1464.60	1458.84
1142.83	1386.65	1376.52
1134.97	1369.63	1367.83
1049.27	1306.90	1292.28
1017.98	1060.68	1016.24
720.33	757.34	730.74
663.59	541.17	500.57
605.40	438.92	378.74
399.70	405.33	337.28
320.39	154.28	140.80
228.26	140.30	121.70
3833.43i	1215.02i	1127.57i

[a] Frequencies are in cm^{-1}.

example, suppose a molecule undergoes C-N bond scission to form $CH_3 + NO_2$. As the radicals recede from one another with rotational motion, it is possible that one of the oxygen atoms on the rotating NO_2 can come within interaction range of the carbon atom on the methyl radical during this rotational recession. If the translational energies and rotational energies of the receding particles are not too large, the ONO group will recombine with the methyl group via one of the oxygens to form methyl nitrite. Results of trajectories run on PES 1 indicate that this mechanism is reasonable; they are presented in the Section 5.

The contour plots of PES 2 and PES 3, shown in Figures 8 and 9, respectively, have common features except for the barrier heights. The transition state on PES 2 (Figure 8) has a value of 55.1 kcal/mol, and is located at a C-N distance of 2.276 Å and a CNO angle of 62.2°. The transition state on PES 3, shown in Figure 9, is located at a C-N bond distance of 2.196 Å and a CNO angle of 61.9°, and has an energy value of 47.6 kcal/mol. The dissociation-recombination mechanism can also occur on these surfaces, but the direct isomerization (i.e., concerted C-N bond scission and C-O bond formation via the transition state) is more probable.

4. DETAILS OF THE CALCULATIONS

Ensembles of trajectories with initial energies in the range 64.6 to 161.4 kcal/mol above the zero-point energy of nitromethane (the total zero point energy of nitromethane is 29.3 kcal/mol), were integrated using a variable-step size Adams-Moulton fourth-order predictor-corrector integrator.[42] Relative error tolerance was set at 10^{-7}. For all three surfaces and for most energies, Reactions I, II, and III were observed.

The initial conditions were selected using Metropolis Monte Carlo sampling.[43,44] Before each ensemble of trajectories is integrated, the structure of the nitromethane molecule is set at the equilibrium geometry, and the desired total energy of the system in the form of kinetic energy is placed in the normal modes. A warm-up Markov walk of 1,000,000 steps is taken to randomize the energy of the system. A trajectory is then integrated until the end tests described below are satisfied, or until the trajectory integration exceeds a maximum time of 30 psec. A sequence of 2,000 Markov moves is taken from the starting point of the previous trajectory, and the integration/Markov walk pattern is repeated until 1,000 trajectories have been integrated. Because of the Monte Carlo sampling technique, approximately 50% of the 1,000 trajectories actually integrated were recounted and included in the averaging.[43,44]

The end tests are based on the values of the weighting functions described in Section II. If $S_{CH_3+NO_2} > S_{Max}$ and all other $S_i < S_{Min}$, then reaction to $CH_3 + NO_2$ has occured and the trajectory is stopped. If $S_{CH_3ONO} > S_{Max}$, then isomerization is noted, but the trajectory is continued until additional end tests are satisfied or the maximum integration time is exceeded. If $S_{CH_3O+NO} > S_{Max}$ and all other $S_i < S_{Min}$, then formation of $CH_3O + NO$ has occurred and the trajectory is stopped. Because the value of the S_i are dependent on geometric factors, these end tests are equivalent to using internal coordinates to determine when reaction has occurred. The value of S_{Max} was chosen to be 0.5 because when $S_i = 0.5$, then the contribution of the corresponding V_i to the total potential energy is approximately 50%. If $S_i > 0.5$, then the character of the total potential energy is dominated by the V_i. If the $S_i = 0.0$, then the V_i contributes nothing to the total potential energy. Upon decomposition to product j, all S_i (i≠j) terms approach zero and S_j approaches unity as the asymptotic limit of the receding decomposition products is approached. Rather than integrate trajectories until this limit is reached and all V_iS_i terms (i≠j) equal zero, we found that when all $S_i < S_{Min}=1 \times 10^{-20}$, reaction had definitely occurred. The end tests were tested extensively by running the same ensemble of trajectories for a full 30 psec without invoking end tests and then manually determining the outcome of the trajectories. The results were the same. Additionally the Markov walk is restricted such that $S_{CH_3NO_2}$ must have a value greater than 0.01, and S_{CH_3ONO}, and $S_{CH_3O NO}$ cannot be greater than S_{Max}. These restrictions ensure that the total potential energy at the beginning of each trajectory has some nitromethane character and will not allow the system to walk into the methyl nitrite well during initial condition selection. Sampling of phase space in this manner, however, included some points in the product region ($CH_3 + NO_2$). These points corresponded to trajectories which did not undergo at least one C-N vibration as nitromethane before forming $CH_3 + NO_2$ and were not included in the ensemble averages.

5. RESULTS AND DISCUSSION

Before presenting and discussing the results of the calculations of ensembles of trajectories, it is worthwhile to consider the mechanisms by which the reactions occur on the three potential energy surfaces. We do this by presenting various plots of selected trajectories that are typical of those that give the ensemble averaged results discussed in Section 5.2. Two types of plots are used to illustrate the behavior of the dissociation and isomerization reactions. The first type are plots as a function of time of the weighting functions S_i that are involved in the reaction. These weighting functions, which were used as "switching" functions in the potential-energy surface formulations, are also useful for following the progress of reactions in the trajectories. The other type are plots as a function of time of the internal coordinates that are involved in the reaction.

35

5.1 Reaction Mechanisms.

5.1.2 PES 1.

$CH_3NO_2 \rightarrow CH_3 + NO_2 \rightarrow CH_3ONO \rightarrow CH_3O + NO$
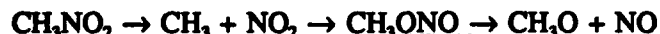
Figures 10a–d and 11a–g show the weighting functions and internal coordinates for a typical trajectory which results in isomerization to methyl nitrite and subsequent dissociation to $CH_3O + NO$. The total energy of the trajectory is 69.2 kcal/mol above the zero-point energy of nitromethane (29.3 kcal/mol).

Figures 10a–d are the weighting functions $S_{CH_3NO_2}$, $S_{CH_3 + NO_2}$, S_{CH_3ONO}, and $S_{CH_3O^\cdot + NO}$, respectively, plotted as functions of time. For the first 0.6 psec of the trajectory, $S_{CH_3NO_2}$ is unity, while all other S_i are zero (with a few minor fluctuations). $S_{CH_3NO_2}$ sharply decreases to zero as $S_{CH_3+NO_2}$ concurrently rises to one, indicating that the total potential energy is no longer characterized mainly by the nitromethane term but rather by the terms which describe methyl and nitrogen dioxide radicals. After approximately 0.1 psec, however, $S_{CH_3 + NO_2}$ drops to zero as S_{CH_3ONO} rises to unity, indicating that the geometry of the system is consistent with that of methyl nitrite wherein O′ is bound to the carbon atom and O is the terminal atom in methyl nitrite. At this time, the total potential energy is described by V_{CH_3ONO}. S_{CH_3ONO} is unity (with minor fluctuations) for approximately 1.75 psec, after which it drops to zero while $S_{CH_3O+ NO}$ rises to one, indicating that formation of $CH_3O + NO$ has occurred. Therefore, by following these weighting functions, it is seen that the reaction mechanism is:

$$CH_3NO_2 \rightarrow CH_3 + NO_2 \rightarrow CH_3ONO \rightarrow CH_3O + NO.$$
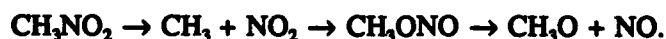
This interpretation of the reaction is confirmed by Figures 11a–g which show various internal coordinates vs. time for the same trajectory. Figure 11a shows the C-N bond distance during the trajectory. For the first 0.6 psec, the C-N bond oscillates about its equilibrium nitromethane value of 1.479 Å. It then begins to increase (indicating bond scission) but then decreases and oscillates about 2.3 Å, which is approximately the equilibrium C-N bond distance in methyl nitrite until the end of the trajectory (about 2.5 psec) where it again increases until it meets the criterion for dissociation. Figures 11b and 11c are the two C-O bond distances throughout the trajectory; for the first 0.6 psec, both C-O bonds oscillate about 2.31 Å, the equilibrium C-O bond distance in nitromethane. As with the C-N

bond, both C-O bond distances become large then decrease until the C-O′ bond distance oscillates about 1.421 Å, the equilibrium C-O bond distance in methyl nitrite (Figure 11c). Figure 11d shows the ONO angle during the trajectory. For the first 0.6 psec of the reaction, the ONO angle oscillates about the nitromethane equilibrium angle of 125.8°, and when the system reaches the methyl nitrite configuration, it oscillates about the equilibrium methyl nitrite value (116.4° or 118.65°, depending on whether the species is in the cis or trans conformation). Perhaps the most dramatic indication of isomerization is the CNO angles as a function of time, shown in Figures 11e–f. At the beginning of the trajectory, both CNO and CNO′ angles oscillate about 117.1°, the equilibrium CNO angle in nitromethane. After isomerization to methyl nitrite, the CNO′ angle drops from 117.1° and oscillates about 32°, the equilibrium CNO angle in methyl nitrite (Figure 11f). Finally, Figure 11g shows the CO′NO dihedral angle as a function of time for the portion of the trajectory during which methyl nitrite exists. The newly formed methyl nitrite undergoes two complete rotations and then settles into the cis conformation (0°) until dissociation occurs.

$CH_3NO_2 \rightarrow CH_3 + NO_2 \rightarrow CH_3ONO \rightarrow CH_3 + NO_2$

Figures 12a–c and 13a–g illustrate a trajectory in which nitromethane isomerizes to methyl nitrite then dissociates to $CH_3 + NO_2$. The total energy of the trajectory is 115.3 kcal/mol above the zero-point energy of nitromethane. Figures 12a–c show the weighting functions $S_{CH_3NO_2}$, $S_{CH_3 + NO_2}$, and S_{CH_3ONO}, respectively; all other S_i throughout the trajectory are zero. For the first 2.5 psec of the trajectory, the $S_{CH_3NO_2}$ undergoes large oscillations from one to approximately 0.2; concurrently, $S_{CH_3 + NO_2}$ undergoes large oscillations from zero to 0.8, indicating that the C-N stretch of nitromethane is highly excited. $S_{CH_3NO_2}$ then drops rapidly to zero as $S_{CH_3 + NO_2}$ rises to unity, indicating C-N bond scission. After another 0.1 psec, $S_{CH_3 + NO_2}$ drops to zero, and S_{CH_3ONO} rises to unity, indicating that isomerization to methyl nitrite has occurred. Large oscillations in $S_{CH_3 + NO_2}$ and S_{CH_3ONO} at t = 2.75 psec indicate that the C-O stretch is highly excited. Dissociation to the products CH_3+NO_2 occurs at 3.0 psec, as S_{CH_3ONO} sharply drops to zero and $S_{CH_3 + NO_2}$ concurrently rises to unity. Therefore, the reaction can be summarized as:

$$CH_3NO_2 \rightarrow CH_3 + NO_2 \rightarrow CH_3ONO \rightarrow CH_3 + NO_2.$$
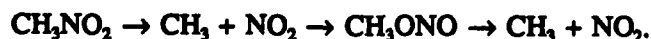
The internal coordinates monitored during the trajectory are illustrated in Figures 13a–g. Figure 13a shows the C-N bond distance throughout the trajectory and for the first 2.5 psec of the trajectory, the C-N bond is highly excited as indicated by the large oscillations of the C-N bond. As

37

in the previous illustration (Figure 11a), the C-N bond distance becomes very large at 2.5 psec, then decreases as the system attains the methyl nitrite conformation. Figures 13b–c show the two C-O bond distances as a function of time, and for the first 2.3 psec of the trajectory both C-O bonds oscillate about the equilibrium C-O distance in nitromethane. The C-O distances undergo large oscillations and then become very large at the same time the C-N distance becomes large, but then the C-O distances decrease. The C-O bond oscillates about the equilibrium C-O bond distance of methyl nitrite indicating that isomerization has occurred while the C-O′ bond oscillates at a larger value, indicating that O′ is the terminal oxygen of the methyl nitrite species. Figure 13d shows the ONO angle during the trajectory. At the beginning of the trajectory, the ONO angle oscillates about 125.8°, the equilibrium value in nitromethane, but upon isomerization, it oscillates about the equilibrium value of methyl nitrite (116.4° or 118.65°, depending on whether the species is in the cis or trans conformation). As in the previous trajectory, the isomerization is most dramatically illustrated by the behavior of the CNO angles during the trajectory. Figures 13e–f show the two CNO angles in time, and upon isomerization the CNO angle changes its oscillation about 117.1° (the equilibrium value in nitromethane) to oscillations about 32° (the equilibrium value in methyl nitrite). Figure 13g shows the CONO′ dihedral angle as a function of time for the portion of the trajectory for which methyl nitrite exists. The newly formed methyl nitrite undergoes one full rotation before dissociation occurs.

$$CH_3NO_2 \rightarrow CH_3 + NO_2$$
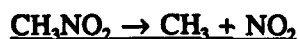
For completeness, we have included a representative trajectory showing the simple C-N bond scission in nitromethane. The total energy of the system is 138.4 kcal/mol above the zero point energy of nitromethane. Figures 14a–b are plots of the weighting functions $S_{CH_3NO_2}$ and $S_{CH_3 + NO_2}$ as functions of time, respectively; all other S_i throughout the trajectory are zero indicating that only the terms $V_{CH_3NO_2}$ and $V_{CH_3 + NO_2}$ contribute to the total potential energy as the reaction proceeds. With a few small oscillations, $S_{CH_3NO_2}$ remains unity throughout the trajectory and then drops sharply to zero, while $S_{CH_3 + NO_2}$ rises to unity indicating that C-N bond scission has occurred. Thus, the reaction is:

$$CH_3NO_2 \rightarrow CH_3 + NO_2.$$
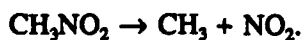
Figures 14c, 14d, and 14e show the C-N, C-O, and C-O′ bond distances, respectively, throughout the trajectory; each bond oscillates about its equilibrium nitromethane value until the bond scission occurs, at which time the C-N, C-O, and C-O′ bond distances simultaneously become large. Figures 14f, 14g, and 14h show the ONO, CNO, and CNO′ angles, respectively, during this trajectory. The

38

angles oscillate about their equilibrium values in nitromethane (125.8° for ONO and 117.1° for CNO) until dissociation.

The trajectory calculations using this potential energy surface indicate that isomerization to methyl nitrite is a two-step process:

(1) CH_3NO_2 undergoes C-N bond rupture to form CH_3 + NO_2;

(2) CH_3 and NO_2 recombine to form CH_3ONO, which then dissociates to either CH_3O + NO or CH_3 + NO_2.

5.1.3 PES 2 and PES 3. Because isomerization on both of these surfaces occurs in the same manner, we have chosen to illustrate the mechanism of isomerization and dissociation using PES 3. The mechanism of isomerization on these surfaces is concerted; as the C-N bond breaks, the C-O bond is formed. As in the previous section, we will present both internal coordinates and weighting functions during the course of the representative trajectories.

$CH_3NO_2 \rightarrow CH_3ONO \rightarrow CH_3O + NO$

Figures 15a–d and 16a–g show, respectively, the weighting functions and internal coordinates during a trajectory that results in the formation of CH_3O + NO. The total energy of the trajectory is 64.6 kcal/mol above the zero point energy of nitromethane.

For the first 6 psec, $S_{CH_3NO_2}$ is unity with minor fluctuations, indicating that the total potential is described by the nitromethane term. At approximately 6 psec, S_{CH_3ONO} shows a sharp peak; immediately thereafter S_{CH_3ONO}· rises to unity as $S_{CH_3NO_2}$ correspondingly goes to zero, suggesting that at the time immediately prior to isomerization both CNO′ and CNO bends are highly excited. Upon isomerization, the methyl nitrite species remains for another 7 psec, at which time O-N bond scission occurs. Therefore, the weighting functions indicate that the mechanism of isomerization and formation of CH_3O + NO is:

$$CH_3NO_2 \rightarrow CH_3ONO \rightarrow CH_3O + NO.$$

Figures 16a, 16b, and 16c are the C-N, C-O, and C-O′ distances throughout the trajectory. For the first 1.75 psec, the C-N and both C-O bonds are oscillating well above their equilibrium values in nitromethane. The NO_2 group settles down for about 2.0 psec, oscillating about the equilibrium values

39

of nitromethane. The C-N and C-O bonds then undergo large oscillations before isomerization at 6.0 psec. At 6.0 psec, the C-O bond begins to oscillate about the equilibrium bond distance in methyl nitrite (1.421 Å) (Figure 16b), while the C-N bond oscillates about the equilibrium distances in methyl nitrite and the C-O′ oscillates at a large bond distance indicating the O′ is the terminal oxygen of the methyl nitrite. Figure 16d shows the ONO angle during the trajectory; for the first 6 psec of the trajectory, the ONO angle oscillates about its equilibrium value in methyl nitrite. Figures 16e and 16f are the CNO and CNO′ angles during the trajectory. Figure 16e is the most dramatic illustration of isomerization: The CNO angle oscillates about 117.1° while the molecule is in the nitromethane configuration, but after isomerization it oscillates around 32°. Figure 16g is the CONO′ torsional angle in methyl nitrite. Upon isomerization, the CONO′ undergoes one full rotation, settles into the cis conformer for approximately 1 psec, undergoes free rotation for the next 2 psec, and again settles down into the cis conformation before once again undergoing free rotation. At 12 psec, the methyl nitrite converts to the trans conformation before finally dissociating.

$CH_3NO_2 \rightarrow CH_3ONO \rightarrow CH_3 + NO_2$

Figures 17a–d and 18a–g illustrate the weighting functions and geometries of a trajectory which results in direct isomerization from nitromethane to methyl nitrite and subsequent C-O bond scission to form $CH_3 + NO_2$. Figures 17a–d show the weighting functions $S_{CH_3NO_2}$, $S_{CH_3ONO'}$, $S_{CH_3O'NO}$, and $S_{CH_3 + NO_2}$, respectively. The total energy of the system is 69.2 kcal/mol above the zero point energy of nitromethane. For the first 4 psec of the trajectory (see Figure 17a), the system is described mainly by the nitromethane terms with fluctuations among the CH_3ONO', $CH_3O'NO$ and $CH_3 + NO_2$ potential terms (Figures 17b, 17c, and 17d, respectively). At 4 psec, $S_{CH_3NO_2}$ decreases to zero as $S_{CH_3O'NO}$ rises to unity. The system is then described by the methyl nitrite term for the next 5 psec, wherein a fluctuation with the $CH_3 + NO_2$ term occurs, indicating excitation of the C-O bond. The C-O bond rupture occurs 1 psec later. Therefore, the weighting functions show the mechanism of isomerization to be

$$CH_3NO_2 \rightarrow CH_3ONO \rightarrow CH_3 + NO_2.$$

Figure 18 shows the internal coordinates during the trajectory. Each coordinate shows distinct changes upon isomerization. As in the trajectories discussed above, the CN, CO, and CO′ distances shown in Figures 18a, 18b, and 18c, respectively, oscillate about their equilibrium nitromethane values. At 4.0 psec, the C-O′ bond in methyl nitrite is formed, as evidenced by the C-O′ oscillation about the equilibrium bond distance for methyl nitrite (Figure 18c). Figures 18d–f are the ONO, CNO, and

CNO´ angles, respectively. All angles oscillate about their nitromethane equilibrium values, but after isomerization they oscillate about the methyl nitrite equilibrium values. The CNO angles (see Figure 18e and 18f) show dramatic change upon isomerization. The CNO angle (see Figure 18e) shows an interesting pattern of oscillation from 7–9 psec that is due to the torsional motion. Note that the torsion angle (Figure 18g) during that time period is highly excited and "free" internal rotation is occurring, whereas for the 3 psec before and 1 psec after the free rotation, the methyl nitrite is in the trans conformation.

5.2. Ensemble Results. Table 18 is a compendium of the results of the ensembles of trajectories integrated at different energies on the three potential energy surfaces. The values under the column labeled "Rejected" are the numbers of trajectories that were not included in the averaging because they did not undergo at least one C-N vibration as nitromethane before forming CH_3 + NO_2. The number of rejected trajectories increases with increasing energy on all three potential energy surfaces. We chose to sample phase space that included some points in the product region (CH_3 + NO_2) and then "reject" those points. This was done to ensure that all of the reactant phase space was covered in the sampling.

The curves in Figure 19 are probabilities of the occurrence of Reaction III, isomerization to methyl nitrite followed by dissociation to CH_3 + NO_2, as a function of energy for the three potential-energy surfaces. For the most part, the probability of Reaction III increases with increasing energy of the system for all three surfaces. The probability of Reaction III for PES 3 (stars) increases dramatically from 64 to 100 kcal/mol and then levels off. The curve which describes the probability of Reaction III for PES 2 (crosses) increases monotonically with energy up to 150 kcal/mol and then drops to a lower value at the highest total energy studied (161.4 kcal/mol above the zero-point energy of nitromethane). The curve for PES 1 (circles) shows a small increase in the probability of Reaction III at the high energy end of the curve. Only a small number of trajectories result in Reaction III on PES 1, and thus statistical error is high. This is expected because of the features of PES 1 discussed in Section III.

Figure 20 shows the probabilities of Reaction II, isomerization to methyl nitrite followed by dissociation to CH_3O + NO, as a function of energy for the three potential energy surfaces. The behavior is quite different among the three surfaces. The probability of Reaction II on PES 3 (stars)

41

Table 18. Numbers of Trajectories and Reactions

Energy[a]	Total			Rejected			Reaction I			Reaction II			Reaction III			Unreacted (CH₃NO₂)			Unreacted (CH₃ONO)		
	I	PES II	III	I	PES II	III	I	PES II	III	I	PES II	III	I	PES II	III	I	PES II	III	I	PES II	III
64.6[b]	-	1847	1699	-	1	0	-	1082	688	-	35	585	-	12	54	-	713	342	-	4	30
69.2	1782	1820	1782	1	5	0	1174	1476	828	0	30	725	0	9	91	607	299	122	0	1	16
80.7	1858	1833	1772	26	7	16	1798	1741	1049	2	61	551	0	22	156	32	2	0	0	0	0
92.2	1891	1780	1823	57	55	15	1823	1614	1229	10	70	370	1	41	209	0	0	0	0	0	0
103.8	1861	1824	1862	70	80	69	1769	1598	1222	12	81	248	10	65	323	0	0	0	0	0	0
115.3	2007	1984	1922	134	220	37	1865	1598	1269	4	63	320	4	103	296	0	0	0	0	0	0
126.8	2004	1823	1862	176	308	45	1804	1314	1171	22	66	357	2	135	289	0	0	0	0	0	0
138.4	1946	1980	1901	219	153	113	1713	1561	1310	7	112	196	7	154	282	0	0	0	0	0	0
149.9	1972	1958	1927	190	151	150	1733	1526	1185	37	84	282	12	197	310	0	0	0	0	0	0
161.4	1949	2025	1961	149	208	234	1720	1641	1114	44	61	290	36	115	323	0	0	0	0	0	0

[a] Energies are in kcal/mol and do not include the zero point energy of nitromethane (29.3 kcal/mol).
[b] Trajectories were not calculated at this energy on PES 1.

decreases with increasing energy over the range of 64 to 100 kcal/mol. At energies above 100 kcal/mol, the reaction probability appears to be less energy dependent. The probabilities of Reaction II on PES 2 and PES 1 (denoted by crosses and circles, respectively) are approximately constant over the energy range studied.

The following ratios were calculated:

B_1 = Reaction II/(Reaction I + Reaction III);

B_2 = (Reaction II + Reaction III)/Reaction I; and

B_3 = Reaction II/Reaction III.

The ratio B_1 corresponds to the Wodtke et al.[2] measurements assuming they did not distinguish between the NO_2 formed in Reaction I to that which might be formed in Reaction III. However, in estimating the isomerization barrier from experimental data, it seems that B_2 would be the ratio which needs to be considered. B_3 is the branching ratio of the decomposition reactions of the methyl nitrite.

Figure 21 shows plots of the branching ratios B_1 (circles) and B_2 (crosses) for PES 1 (Figure 21a), PES 2, (Figure 21b) and PES 3 (Figure 21c). Figure 22 shows plots of the branching ratio B_3 for PES 1 (Figure 22a), PES 2 (Figure 22b) and PES 3 (Figure 22c). The B_1, B_2, and B_3 for PES 1 have been included for completeness; however, the statistical errors are very large for the ratios due to the small number of isomerization trajectories. The behavior of the curves reflect the energy dependences of the reaction probabilities discussed above. However, the only experimental value for B_1 available for comparison corresponds to an energy near the threshold of C-N bond dissociation. The calculated value at this energy for PES 2 is 0.032 whereas the value for PES 3 at the same energy is 0.79, in reasonable agreement with experiment (0.60)[2]. This suggests that the barrier height of a tight transition state such as those described by PES 2 and 3 should be slightly larger than 47 kcal/mol.

The curves for B_3 for PES 2 and PES 3 (Figure 22) have similar energy dependences. At lower energies (below 100 kcal/mol), B_3 is larger than 1.0, indicating that upon isomerization, O-N bond scission in methyl nitrite is more probable than C-O bond scission. However, at higher energies, B_3 is approximately constant and less than unity, indicating that C-O bond scission is more probable following isomerization than O-N bond scission.

Two questions arise from the behavior of the reaction probabilities and the branching ratios:

(1) Why does the C-O bond scission (Reaction III) occur at all energies, and why is it more probable than O-N bond scission (Reaction II) in methyl nitrite at high energies, even though Reaction III requires 16 kcal/mol more energy?

(2) Why is the probability of Reaction II essentially not energy dependent on PES 2 but decreases as a function of energy on PES 3?

Unimolecular decomposition of methyl nitrite under the experimental conditions of Wodtke et al.[2] would most likely result solely in O-N bond breaking to form CH_3O + NO because of the large difference in the dissociation energies of the O-N and C-O bonds. However, the C-O bond that is formed when nitromethane isomerizes to methyl nitrite is very likely initially highly excited. That is, energy is selectively deposited in this bond in the isomerization reaction, and the transfer of only a small amount of energy from other molecular modes will result in the breaking of the bond. Thus, this mode selectivity in the energy distribution of the nascent methyl nitrite leads to the rupture of the stronger C-O bond (preferentially at high energies) seen in our results.

The observed increasing probability of Reaction III with increasing energy is simply due to the increasing amount of energy that is available among the various modes for transfer to the C-O bond. Why then is Reaction II essentially constant as a function of energy for PES 2 but not for PES 3? This can be attributed to the difference in the barrier heights for isomerization from nitromethane to methyl nitrite for the two surfaces. The barrier height for isomerization on PES 2 is 55.1 kcal/mol and 47.6 kcal/mol for PES 3. If we assume that all of the energy of isomerization goes into the newly-formed C-O bond, then the C-O bond on PES 2 will have 7.5 kcal/mol more energy than the C-O bond on PES 3 because of the difference in the barrier heights. On PES 2 only 2 kcal/mol of energy must transfer from other modes to provide the energy needed to break the C-O bond (bond dissociation energy is 57 kcal/mol), and thus the reaction is essentially independent of the total energy. However, on PES 3 9.4 kcal/mol must flow into the C-O bond to break it. The higher energy requirement for C-O bond scission on PES 3 could explain the observed energy dependence of Reaction II on this surface.

Figure 23 show the translational energy distribution of products from Reaction I (hollow bars) and Reaction III (filled bars) for PES 3 at 69.2 (Figure 23a), 115.3 (Figure 23b), and 161 kcal/mol

44

(Figure 23c) above the zero-point energy of nitromethane. Although there are no exit barriers for Reaction I and III on PES 3, the distributions do not peak at zero as expected for simple bond scission reactions. This behavior has been observed in classical trajectory studies of unimolecular reactions of NH_3, CH_4, and SiH_4.[45]

There is an increase in the release of product translational energy with increasing total energy, as shown by the distributions in Figure 23 and by the average values given in Table 19. Note that the distribution of products for Reaction III are strikingly similar to those of Reaction I.

Figures 24 and 25 are the same as Figure 23, except they are for the product translational energy distributions for PES 2 and PES 1, respectively. The probability of the formation of methyl and nitrogen dioxide radicals from C-O bond dissociation in methyl nitrite (Reaction III) is much smaller than that of Reaction I for all surfaces; however, the product translational energy distribution for both reactions appear to have the same features. Figures 26 and 27 are plots of the average relative translational energies of the products for Reactions I, II, and III on PES 3 and PES 2, respectively, as functions of energy. The average translational energy of the products of Reaction II are, for the most part, larger than the average translational energy of the products of Reaction I and Reaction III at all energies studied. This is expected because the energy required for Reaction II (O-N bond scission in methyl nitrite, 41 kcal/mol) is much less than that required for Reaction I or Reaction III (60 and 57 kcal/mol, respectively). The molecules, whether nitromethane or methyl nitrite, have essentially the same internal energy before decomposition and, therefore, products of Reaction II have at least 17 kcal/mol more energy to be distributed among internal and translational degrees of freedom.

Figures 28 and 29 are plots of the average rotational energy of the methyl radicals formed from Reaction I (circles) and Reaction III (crosses) on PES 3 and PES 2, respectively. Figures 30 and 31 are plots of the average rotational energy of the nitrogen dioxide radicals formed from Reaction I and Reaction III on PES 3 and PES 2, respectively. As for the product translational energy distributions, remarkable similarities are apparent in the average translational and rotational energies of the product of Reactions I and III shown in Figures 26–31. These similarities indicate that products from Reactions I and III might be very difficult to distinguish experimentally.

Figure 32 shows the product translational energy distribution of products for Reaction II for PES 2 (Figure 32a) and PES 3 (Figure 32b) at 69.2 kcal/mol. The distributions are quite dissimilar; however,

45

Table 19. Average Product Translational Energies[a]

Energy	Reaction I			Reaction III			Reaction II		
	I	PES II	III	I	PES II	III	I	PES II	III
64.6[b]	—	5.16	5.13	—	4.33	4.47	—	5.45	6.04
69.2	6.04	6.14	6.43	—	5.25	5.32	—	9.32	6.82
80.7	7.64	7.60	7.00	—	5.91	7.17	6.21	8.16	8.13
92.2	9.44	8.88	8.31	13.74	7.00	8.38	6.95	9.94	10.03
103.8	10.37	8.63	12.66	7.03	8.09	11.40	7.29	10.61	12.25
115.3	13.65	10.41	10.82	8.59	10.08	11.20	15.27	19.11	14.14
126.8	11.53	11.16	12.12	11.92	11.14	9.87	7.92	20.10	13.61
138.4	15.02	12.11	14.77	23.50	13.62	13.80	5.38	17.94	17.68
149.9	14.97	13.00	13.83	7.79	13.90	14.04	13.76	13.46	17.70
161.4	16.22	16.42	15.60	14.77	14.64	16.58	14.19	21.80	18.07

[a] Energies are in kcal/mol and do not include the zero point energy of nitromethane (29.3 kcal/mol).
[b] Trajectories were not calculated at this energy on PES 1.

this could be due to the small number of trajectories resulting in Reaction II on PES 2 at this energy, thus giving large statistical error. The distribution in Figure 32b, however, has a shape very similar to the translational energy distributions of the products of Reactions I and III (Figures 23–25). Tables 20 and 21 give the average rotational energies of products from Reactions I and III and Reaction II, respectively. The internal energy of all decomposition products increase with increasing energy. Exceptions appear in Reactions II and III on PES 1 and are attributed to the poor statistics.

6. SUMMARY

We have performed a classical dynamics study of the unimolecular decomposition of nitromethane. Three model potential energy surfaces were used in the study. The surfaces differ mainly in the heights of the barrier to the isomerization of nitromethane to methyl nitrite. PES 1 has a very high barrier to isomerization (216.4 kcal/mol) whereas the barrier for PES 2 is 55.1 kcal/mol, the value suggested by Wodtke, Hintsa, and Lee[2] and PES 3 has a barrier of 47.6 kcal/mol, which compares well with the predicted MINDO/3 value of Dewar and Ritchie.[16] Two primary unimolecular decomposition pathways were suggested by Wodtke et al.[2] in interpreting the results of their infrared multiphoton dissociation experiments:

[I] $$CH_3NO_2 \rightarrow CH_3NO_2^\dagger \rightarrow CH_3 + NO_2 \; ;$$

[II] $$CH_3 NO_2^\dagger \rightarrow CH_3ONO^\dagger \rightarrow CH_3O + NO \; .$$

An additional primary unimolecular decomposition pathway was observed in the trajectory results for all three potential energy surfaces,

[III] $$CH_3NO_2^\dagger \rightarrow CH_3ONO^\dagger \rightarrow CH_3 + NO_2 \; .$$
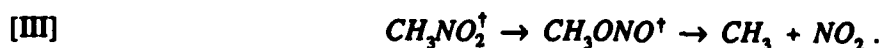
Reaction I occurs by the same mechanism for all three potential energy surfaces. The isomerizing reactions, Reactions II and III, however, occur by different mechanisms for PES 1 and PES 2 and 3. The energy of the barrier to isomerization on PES 1 is larger than any of the total energies of the

Table 20. Average Rotational Energies[a] of Products CH_3 + NO_2.

Energy	CH₃ Radical						NO₂ Radical					
	Reaction I			Reaction III			Reaction I			Reaction III		
	PES			PES			PES			PES		
	I	II	III	I	II	III	I	II	III	I	II	III
64.6[b]	—	3.54	3.63	—	3.92	3.56	—	4.21	3.91	—	3.92	4.25
69.2	3.96	3.88	4.15	—	6.18	4.53	4.04	4.77	4.51	—	3.21	4.27
80.7	5.56	5.04	5.62	—	6.53	6.06	5.18	5.96	5.71	—	4.29	5.33
92.2	6.34	6.44	6.78	3.02	7.84	6.26	6.51	6.99	6.58	7.49	6.24	6.79
103.8	7.75	7.41	9.54	14.70	7.36	10.24	8.18	8.03	8.39	5.03	8.10	8.63
115.3	8.47	9.09	8.64	6.24	7.43	8.53	9.57	7.97	9.33	21.24	8.91	9.47
126.8	10.17	10.27	9.60	2.55	11.28	11.54	9.29	10.07	10.04	18.22	10.61	10.19
138.4	12.21	11.90	10.74	2.61	11.48	11.94	11.02	11.85	11.04	24.87	12.02	12.85
149.9	12.39	13.33	13.24	6.69	13.68	13.39	12.52	11.39	11.27	10.71	15.23	14.04
161.4	13.61	13.85	15.28	14.45	11.51	16.33	13.04	12.50	13.66	10.85	14.59	14.06

[a] Energies are in kcal/mol and do not include the total zero point energy of nitromethane (29.3 kcal/mol).
[b] Trajectories were not calculated at this energy on PES 1.

48

Table 21. Average Rotational Energies[a] of Products CH_3O + NO

Energy	CH₃O Radical Reaction II			NO Radical Reaction III		
	I	PES II	III	I	PES II	III
64.6[b]	-	5.32	4.87	-	3.48	3.40
69.2	-	5.50	5.09	-	3.67	3.84
80.7	4.07	7.49	6.44	6.48	5.69	4.36
92.2	4.63	7.95	7.19	6.36	6.23	5.33
103.8	4.38	8.76	9.69	7.53	7.24	7.35
115.3	14.72	9.29	9.94	5.79	7.34	7.05
126.8	11.93	12.56	12.30	10.79	8.60	7.55
138.4	14.64	13.20	11.10	2.94	6.84	8.35
149.9	15.68	15.22	11.94	11.25	5.90	9.97
161.4	9.30	13.00	13.92	16.03	9.02	9.95

a Energies are in kcal/mol and do not include the total zero point energy of nitromethane (29.3 kcal/mol).
b Trajectories were not calculated at this energy on PES 1.

trajectories calculated, precluding isomerization via the transition state region on this surface. However, isomerization occurs on this surface by a mechanism of dissociation of nitromethane to $CH_3 + NO_2$, followed by recombination of the radicals to form methyl nitrite. The probability of isomerization on this surface increases with increasing energy.

The mechanism of isomerization for PES 2 and PES 3 is a concerted C-N bond-breaking and C-O bond-forming process. PES 2, the surface which has the barrier height suggested by Wodtke et al.[2], predicts a branching ratio at least an order of magnitude smaller than that determined from the experimental results. PES 3, the surface with the lowest barrier to isomerization, predicts a branching ratio in reasonable agreement with that reported by Wodtke et al.[2]

Although PES 2 and PES 3 differ by only a few kcal/mol in barrier heights and show the same mechanisms for isomerization and decomposition, the dynamics results are dramatically different. The energy-dependent branching ratios of isomerization reactions to C-N bond scission reactions for PES 2 increase with increasing energy. The same branching ratios for PES 3 decrease with increasing energies from 64.1 kcal/mol to 103 kcal/mol, then remain constant up to 161.4 kcal/mol. There is a strong energy dependence of the probability of Reaction II for PES 3, whereas the probability of Reaction II remains approximately constant as a function of energy on PES 2. However, the probability of Reaction III increases with increasing energy for both PES 2 and PES 3.

Average translational energies of the products for Reaction II are higher than those of Reactions I and III at all energies. The product translational energy distributions, as well as the average translational and rotational energies of the products of Reactions I and III are similar for all three surfaces, indicating that the products of Reaction I and Reaction III might be indistinguishable in experiments.

Although the trajectory results suggest that the barrier height of the transition state should be slightly higher than 47 kcal/mol, several good quality ab initio calculations[14,15,17] predict a much higher barrier to isomerization for a tight transition state of the type described by the potential energy surfaces in this study. It is not known whether a much better electronic structure calculation would lower the energy value of this transition state by 20 to 30 kcal/mol. However, there have been suggestions that another transition state might exist which resembles a van der Waals complex.[18,19] Isomerization through this transition state would resemble the dissociation-recombination mechanism seen in the results for PES 1.

Although gains have been made previously in understanding the electronic structure and dynamics of this system, this study uncovers complexities in the unimolecular decomposition of nitromethane. Our models predict that nitromethane has three decomposition pathways rather than the two observed in the experiment.[2] Therefore, experiments need to be performed on this system in an effort to determine the occurrence of Reaction III. If Reaction III is found to exist, this will affect the analysis used to estimate the isomerization barrier. Additionally, our models indicate that there are two possible mechanisms for isomerization of nitromethane to methyl nitrite. An accurate description of the transition state from higher quality ab initio quantum chemical calculations could help determine which isomerization mechanism is most probable.
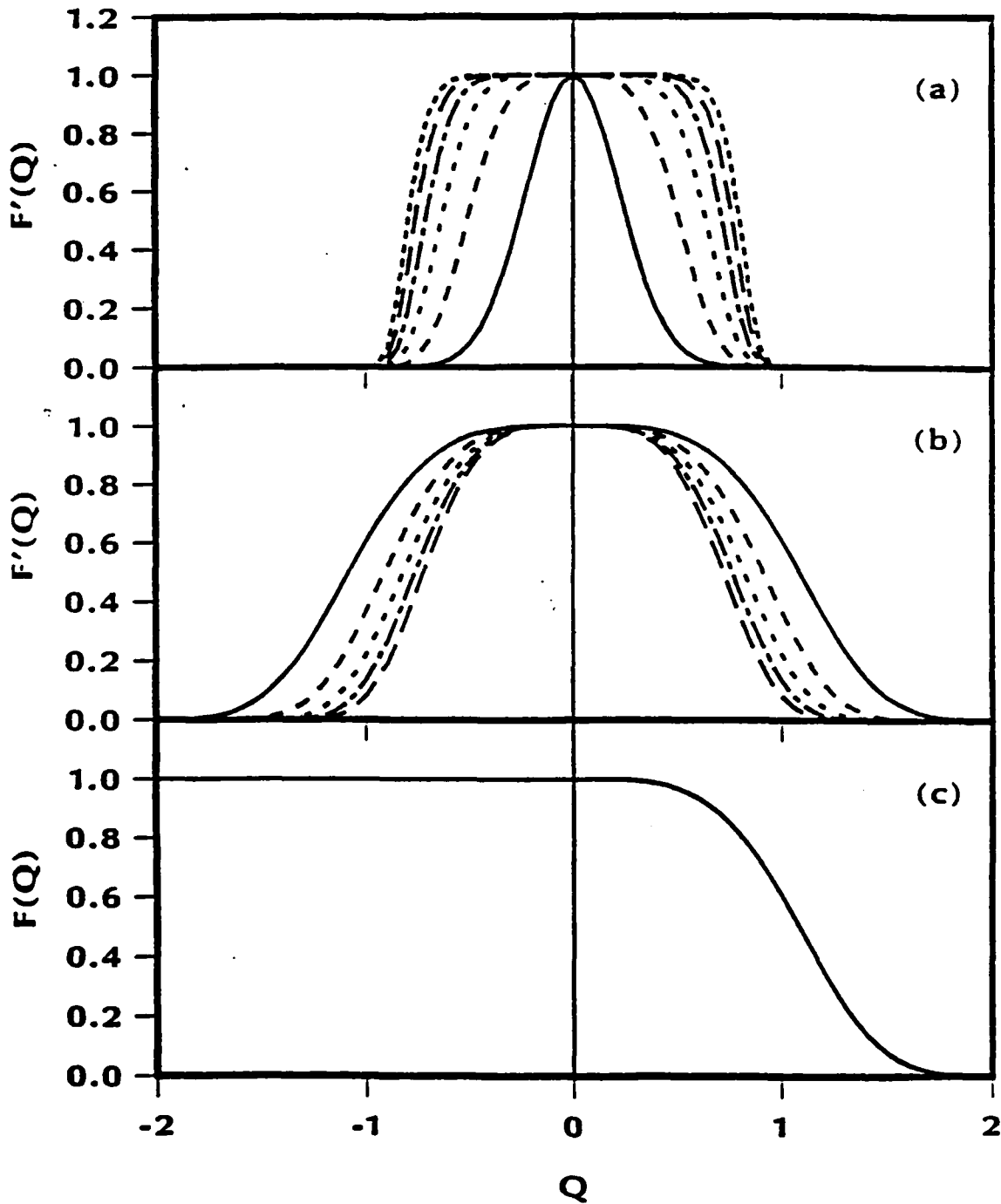
Figure 1. (a) F′ (Defined in Equation 6) for N=2 (——), 4(– – –), 6 (· · ·), 8 (— · — ·),
10 (— — —,) and 12 (-----). G=10.0 and Q_{eq}=0 for All Curves; (b) F′ (Defined in
Equation 6) for G=0.5(——), 1.0 (– – –), 1.5 (· · ·), 2.0 (— · — ·), and 2.5 (— — —).
· N=4 and Q_{eq} =0 for All Curves; (c) F (Defined in Equation 7) for N=4, G=0.5, and
Q_{eq} = 0.
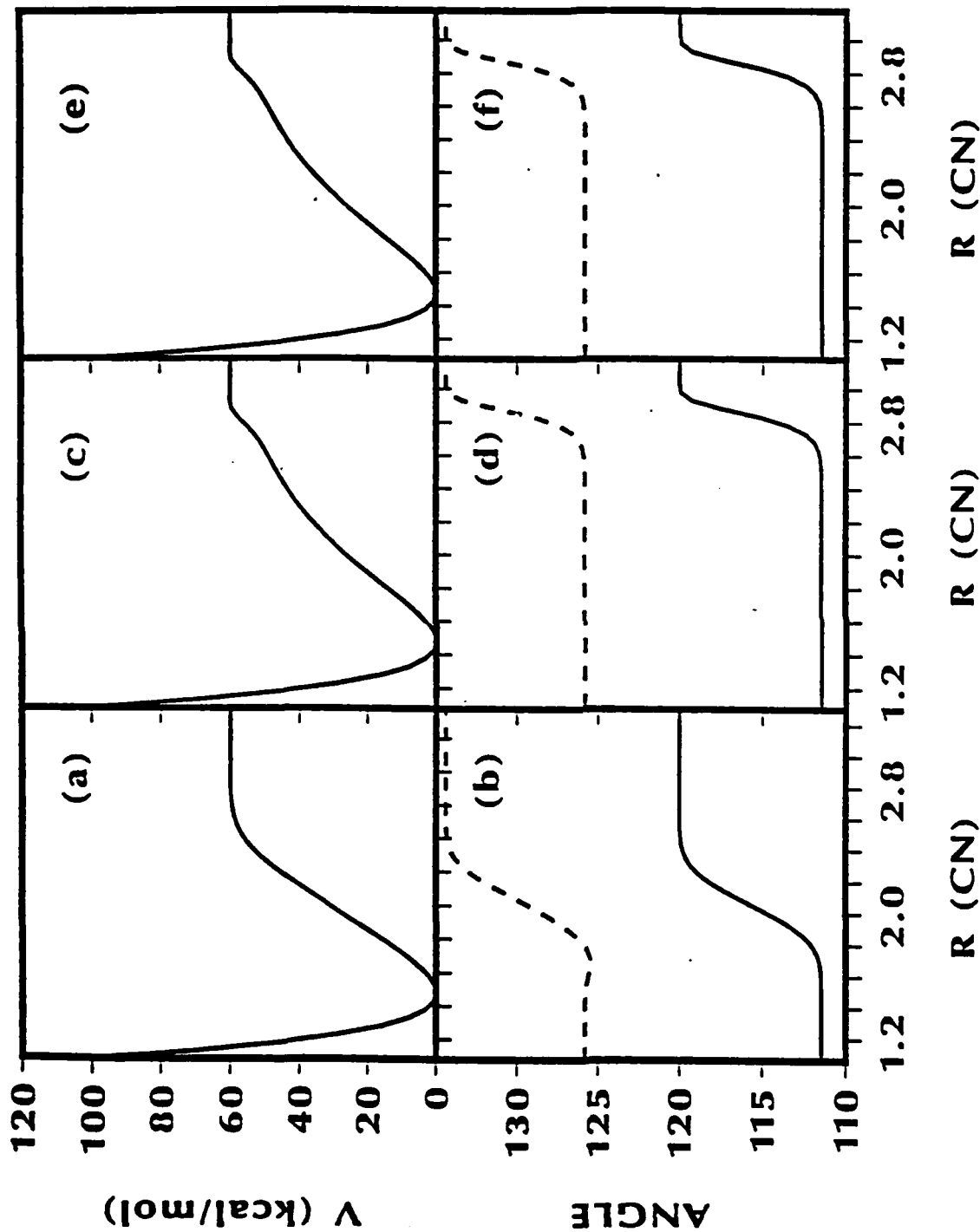
Figure 2. Top Half: Potential Energy as a Function of the C-N Bond Distance in Nitromethane for (a) PES 1, (c) PES 2, and (e) PES 3. All Other Internal Coordinates Are Optimized to Minimize the Energy at Each C-N Distance. Bottom Half: Optimized HCH angle (Solid Line) and ONO Angle (Dashed Line) as a Function of C-N Bond Distance for (b) PES 1, (d) PES 2, and (f) PES 3.

53
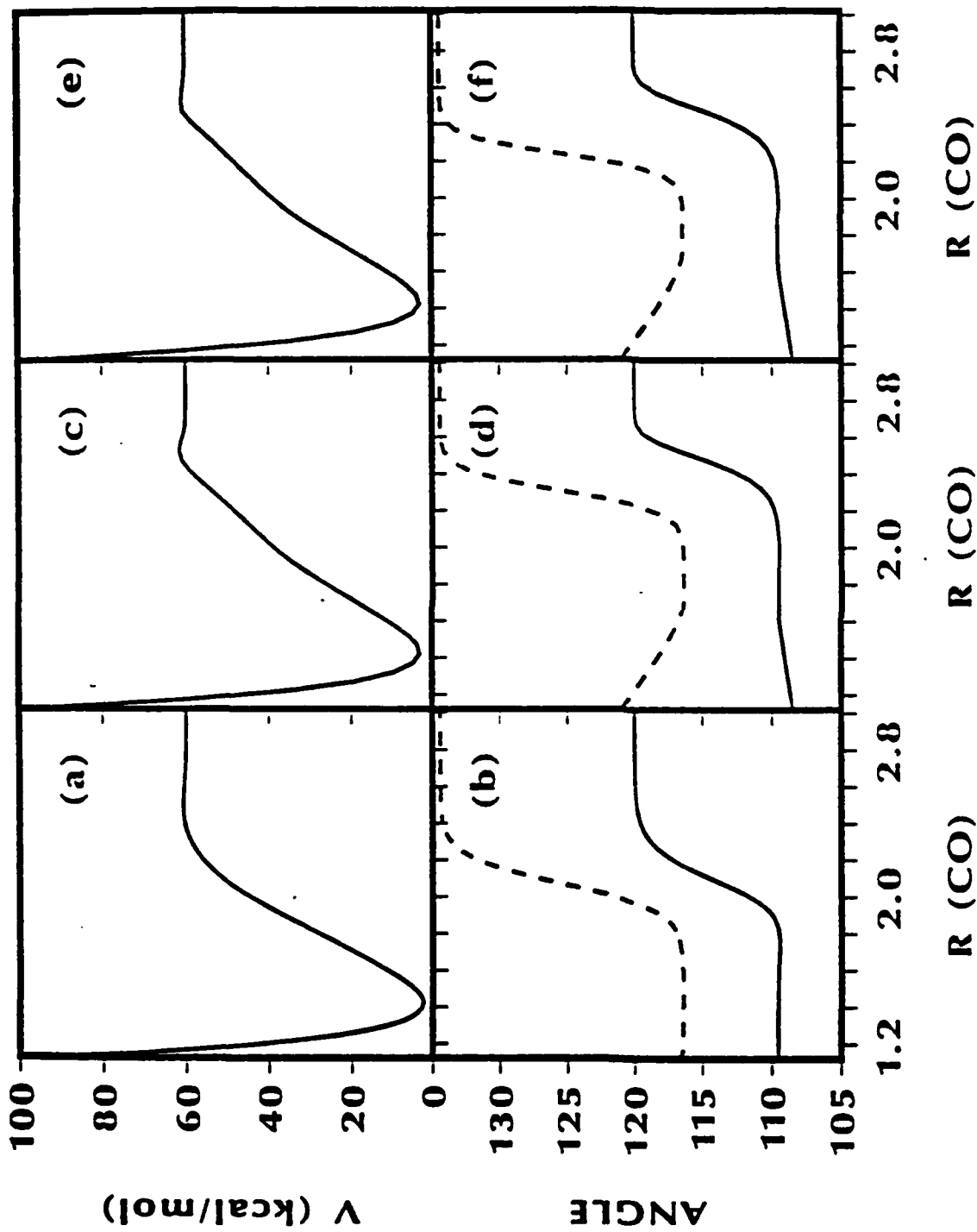
Figure 3. Top Half: Potential Energy as a Function of the C-O Bond Distance in Cis-Methyl Nitrite for (a) PES 1, (c) PES 2, and (e) PES 3. All Other Internal Coordinates Are Optimized to Minimize the Energy at Each C-O Distance. Bottom Half: Optimized HCH Angle (Solid Line) and ONO Angle (Dashed Line) as a Function of C-O Bond Distance for (b) PES 1, (d) PES 2, and (f) PES 3.
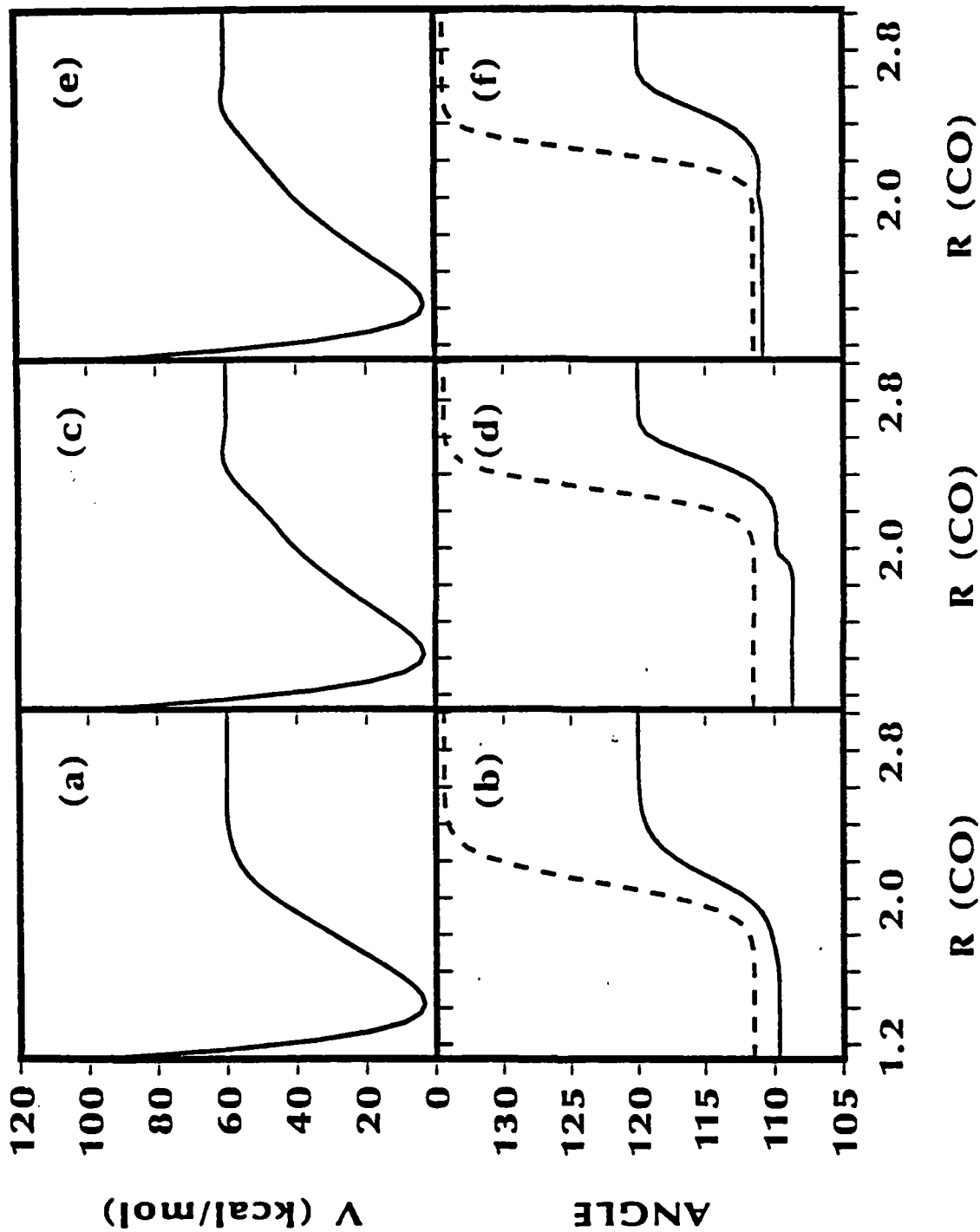
Figure 4. Top Half: Potential Energy as a Function of the C-O Bond Distance in Trans-Methyl Nitrite for (a) PES 1, (c) PES 2, and (e) PES 3. All Other Internal Coordinates Are Optimized to Minimize the Energy at Each C-O Distance. Bottom Half: Optimized HCH Angle (Solid Line) and ONO angle (Dashed Line) as a Function of C-O Bond Distance for (b) PES 1, (d) PES 2, and (f) PES 3.

55
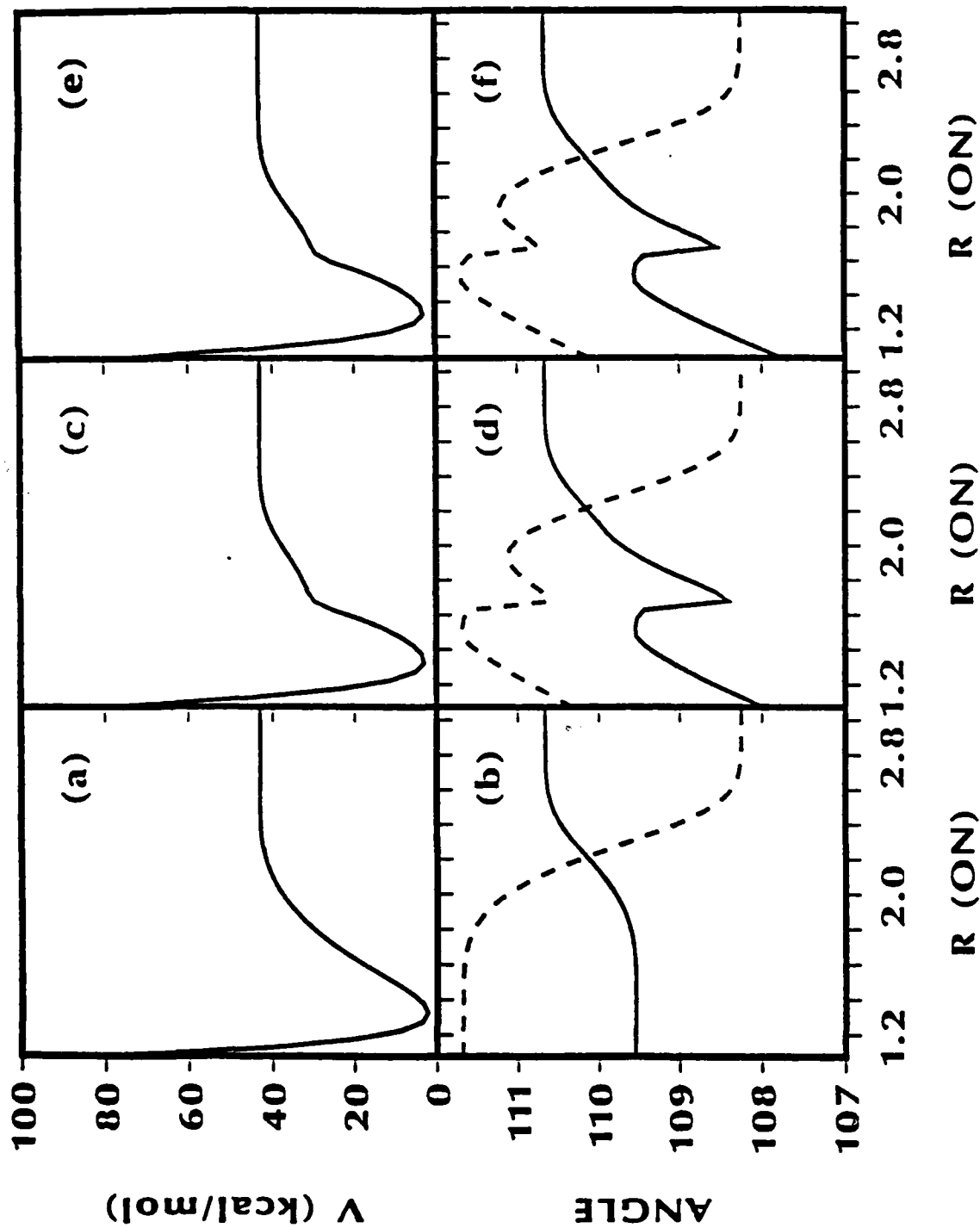
Figure 5. Top Half. Potential Energy as a Function of the O-N Bond Distance in Cis-Methyl Nitrite For (a) PES 1, (c) PES 2, and (e) PES 3. All Other Internal Coordinates Are Optimized to Minimize the Energy at Each O-N Distance. Bottom Half: Optimized HCH Angle (Solid Line) and HCO Angle (Dashed Line) as a Function of O-N Bond Distance for (b) PES 1, (d) PES 2, and (f) PES 3.

56
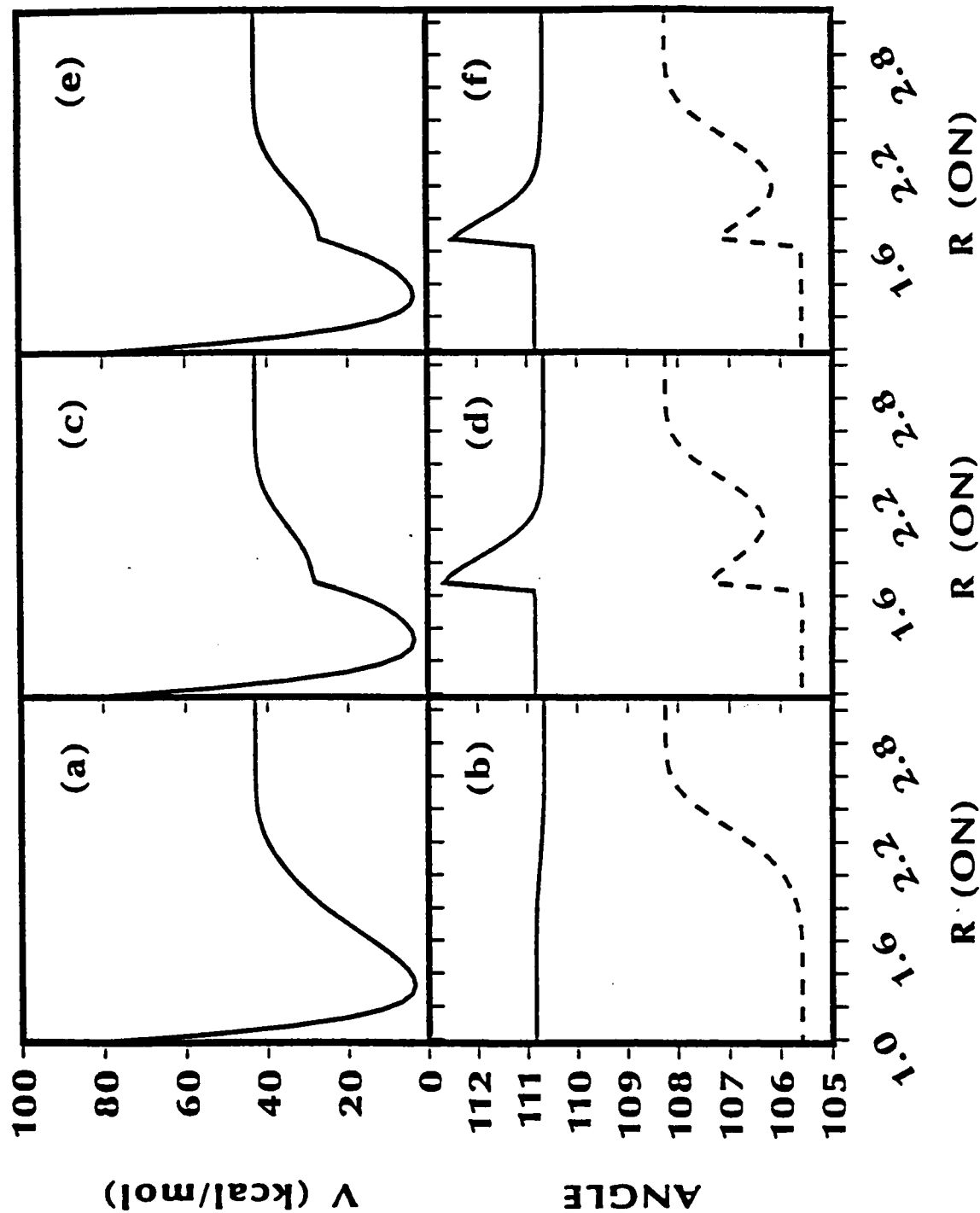
Figure 6. Top Half: Potential Energy as a Function of the O-N Bond Distance in Trans-Methyl Nitrite For (a) PES 1, (c) PES 2, and (e) PES 3. All Other Internal Coordinates Are Optimized to Minimize the Energy at Each O-N Distance. Bottom Half: Optimized HCH Angle (Solid Line) and HCO Angle (Dashed Line) as a Function of O-N Bond Distance for (b) PES 1, (d) PES 2, and (f) PES 3.

57
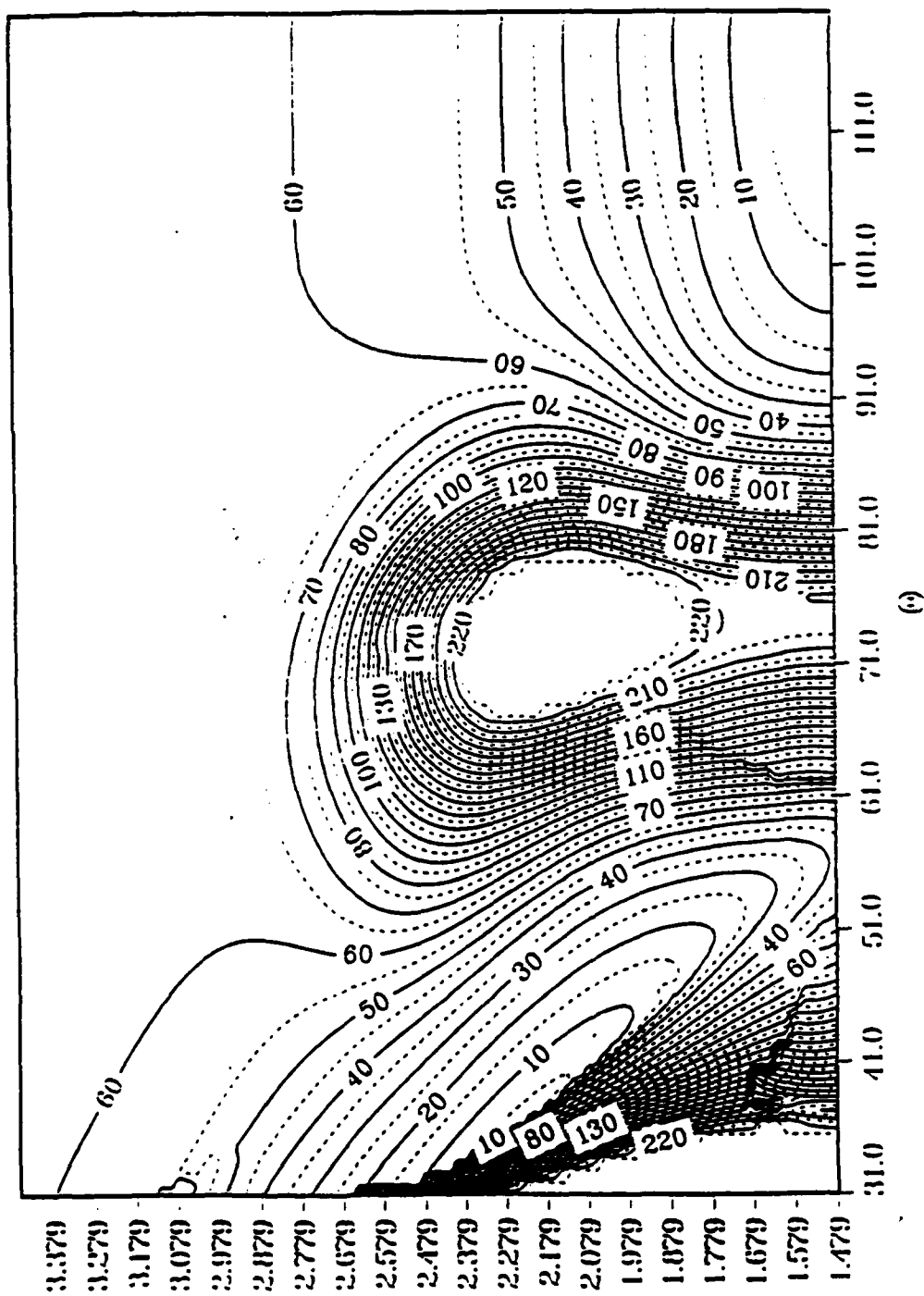
Figure 7. Contour Plot of Potential Energy (PES 1) as a Function of the C-N Bond Distance and CNO Angle. All Other Internal Coordinates Are Optimized to Minimize the Energy at Each C-N, CNO Grid Point. Energy Contour Values Are in kcal/mol, and Contour Values From 0.0 to 225 kcal/mol at 5 kcal/mol Increments Are Shown.

58
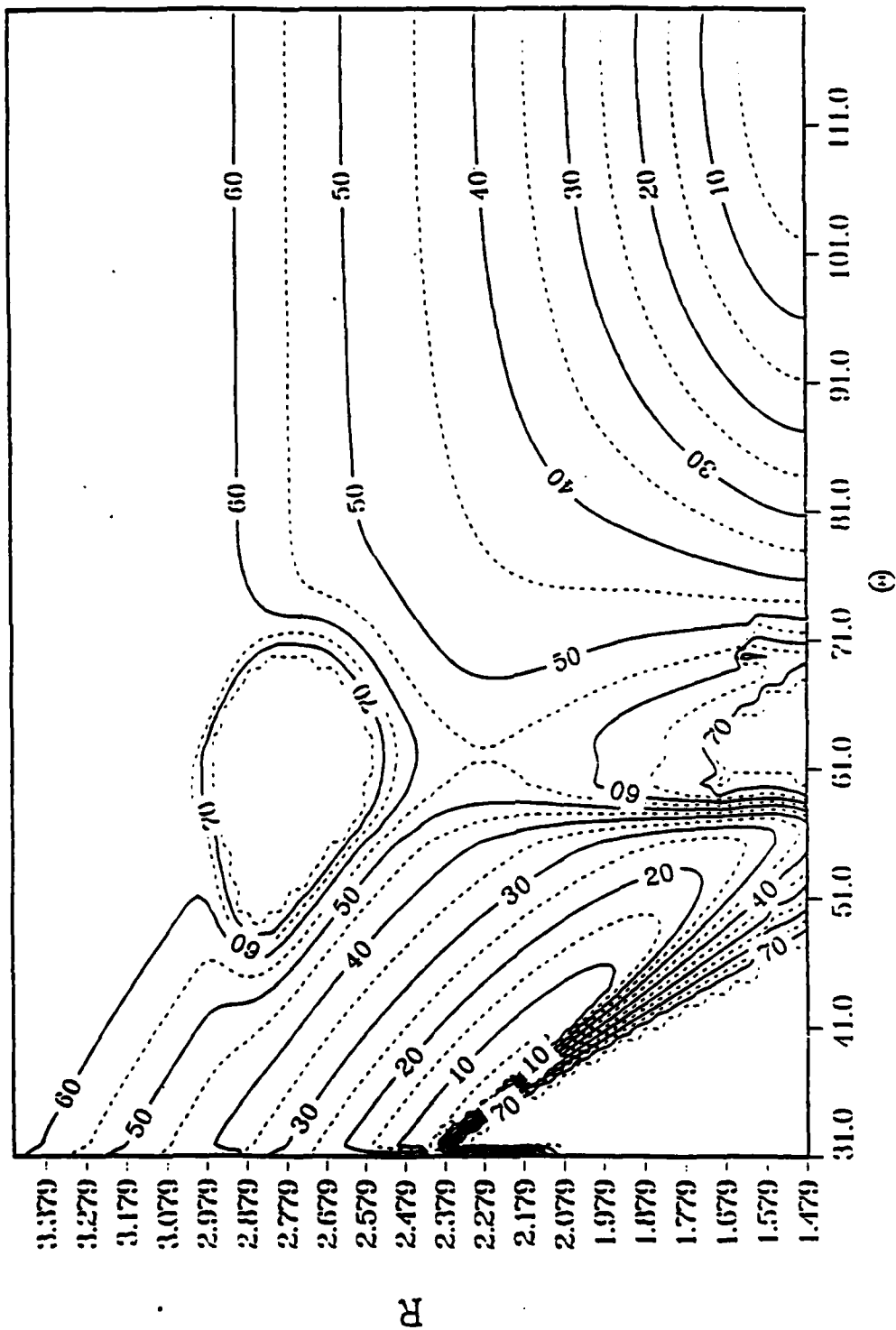
Figure 8. Contour Plot of Potential Energy (PES 2) as a Function of the C-N Bond Distance and CNO Angle. All Other Internal Coordinates Are Optimized to Minimize the Energy at Each C-N, CNO Grid Point. Energy Contour Values Are in kcal/mol, and Contour Values From 0.0 to 75 kcal/mol at 5 kcal/mol Increments Are Shown.

59
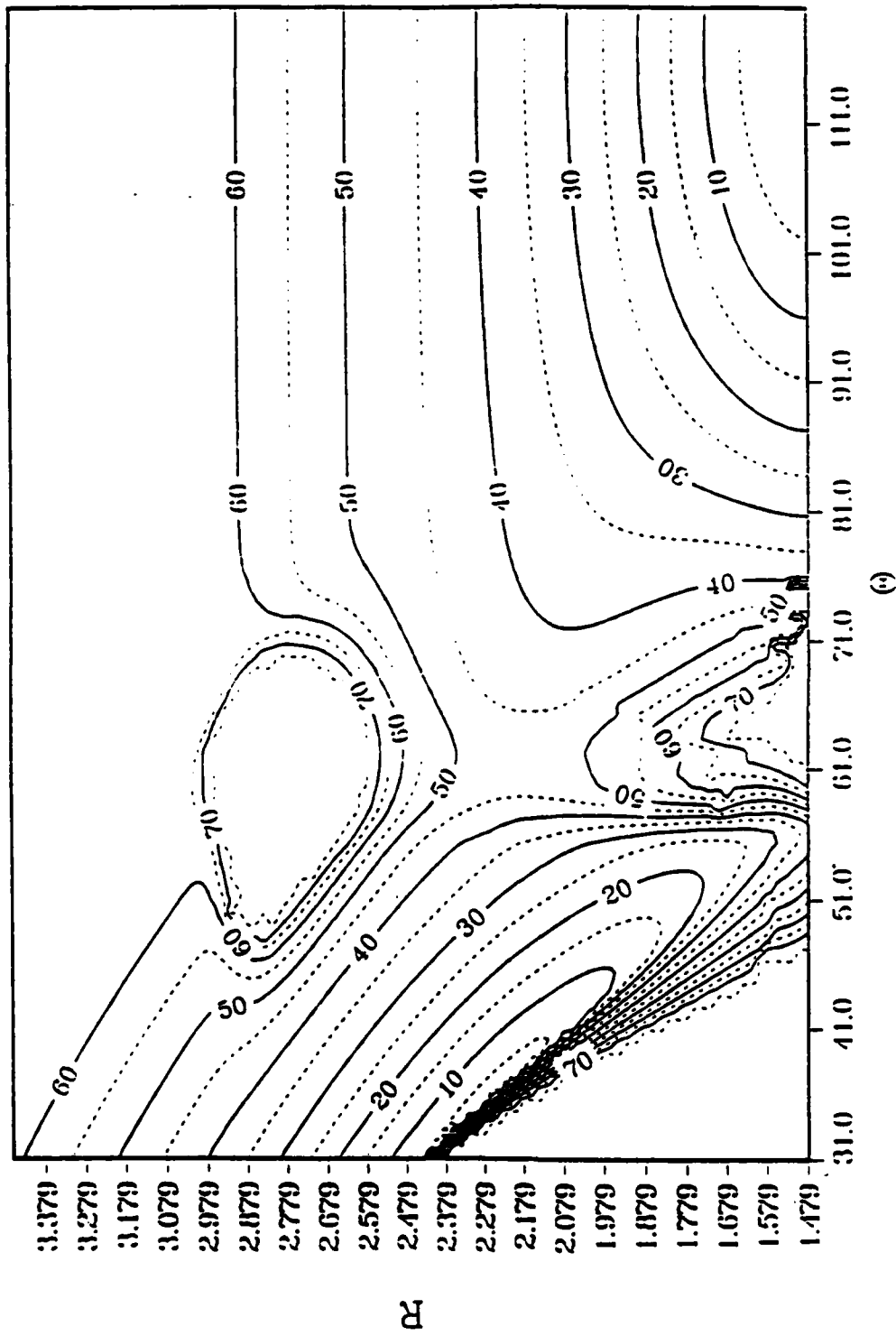
Figure 9. Contour Plot of Potential Energy (PES 3) as a Function of the C-N Bond Distance and CNO Angle. All Other Internal Coordinates Are Optimized to Minimize the Energy at Each C-N, CNO Grid Point. Energy Contour Values are in kcal/mol, and Contour Values From 0.0 to 75 kcal/mol at 5 kcal/mol Increments Are Shown.
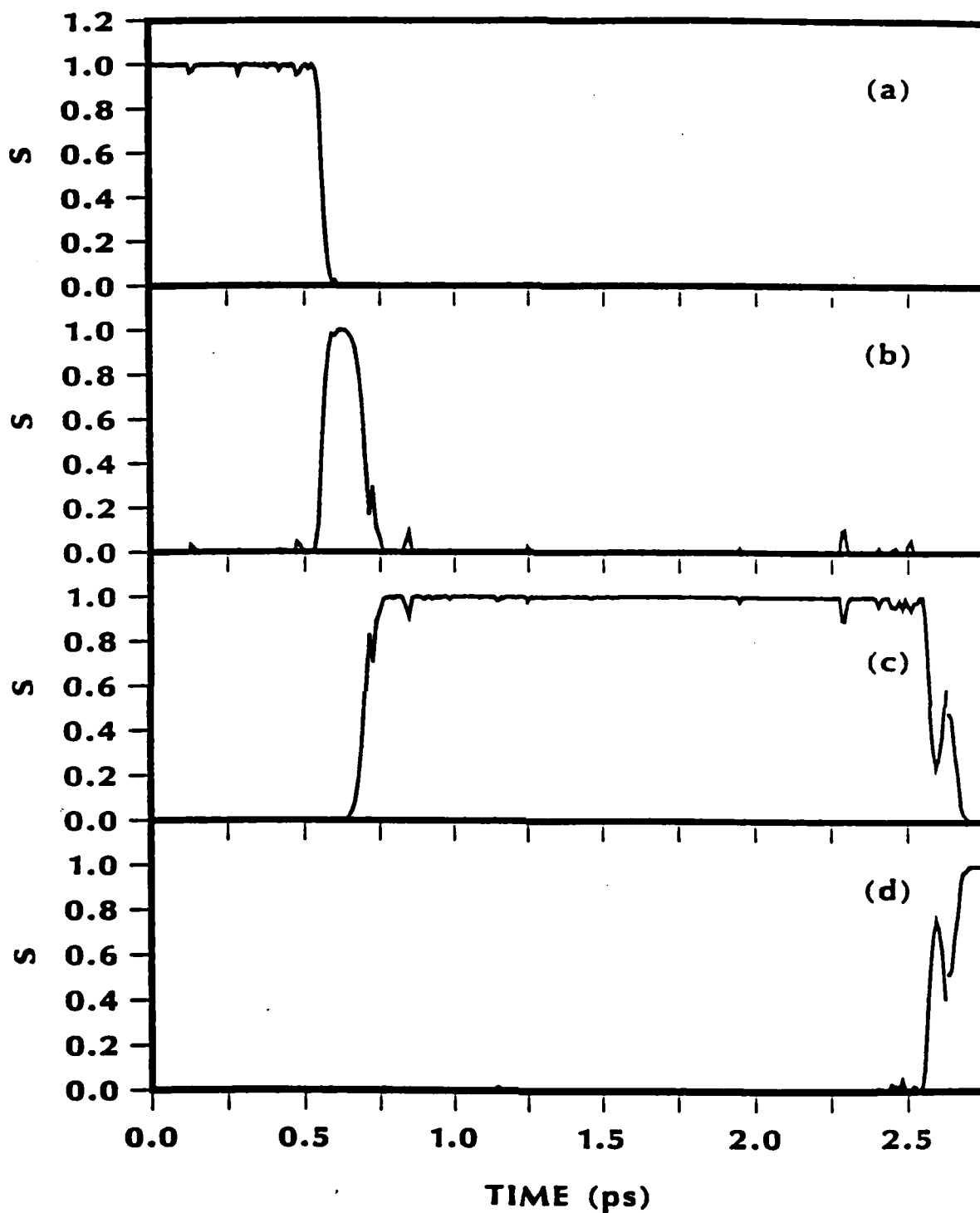
Figure 10. Weighting Functions (a) $S_{CH_3NO_2}$, (b) $S_{CH_3+NO_2}$, (c) S_{CH_3ONO}, and (d) $S_{CH_3O^{\bullet}+NO}$ During a Trajectory Integrated on PES 1 Which Results in Formation of Methyl Nitrite and Subsequent Dissociation to CH_2O + NO Via a Dissociation-Recombination Mechanism.
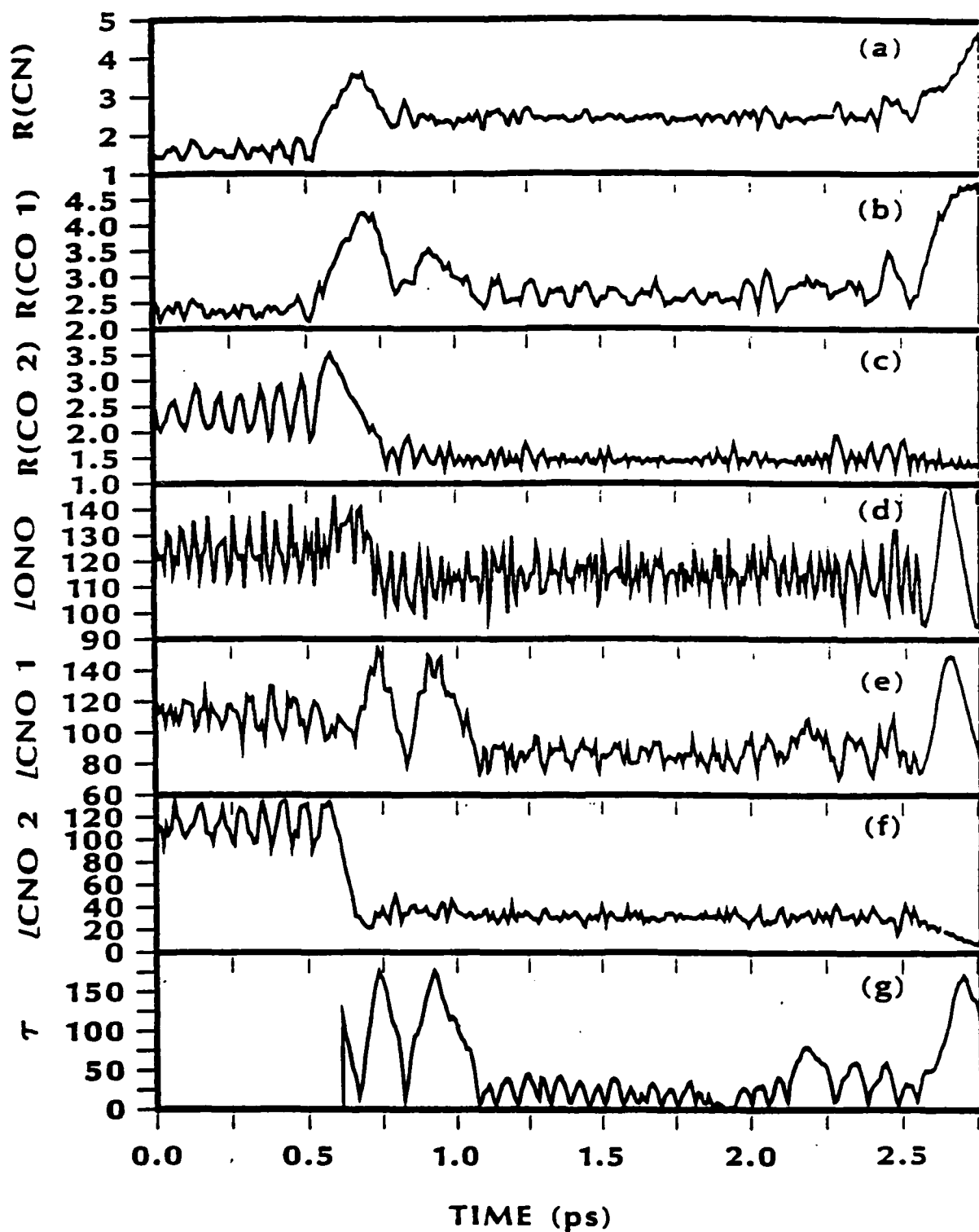
Figure 11. Internal Coordinated During the Trajectory Described in Figure 10. (a) C-N Bond Distance; (b) C-O Bond Distance; (c) C-O´ Bond Distance; (d) ONO Angle; (e) CNO Angle; (f) CNO´Angle; and (g) CO'NO Dihedral Angle.
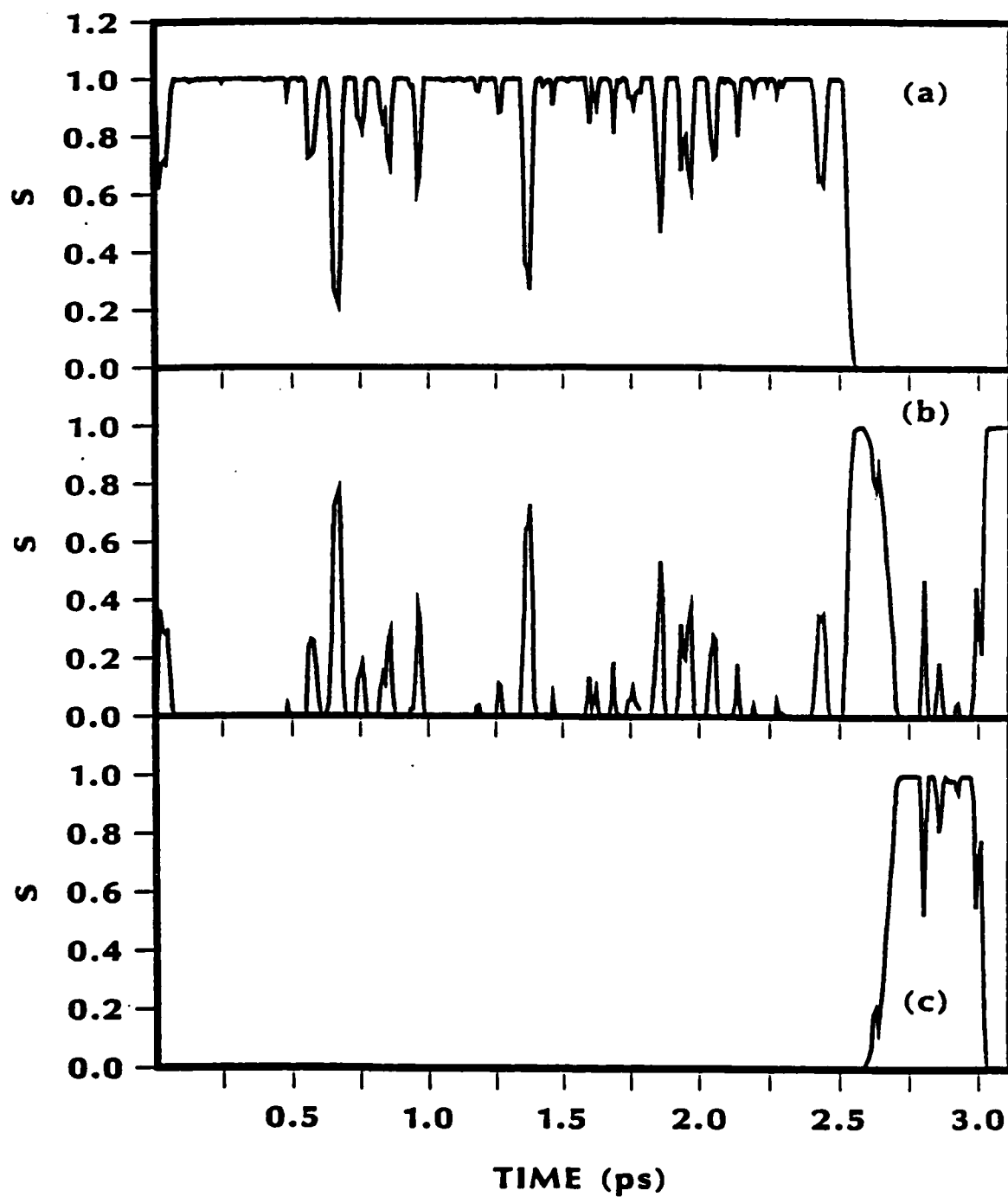
Figure 12. Weighting Functions (a) $S_{CH_3NO_2}$, (b) $S_{CH_3+NO_2}$, and (c) S_{CH_3ONO} During a Trajectory Integrated on PES 1 Which Results in Formation of Methyl Nitrite and Subsequent Dissociation to $CH_3 + NO_2$ Via a Dissociation-Recombination Mechanism.
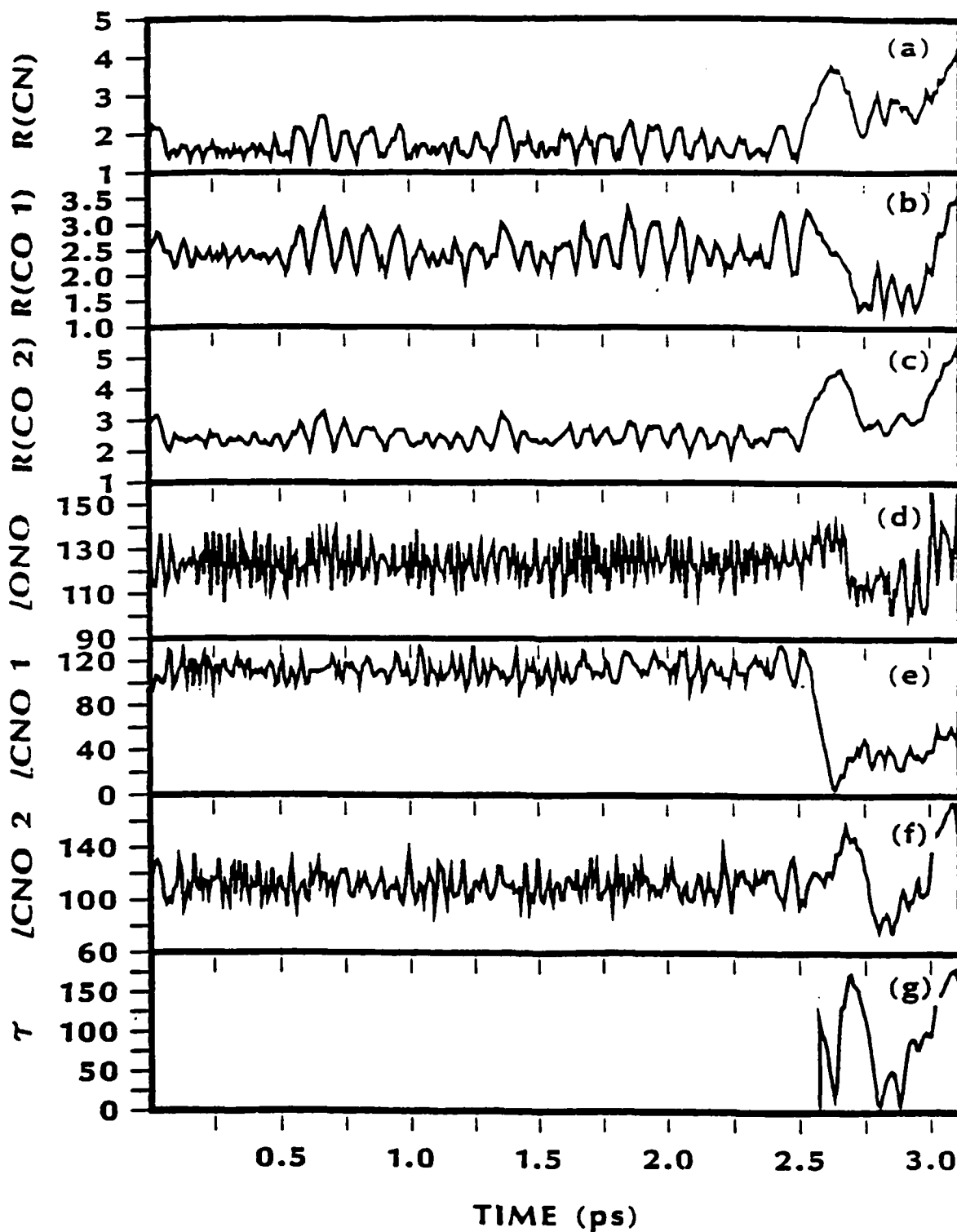
Figure 13. Internal Coordinates During the Trajectory Described in Figure 12. (a) C-N Bond Distance; (b) C-O Bond Distance; (c) C-O´ Bond Distance; (d) ONO Angle; (e) CNO Angle; (f) CNO´ Angle; and (g) CONO´ Dihedral Angle.

64
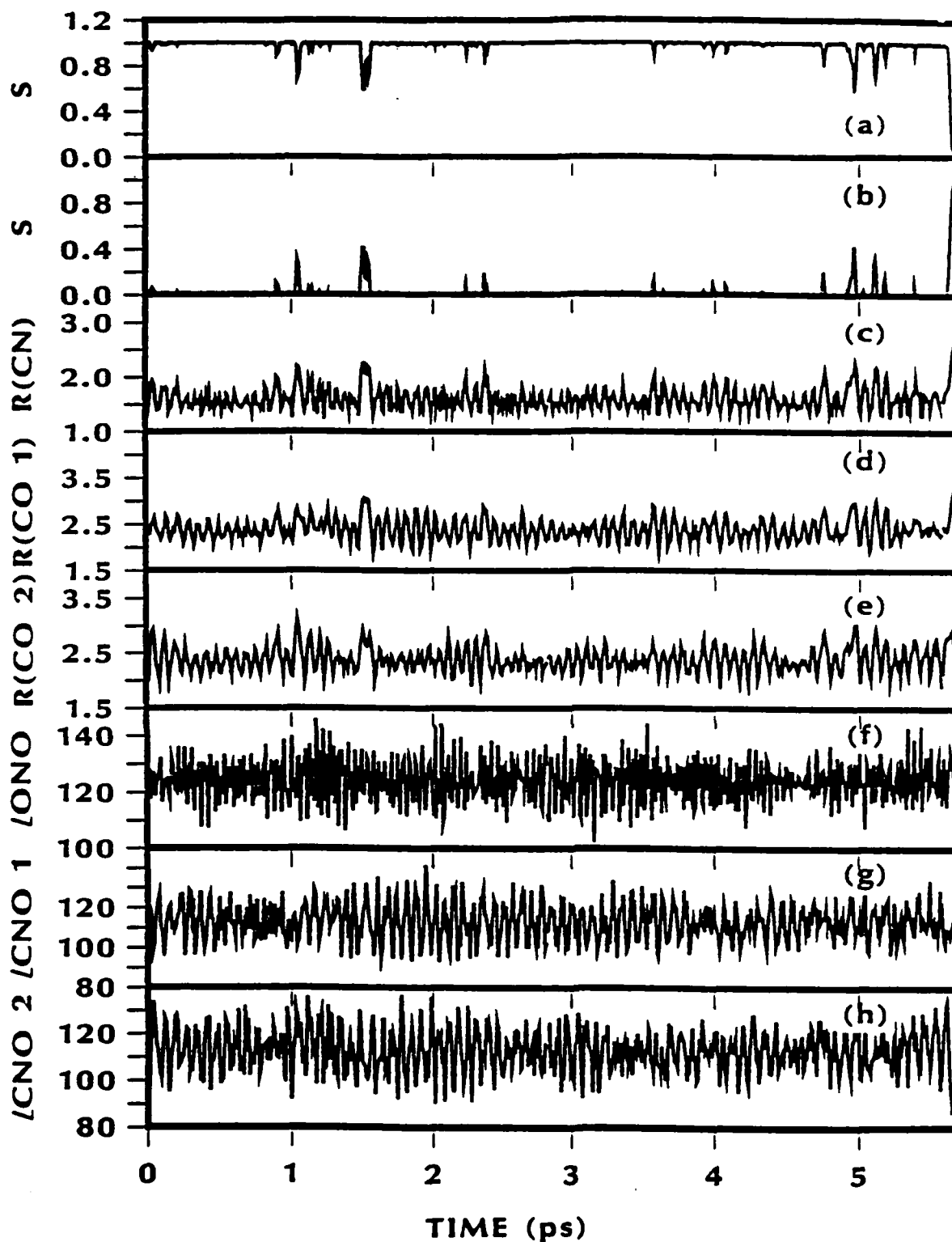
Figure 14. Weighting Functions (a) $S_{CH_3NO_2}$ and (b) $S_{CH_3+NO_2}$ During a Trajectory Integrated on PES 1 Which Results in C-N Bond Scission in Nitromethane to Form Methyl and Nitrogen Dioxide Radicals. Internal Coordinates During the Same Trajectory Are Shown in (c) C-N Bond Distance, (d) C-O Bond Distance, (f) ONO Angle, (g) CNO Angle, and (h) CNO' Angle.
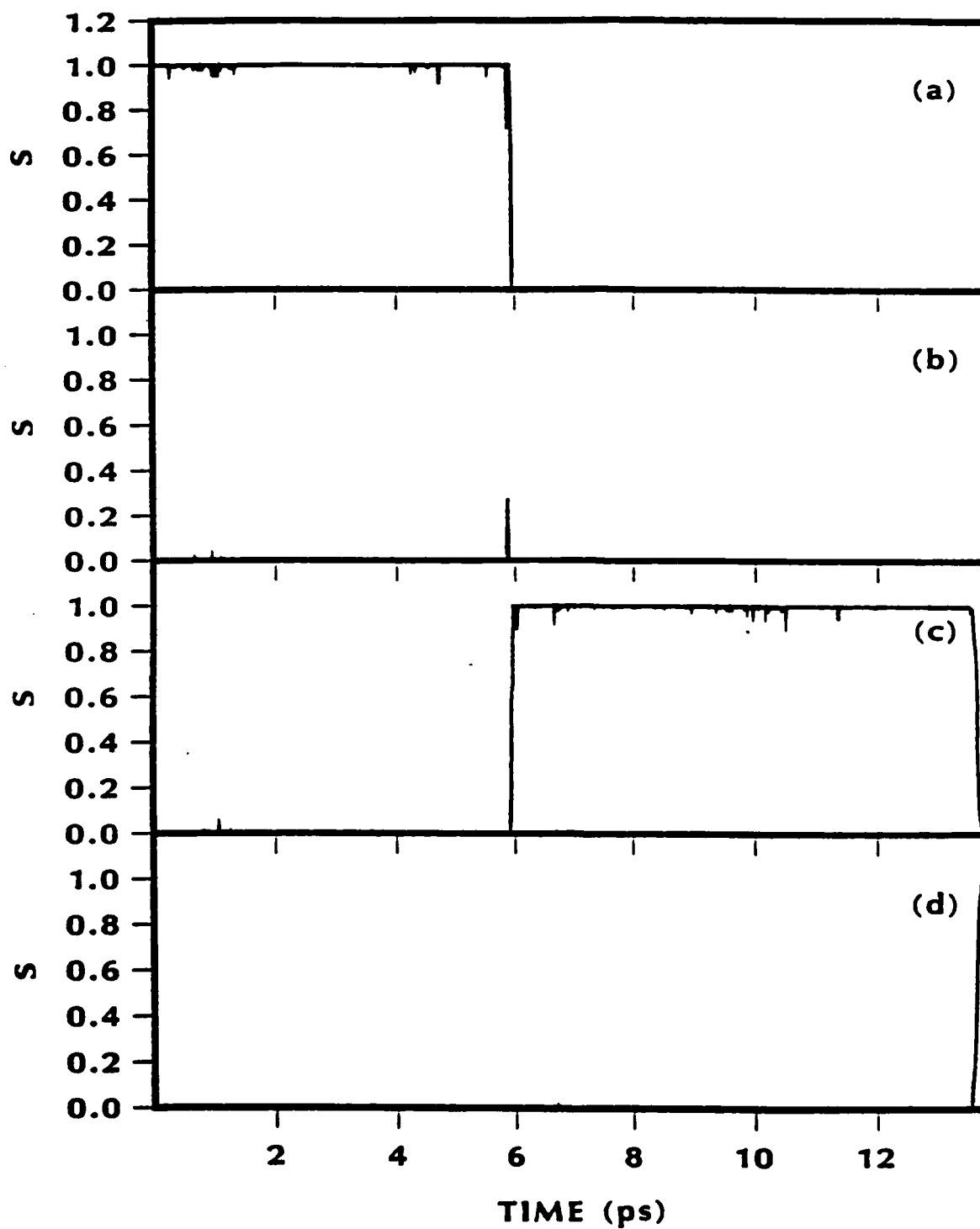
Figure 15. Weighting Functions (a) $S_{CH_3NO_2}$, (b) $S_{CH_3O\cdot NO}$, (c) S_{CH_3ONO}, and (d) S_{CH_3O+NO} During a Trajectory Integrated on PES 3 Which Results in Formation of Methyl Nitrite and Subsequent Dissociation to CH_2O + NO Via a Direct Isomerization Mechanism.
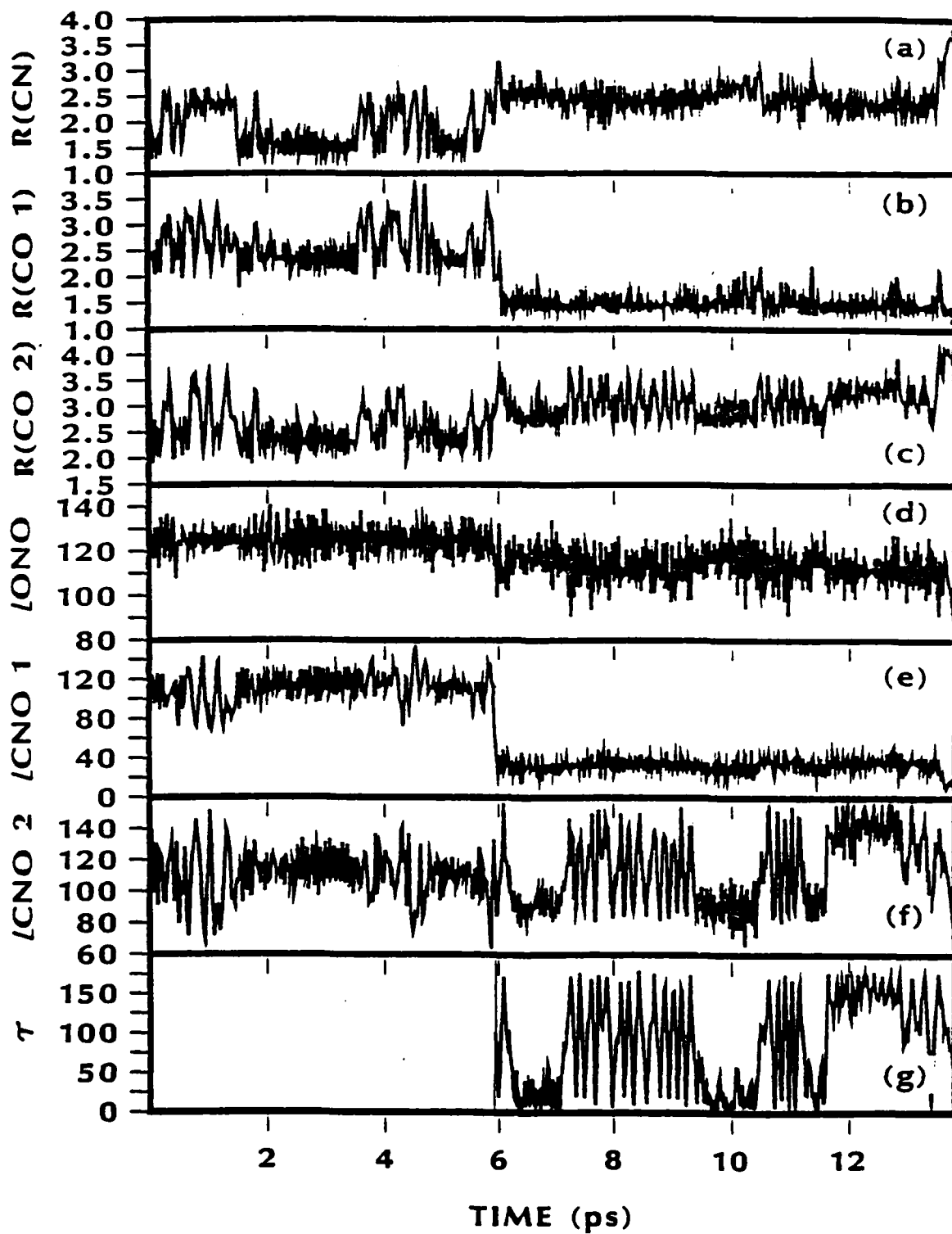
Figure 16. Internal Coordinates During the Trajectory Described in Figure 15. (a) C-N Bond Distance; (b) C-O Bond Distance; (c) C-O′ Bond Distance; (d) ONO Angle; (e) CNO Angle; (f) CNO′ Angle; and (g) CO′NO Dihedral Angle.
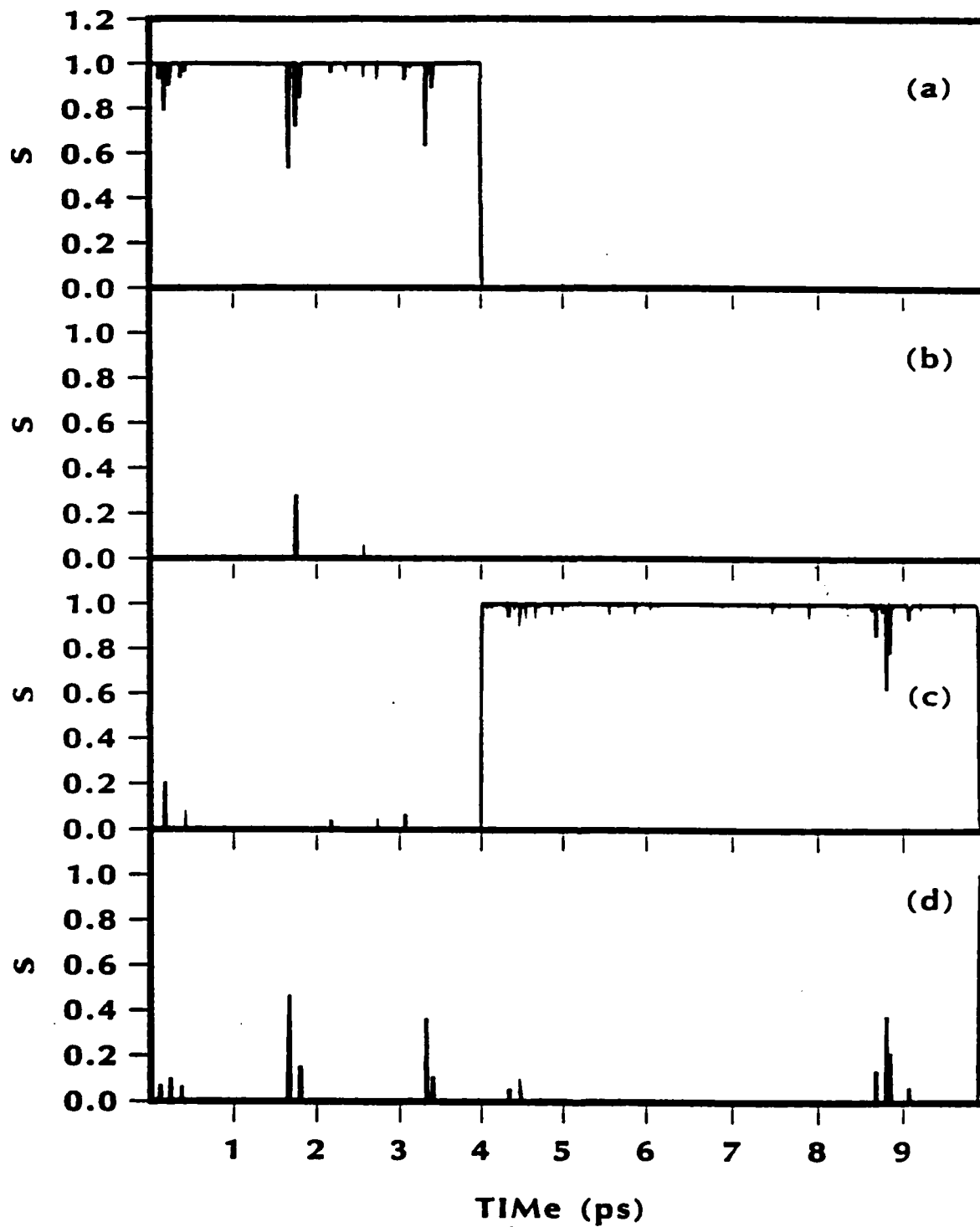
Figure 17. Weighting Functions (a) $S_{CH_3NO_2}$ (b) S_{CH_3ONO} (c) S_{CH_3O-NO} and (d) $S_{CH_3 + NO_2}$ During a Trajectory Integrated on PES 3 Which Results in Formation of Methyl Nitrite and Subsequent Dissociation to $CH_3 + NO_2$ Via a Direct Isomerization Mechanism.
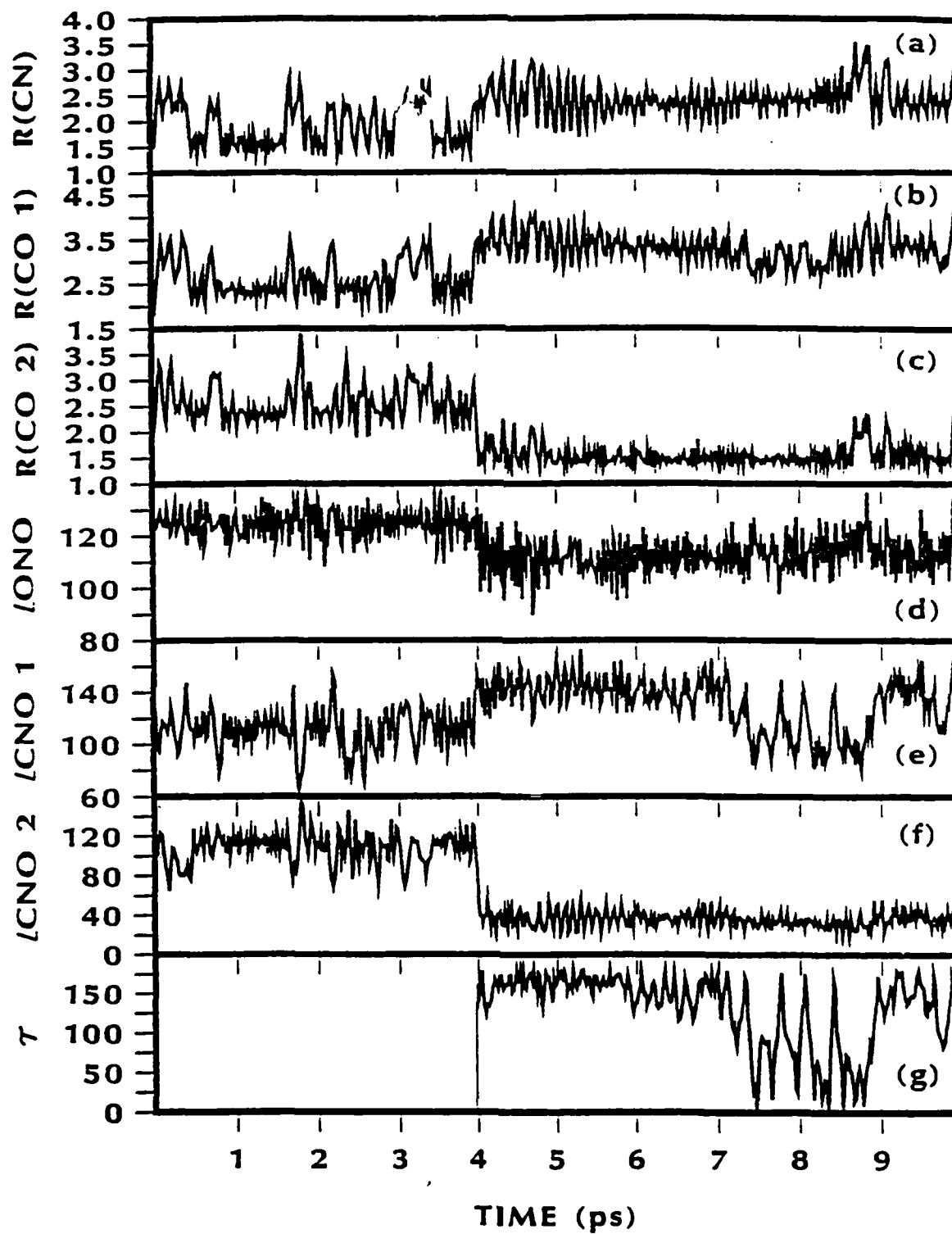
Figure 18. Internal Coordinates During the Trajectory Described in Figure 17. (a) C-N Bond Distance; (b) C-O Bond Distance; (c) C-O´ Bond Distance; (d) ONO Angle; (e) CNO Angle; and (g) CO´NO Dihedral Angle.

69
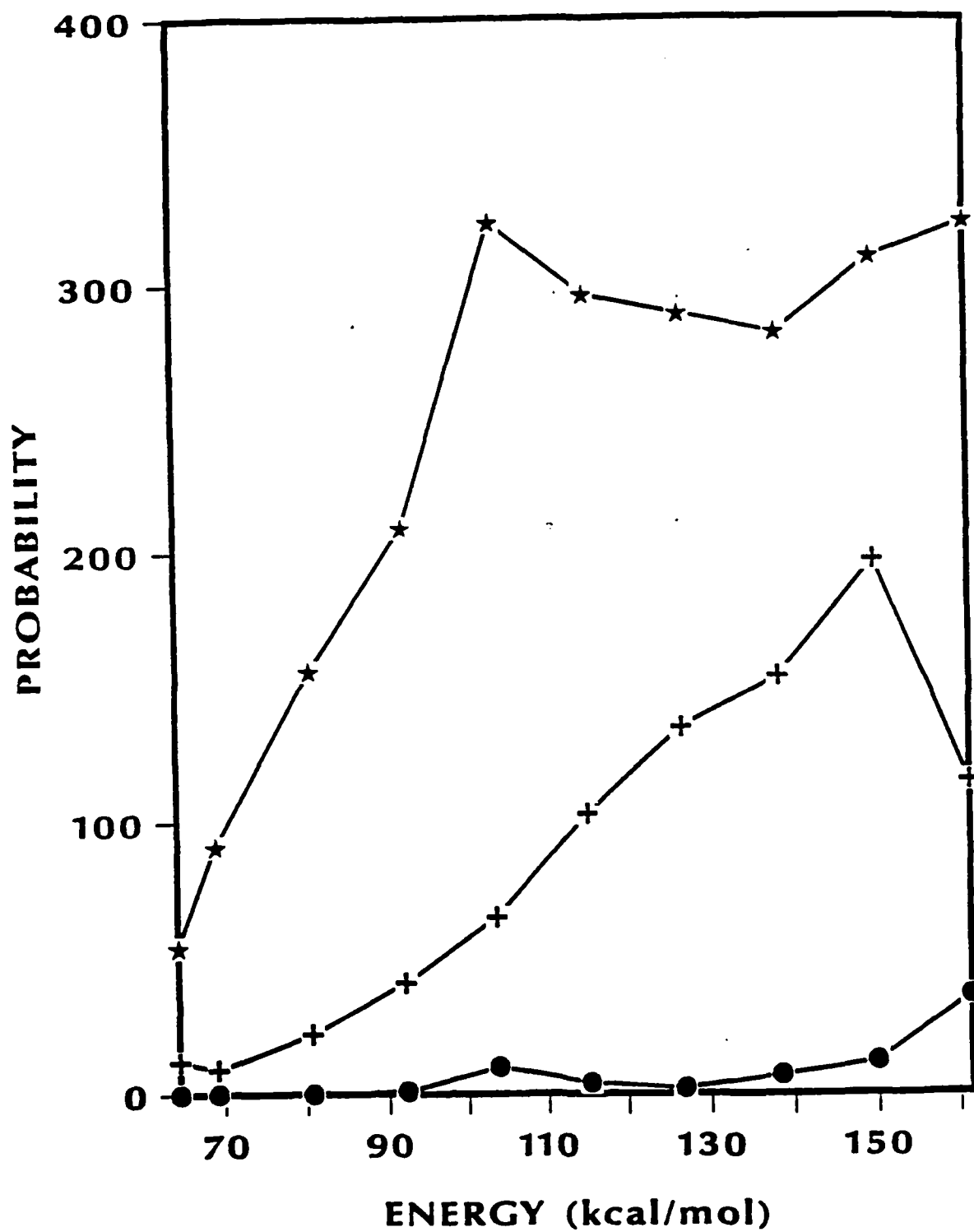
Figure 19. Probability of Reaction III Occurring as a Function of Energy for PES 1 (Circles), PES 2 (Crosses), and PES 3 (Stars). The Energy Along the Abscissa Is the Total Energy Above the Zero Point Energy of Nitromethane.
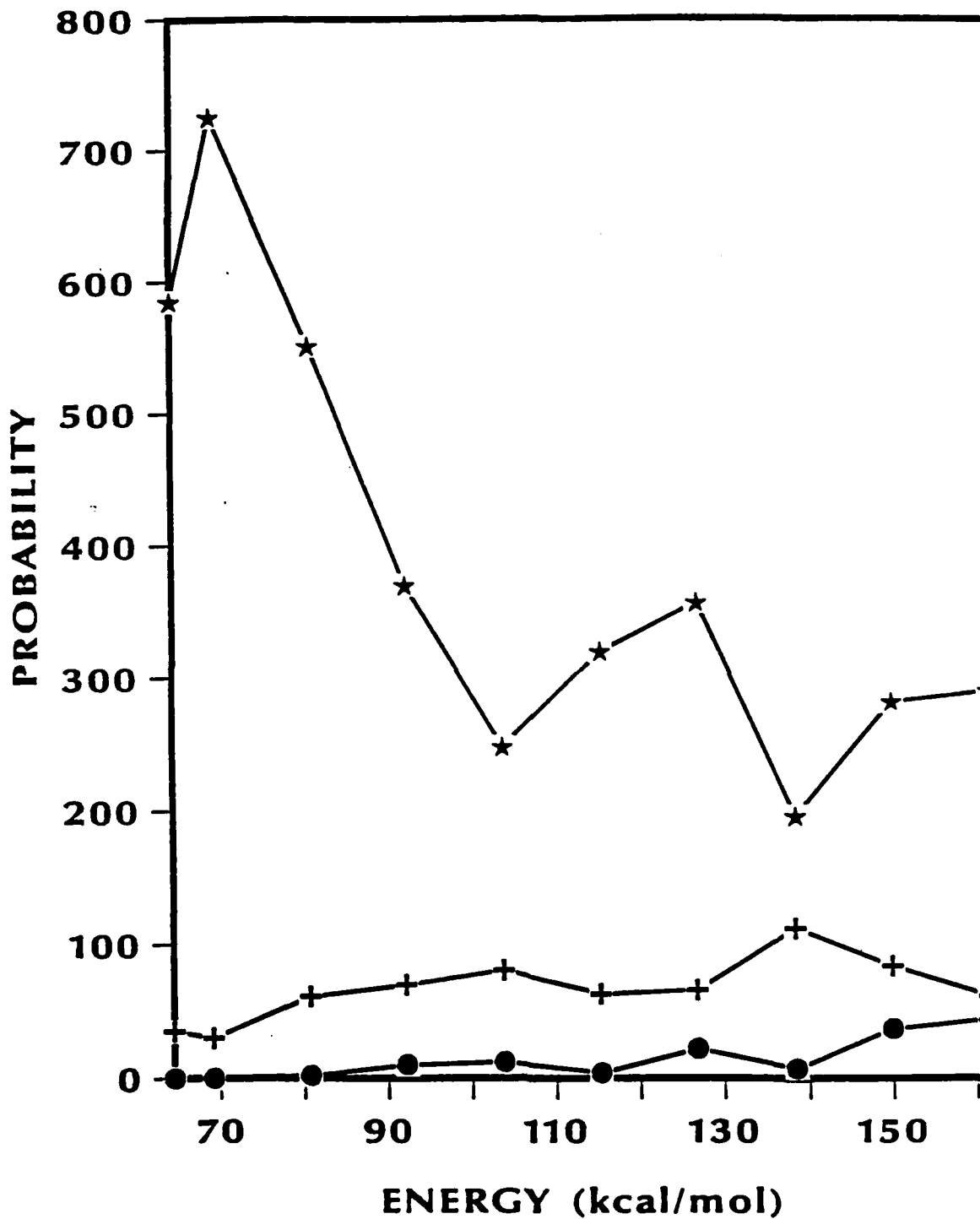
Figure 20. Probability of Reaction II occurring as a Function of Energy for PES 1 (Circles), PES 2 (Crosses), and PES 3 (Stars). The Energy Along the Abscissa Is the Total Energy Above the Zero Point Energy of Nitromethane.
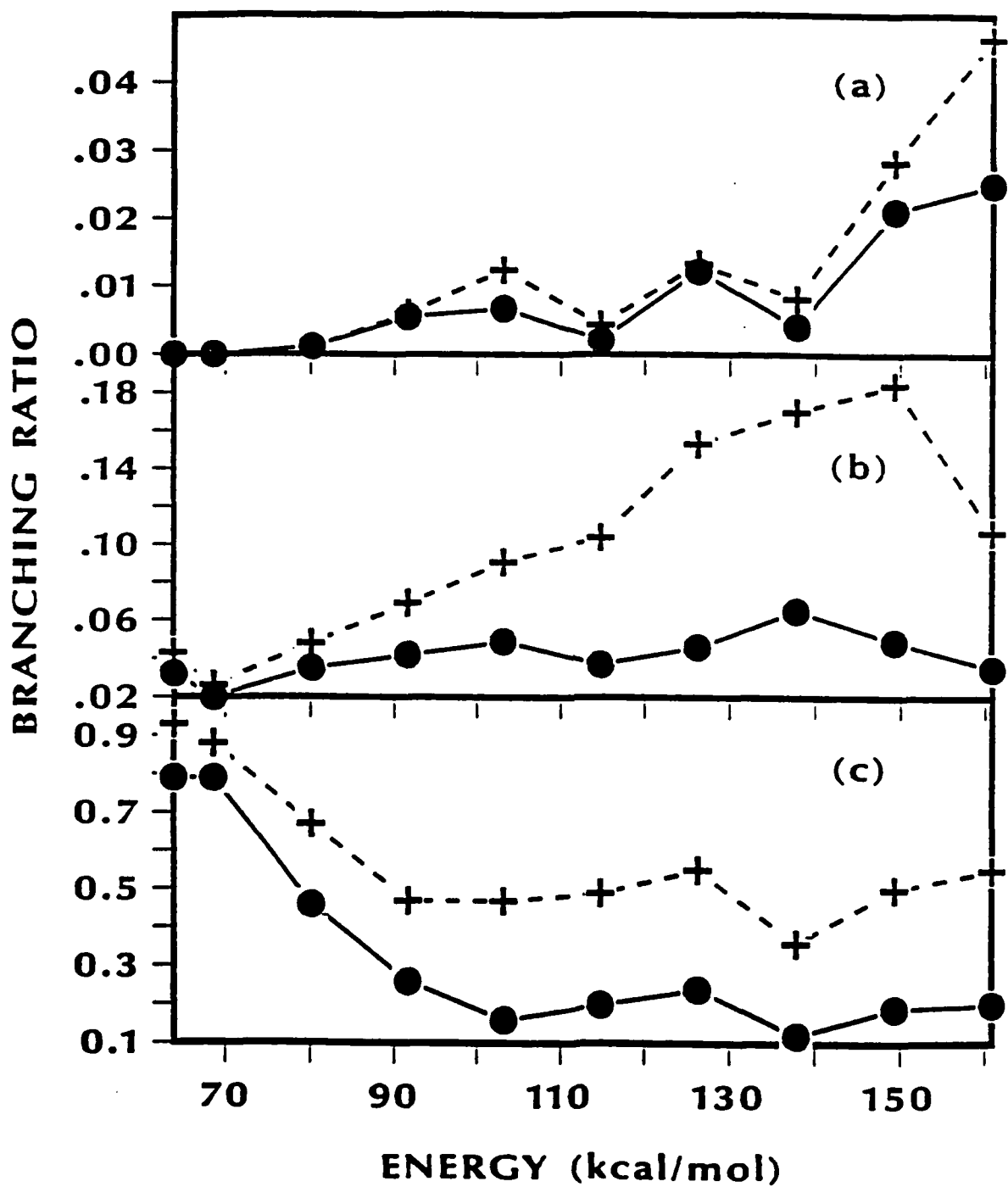
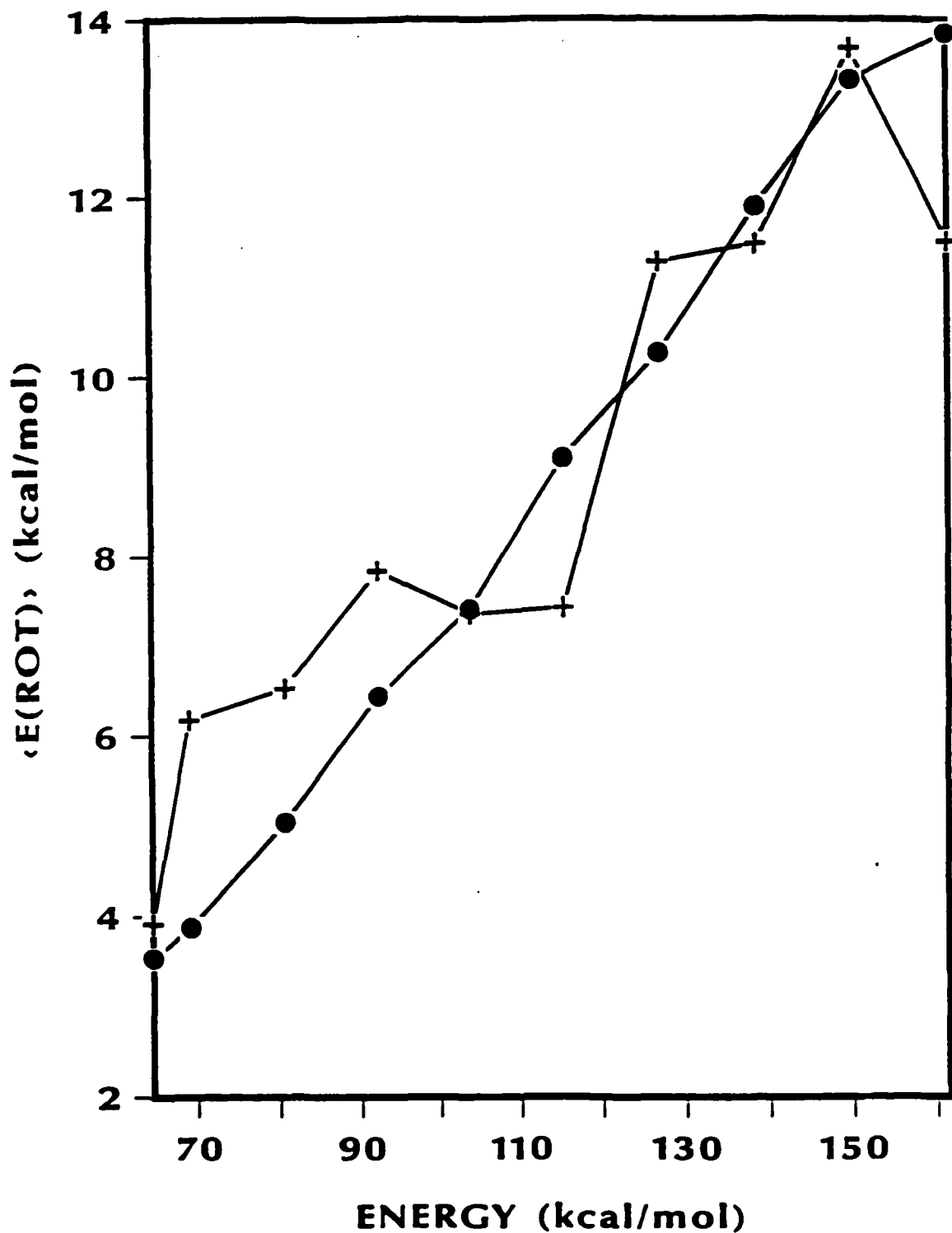Figure 21. Branching Ratios B₁ (Circles) and B₂ (Crosses) for (a) PES 1, (b) PES 2, and (c) PES 3. The Energy Along the Abscissa Is the Total Energy Above the Zero Point Energy of Nitromethane.

72
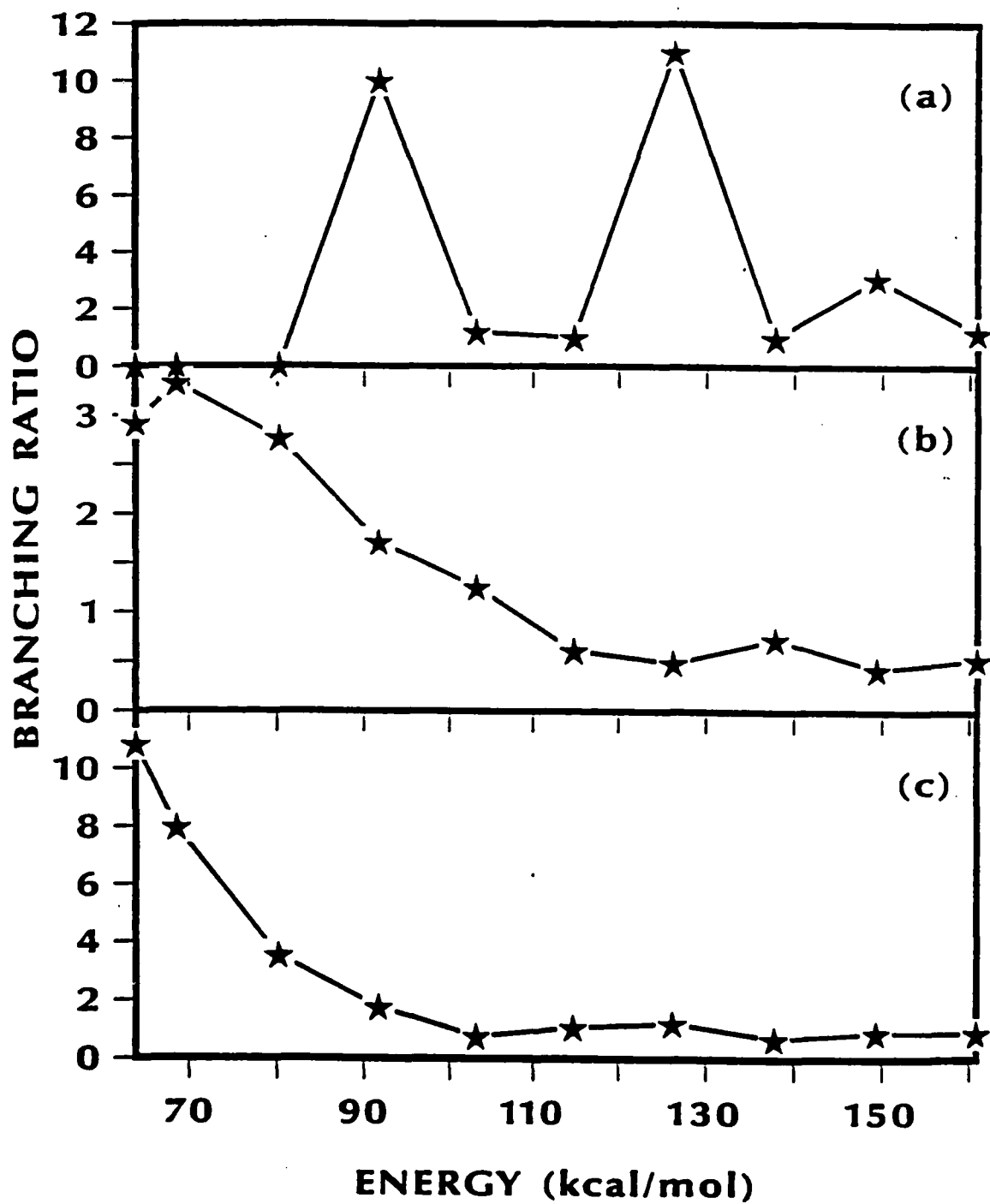
Figure 22. Branching Ratios B, for (a) PES 1, (b) PES 2, and (c) PES 3. The Energy Along the Abscissa Is the Total Energy Above the Zero Point Energy of Nitromethane.
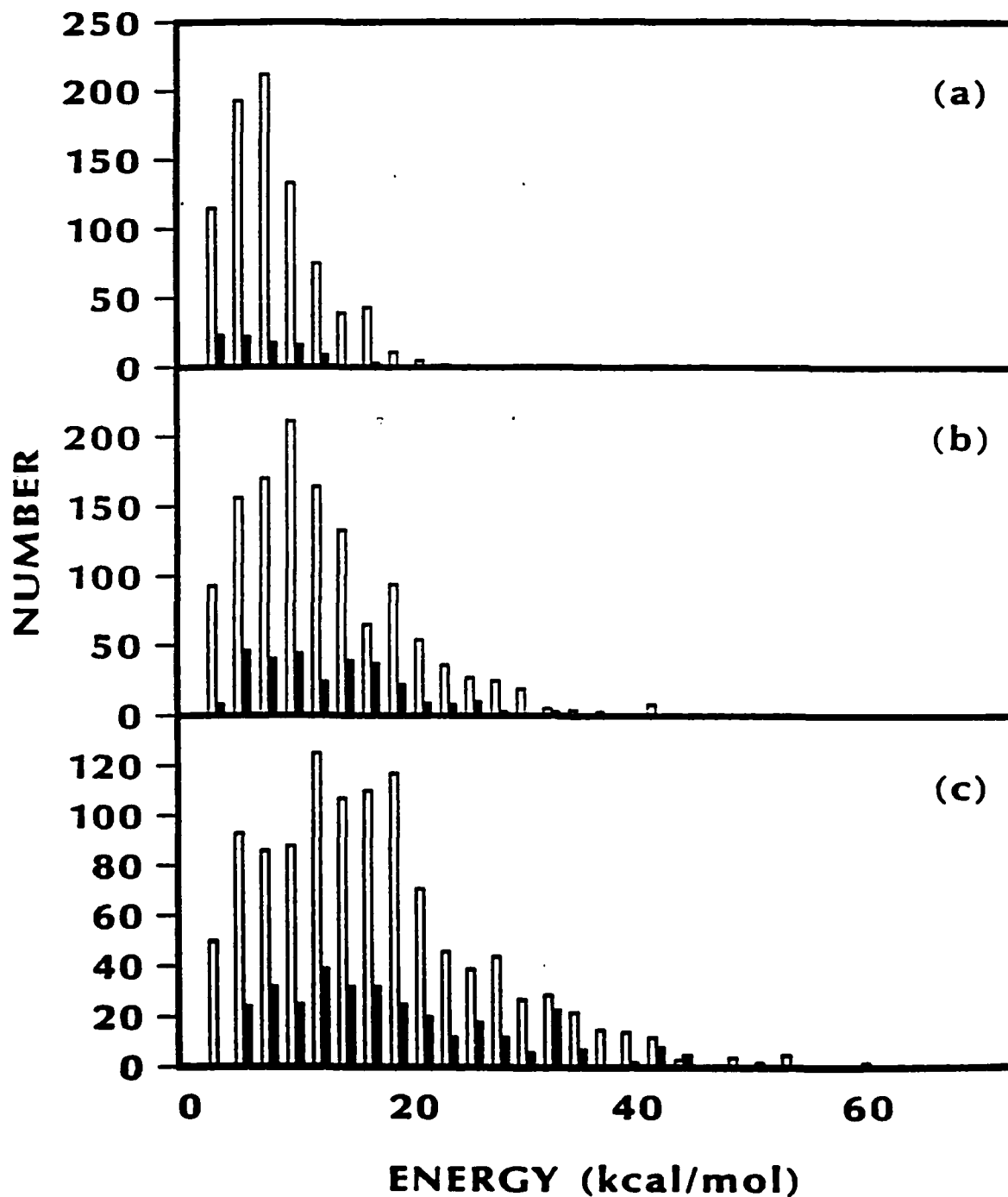
Figure 23. Distributions of the Product Relative Translational Energies for CH_3 + NO_2 Formed From Reaction I (Hollow Bars) and Reaction III (Filled Bars) on PES 3 at Energies (a) 69.2, (b) 115.3, and (c) 161 kcal/mol Above the Zero Point Energy of Nitromethane.
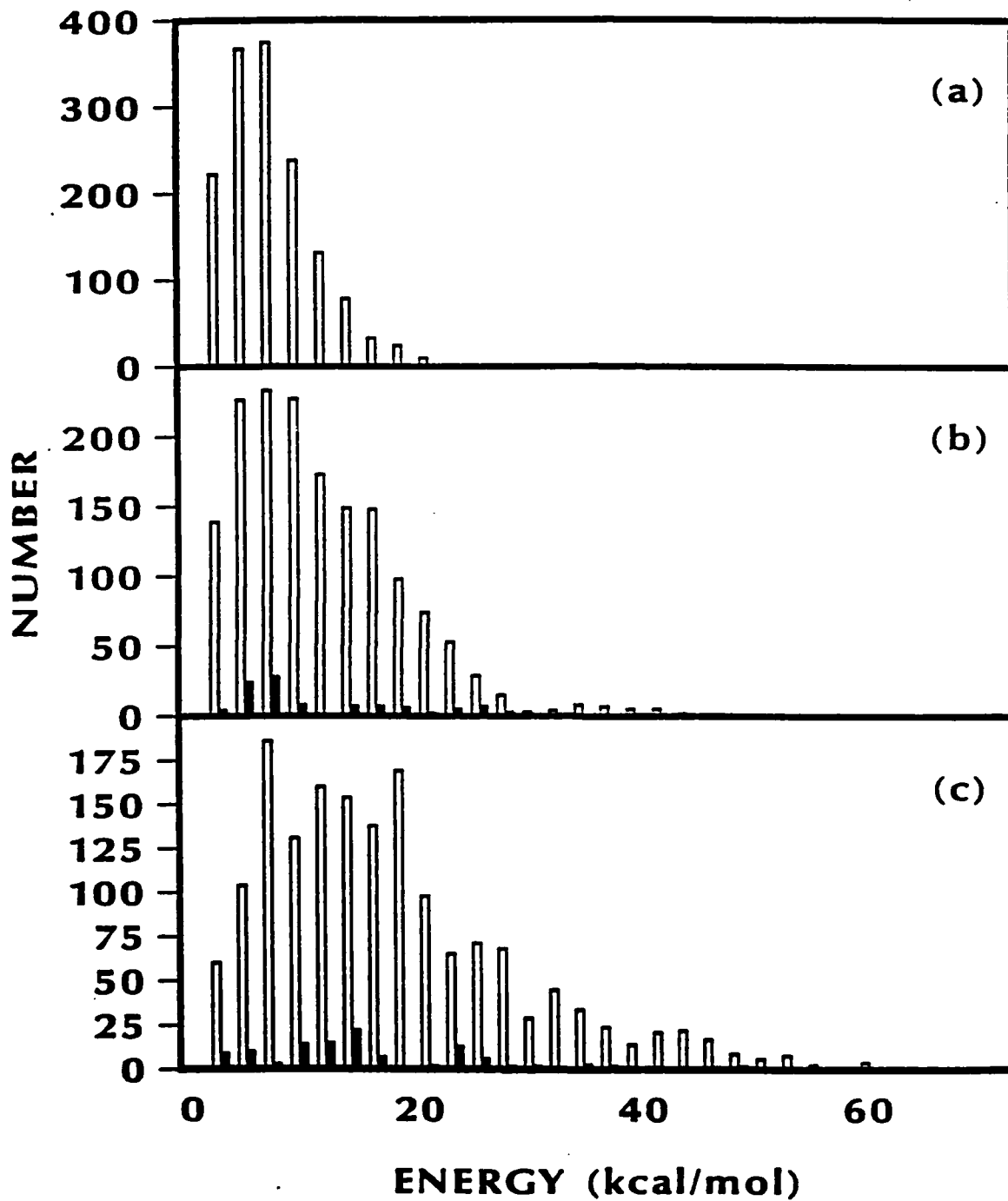
Figure 24. Distributions of the Product Relative Translational Energies for CH₃ + NO₂ Formed From Reaction I (Hollow Bars) and Reaction III (Filled Bars) on PES 2 at Energies (a) 69.2, (b) 115.3, and (c) 161 kcal/mol Above the Zero Point Energy of Nitromethane.
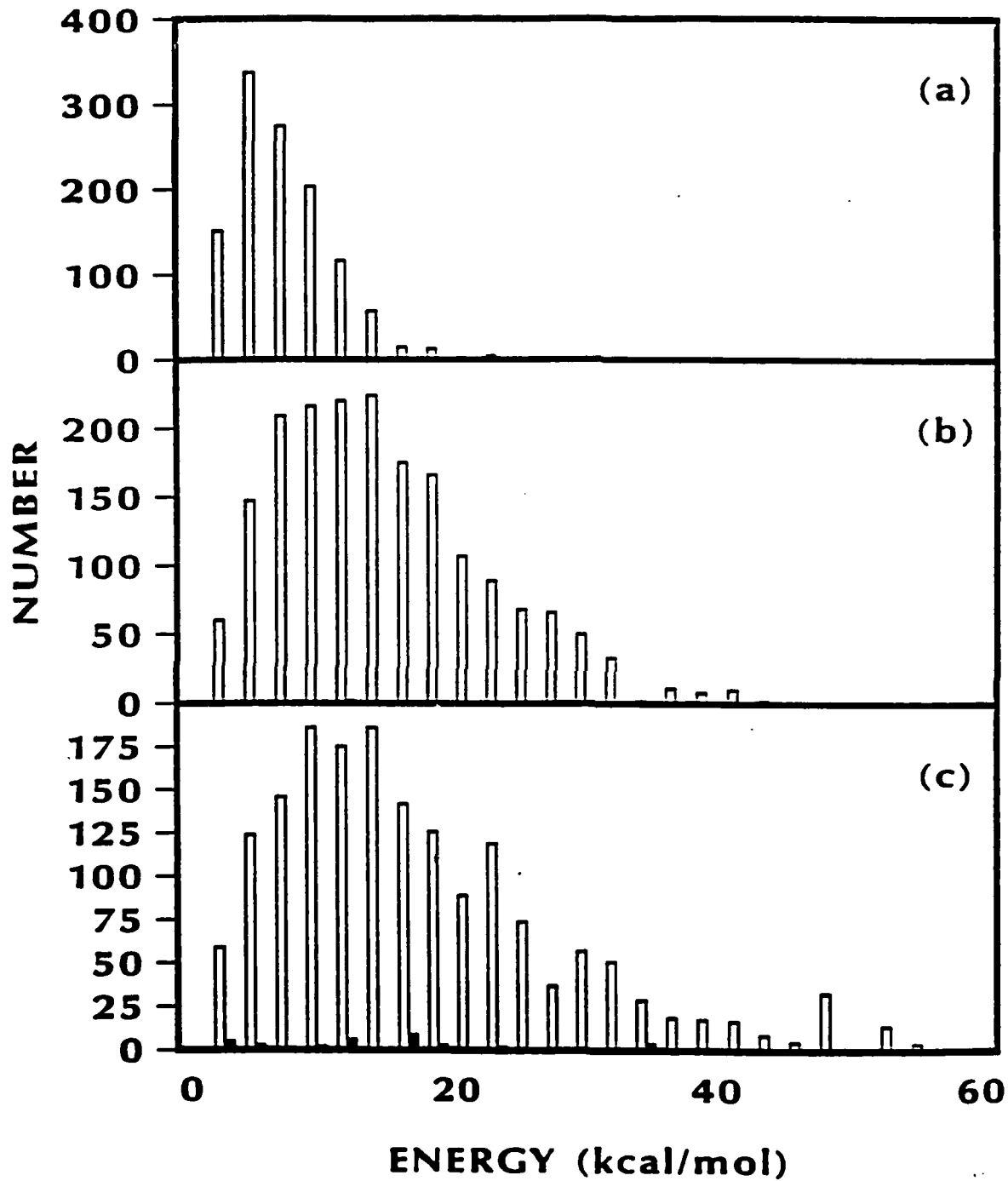
Figure 25. Distributions of the Product Relative Translational Energies for CH_3 + NO_2 Formed From Reaction I (Hollow Bars) and Reaction III (Filled Bars) on PES 1 at Energies (a) 69.2, (b) 115.3, and (c) 161 kcal/mol Above the Zero Point Energy of Nitromethane.
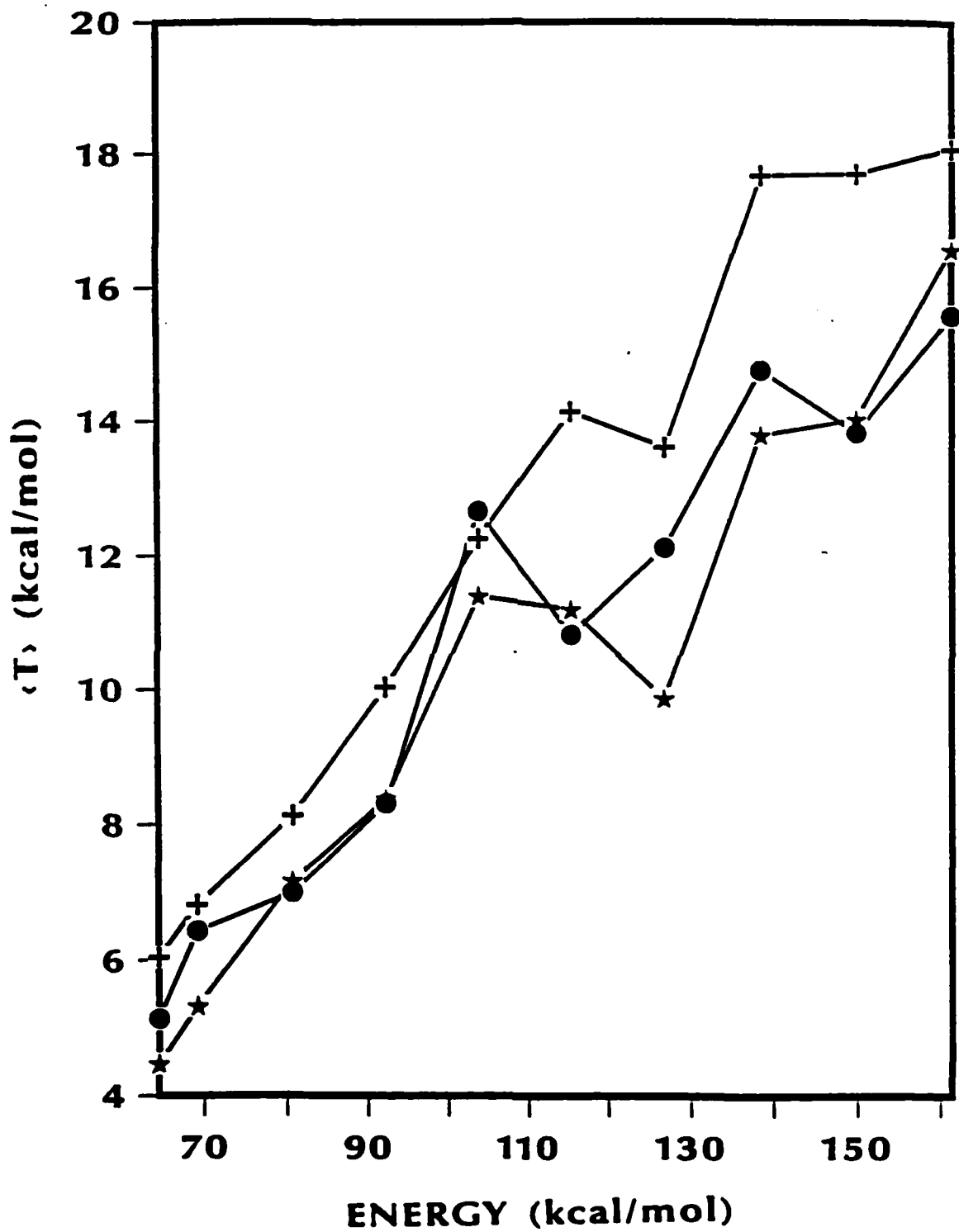
Figure 26. Average Relative Translational Energy of the Products From Reactions I (Circles), II (Crosses), and III (Stars) on PES 3 as a Function of Energy. The Energy Along the Abscissa Is the Total Energy Above the Zero Point Energy of Nitromethane.
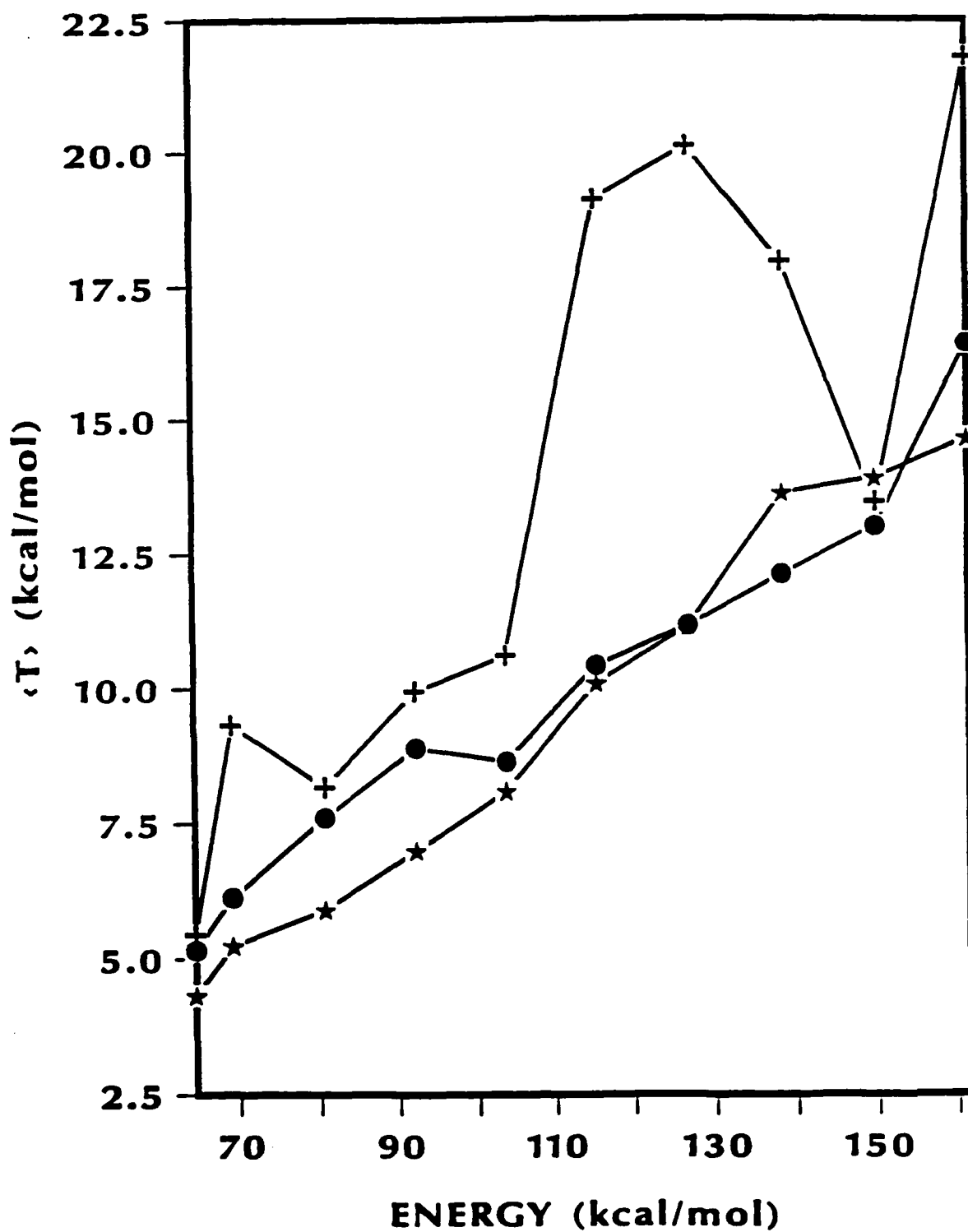
Figure 27. Average Relative Translational Energy of the Products From Reactions I (Circles), II (Crosses), and III (Stars) on PES 2 as a Function of Energy. The Energy Along the Abscissa Is the Total Energy Above the Zero Point Energy of Nitromethane.
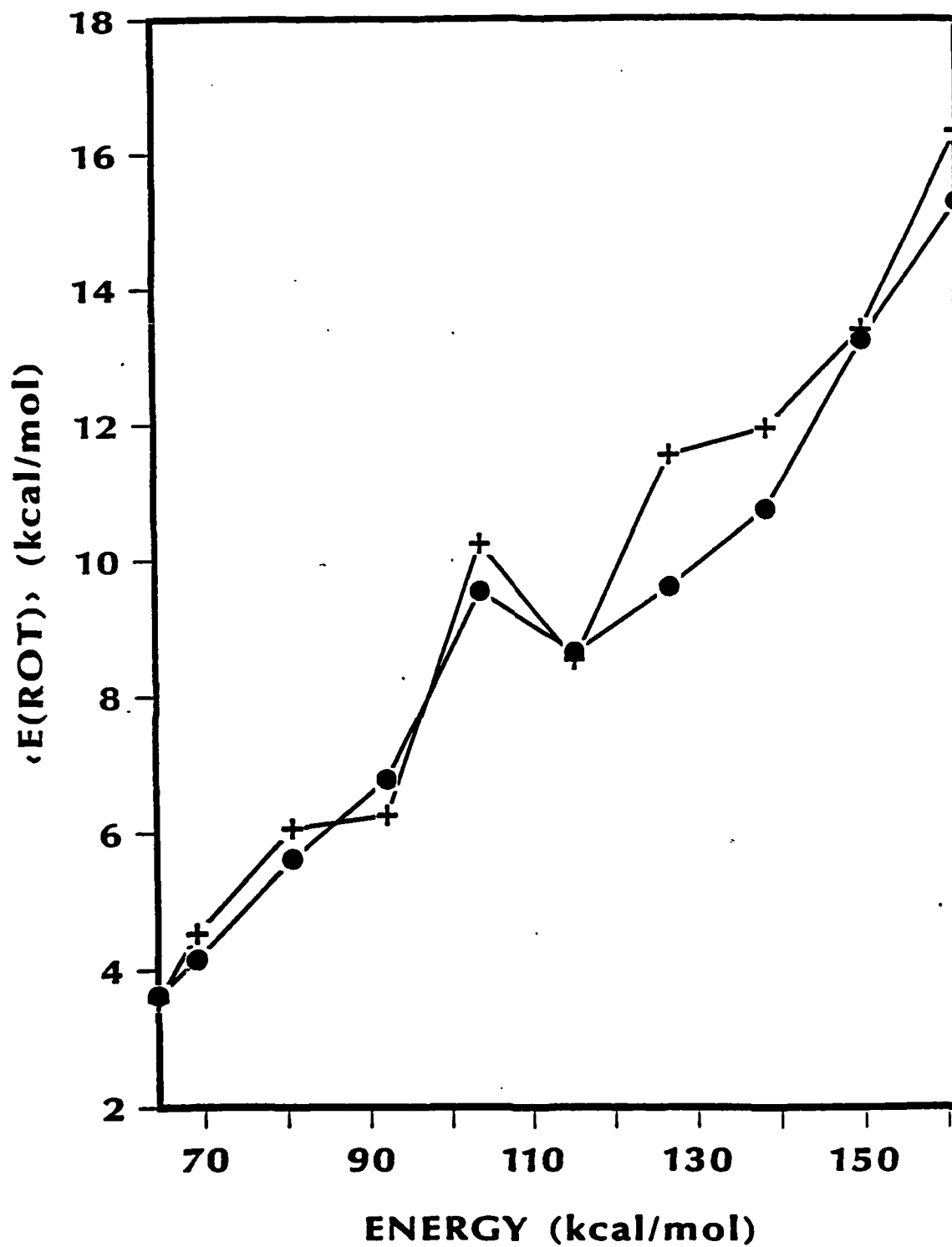
Figure 28. Average Rotational Energy of Methyl Radical Formed From Reactions I (Circles) and III (Crosses) on PES 3 as a Function of Energy. The Energy Along the Abscissa Is the Total Energy Above the Zero Point Energy of Nitromethane.

79

Figure 29. Average Rotational Energy of Methyl Radical Formed From Reactions I (Circles) and III (Crosses) on PES 2 as a Function of Energy. The Energy Along the Abscissa Is the Total Energy Above the Zero Point Energy of Nitromethane.

80
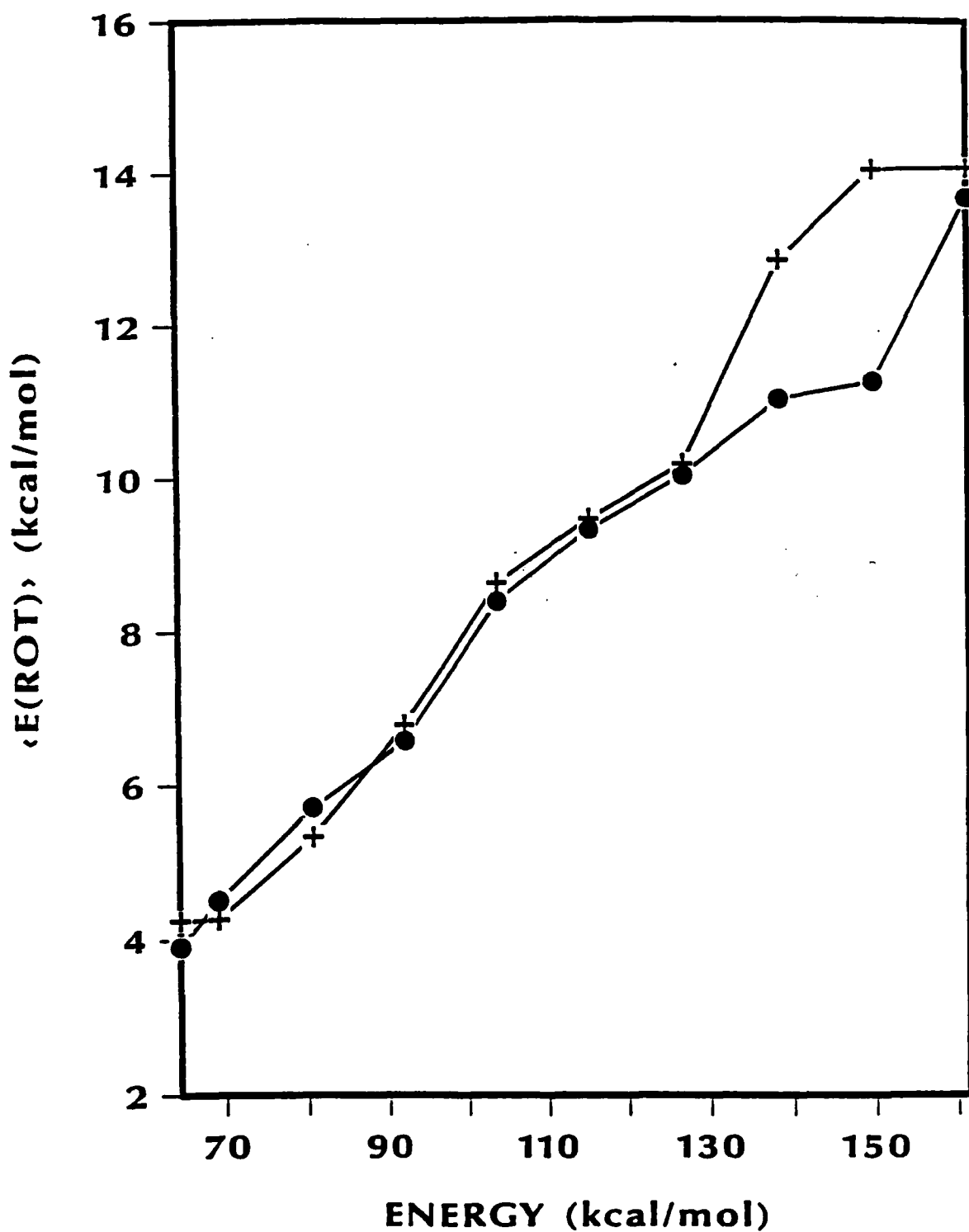
Figure 30. <u>Average Rotational Energy of Nitrogen Dioxide Radical Formed From Reaction I (Circles) and III (Crosses) on PES 3 as a Function of Energy. The Energy Along the Abscissa Is the Total Energy Above the Zero Point Energy of Nitromethane.</u>

81
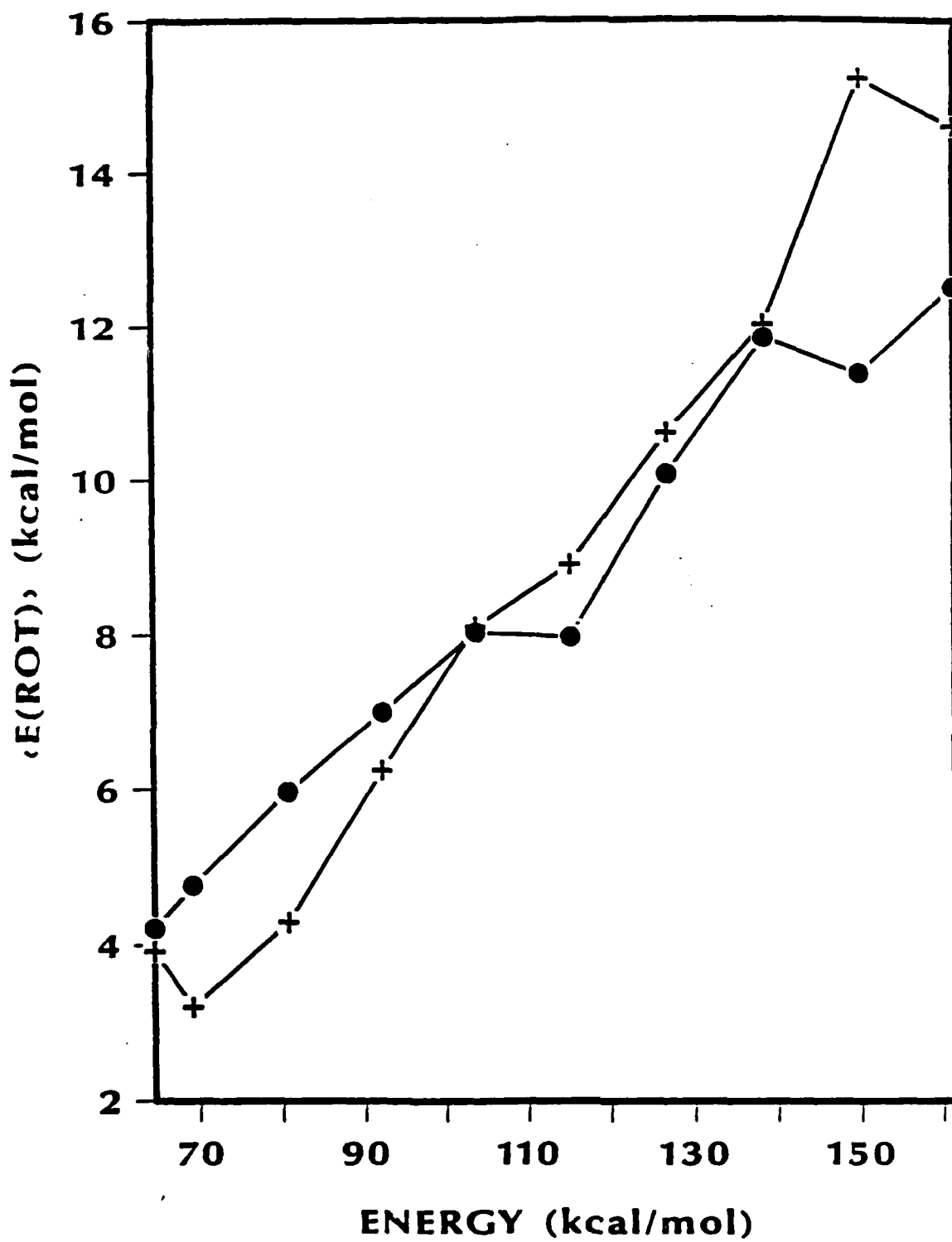
Figure 31. Average Rotational Energy of Nitrogen Dioxide Radical Formed From Reaction I (Circles) and III (Crosses) on PES 2 as a Function of Energy. The Energy Along the Abscissa Is the Total Energy Above the Zero Point Energy of Nitromethane.

END
FILMED
- 91
DTIC
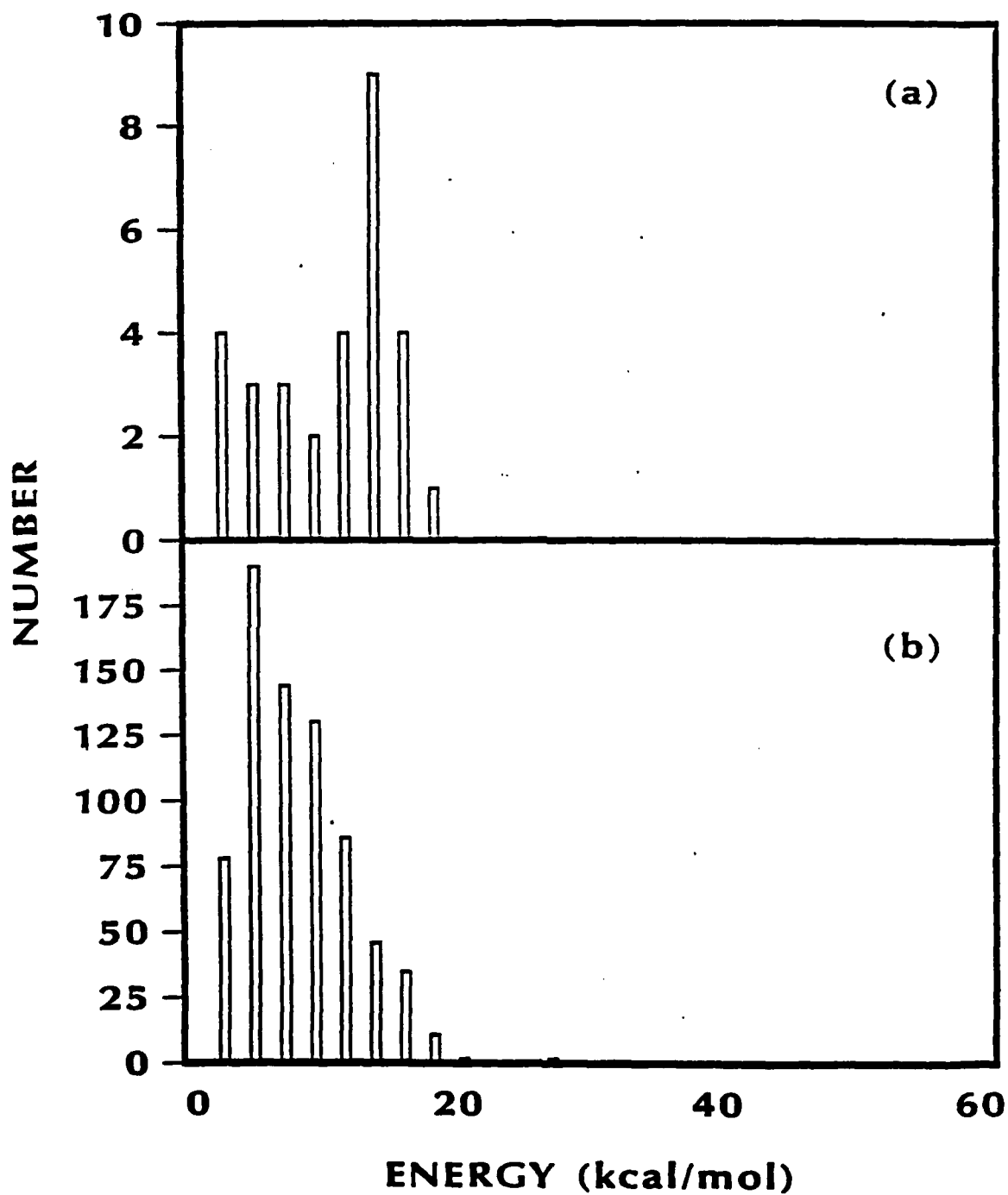
Figure 32. Distribution of the Product Relative Translational Energies for CH_3O + NO Formed From Reaction II on (a) PES 2 and (b) PES 3 at 69.2 kcal/mol Above the Zero Point Energy of Nitromethane.

7. REFERENCES

1. Hershkowitz, J., and B. M. Dobratz. U. S. Army ARDEC Special Publication ARFSD-SP-89001, AD-E401-909, April 1989.

2. Wodtke, A. M., E. J. Hintsa, and Y. T. Lee. Journal of Chemical Physics. Vol. 84, p. 1044, 1986; Journal of Physical Chemistry. Vol. 90, p. 3549, 1986.

3. Rockney, B. H., and E. R. Grant. Journal of Chemical Physics. Vol. 79, p. 708, 1983.

4. Brockway, L. O., J. Y. Beach, and L. Pauling. Journal of the American Chemical Society. Vol. 57, p. 2693, 1935.

5. Tannenbaum, E., R. D. Johnson, R. J. Myers, and W. D. Gwinn. Journal of Chemical Physics. Vol. 22, p. 949, 1954.

6. Tannenbaum, E., R. J. Myers, and W. D. Gwinn. Journal of Chemical Physics. Vol. 25, p. 42, 1956.

7. Cox, A. P., and S. Waring. Journal of the Chemical Society, Faraday Transactions II. Vol. 68 p. 1060, 1972.

8. Sorensen, G. O., T. Pederson, H. Dreizler, A. Guarnieri, and A. P. Cox. Journal of Molecular Structure. Vol. 97, p. 77, 1983.

9. McKean, D. C., and R. A. Watt. Journal of Molecular Spectroscopy. Vol. 61, p. 184, 1976.

10. Wells, A. J., and E. B. Wilson. Journal of Chemical Physics. Vol. 9, p. 314, 1941.

11. Smith, D. C., C. Pan, and J. R. Nielsen. Journal of Chemical Physics. Vol. 18, p. 706, 1950.

12. Jones, W. J., and N. Sheppard. Proceedings of the Royal Society, Series A. Vol. 304, p. 135, 1968.

13. Trinquecoste, C., M. Rey-Lafon, and M. T. Forel. Spectrochimica Acta. Vol. 30A, p. 813, 1974.

14. Adams, G. F. Unpublished results.

15. McKee, M. L. Journal of the American Chemical Society. Vol. 108, p. 5784, 1986; Vol. 107, p. 1900, 1985.

16. Dewar, M. J. S., and J. P. Ritchie. Journal of Organic Chemistry. Vol. 50, p. 1031, 1985.

17. Melius, C. F. Private communication. 15 June 1989.

18. McKee, M. L. Journal of Physical Chemistry. Vol. 93, p. 7365, 1989.

19. Saxon, Roberta P. Private communication. 8 November 1989.

20. Kleier, D. A., and M. A. Lipton. Journal of Molecular Structure (THEOCHEM). Vol. 109, p. 39, 1984; D. S. Marynick, A. K. Ray, J. L. Fry, and D. A. Kleier. Journal of Molecular Structure. Vol. 108, p. 45, 1984; C. Chabalowski, P. C. Hariharan, J. J. Kaufman, and R. Buenker. International Journal of Quantum Chemistry Symposium. Vol. 17, p. 643, 1983; J. J. Kaufman, P. C. Hariharan, C. Chabalowski, and M. Hotokka. International Journal of Quantum Chemistry Symposium. Vol. 19, p. 221, 1986; G. A. Jeffrey, J. R. Ruble, L. M. Wingert, J. H. Yates, and R. K. McMullan. Journal of the American Chemical Society. Vol. 107, p. 6227, 1985; H. M. Niemeyer. Tetrahedron. Vol. 35, p. 1297, 1979; J. R. Murdoch, A. Streitwieser, Jr., and S. Gabriel. Journal of the American Chemical Society. Vol. 100, p. 6338, 1978; and C. W. Bock, S. V. Krasnoshchiokov, L. V. Khristenko, Yu. N. Panchenko, and Yu. A. Pentin. Journal of Molecular Structure (THEOCHEM). Vol. 149, p. 201, 1987.

21. Batt, L., and G. N. Robinson. The Chemistry of Amino, Nitroso, and Nitro Compounds and Their Derivatives. S. Patai, ed; Wiley, NY, 1982.

22. Knobel, Yu. K., E. A. Miroshnichenko, Lebedev, Yu. Izvestiya Akademii Nauk SSSR Seriya Khimicheskaya. Vol. 20, p. 425, 1971.

23. Butler, L. J., D. Krajnovich, Y. T. Lee, G. Ondrey, and R. Bersohn. Journal of Chemical Physics. Vol. 79, p. 1708, 1983.

24. Darsey, J. A., and D. L. Thompson. Chemical Physics Letters. Vol. 145, p. 523, 1988. Note: the form of the potential in Equation 2 of this reference should not include the factor of 0.5.

25. Turner, P. H., M. J. Corkill, and A. P. Cox. Journal of Physical Chemistry. Vol. 83, p. 1473, 1979.

26. Gwinn, W. D., R. J. Anderson, and D. Stelman. Bulletin of the American Physical Society. Vol. 13, p. 831, 1968.

27. Ha, T. K., R. Meyer, P. N. Ghosh, A. Bauder, and Hs. H. Günthard. Chemical Physical Letters. Vol. 81, p. 610, 1981.

28. Ghosh, P. N., and Hs. H. Günthard. Spectrochimica Acta. Vol. 37A, p. 347, 1981.

29. (a) Duchovic, R. J., W. L. Hase, and H. B. Schlegel. Journal of Physical Chemistry. Vol. 88, p. 1339, 1984; (b) T. Valencich and D. L. Bunker. Journal of Chemical Physics. Vol. 61, p. 21, 1974; (c) S. Chapman and D. L. Bunker, Journal of Chemical Physics. Vol. 62, p. 2890, 1975; (d) L. M. Raff. Journal of Chemical Physics. Vol. 60, p. 2220, 1974; (e) R. Steckler, K. J. Dykema, F. B. Brown, G. C. Hancock, D. G. Truhlar, and T. Valencich. Journal of Chemical Physics. Vol. 87, p. 7024, 1987; (f) T. Joseph, R. Steckler, and D. G. Truhlar. Journal of Chemical Physics. Vol. 87, p. 7036, 1987.

30. Herzberg, G. Proceedings of the Royal Society, Series A. Vol. 262, p. 291, 1961.

31. (a) Bird, G. R., J. C. Baird, A. W. Jache, J. A. Hodgeson, R. F. Curl, Jr., A. C. Kunkle, J. W. Bransford, J. Rastrup-Andersen, and J. Rosenthal. Journal of Chemical Physics. Vol. 40, p. 3378, 1964; (b) A. Cabana, M. Laurin, W. J. Lafferty, and R. L. Sams, Canadian Journal of Physics. Vol. 53, p. 1902, 1975.

86

32. See references 30–41 cited in Duchovic et al., Ref. 29(a) of this paper.

33. Jacox, M. E. Journal of Physical and Chemical Reference Data. Vol. 17, pp. 269, 352, 1988.

34. Sams, R. L., and W. J. Lafferty. Journal of Molecular Spectroscopy. Vol. 56, p. 399, 1975.

35. Benson, S. W., and H. E. O'Neal. Kinetic Data on Gas Phase Unimolecular Reactions: National Standard Reference Data Series. National Bureau of Standards: Washington, DC, 1970; Library of Congress Card Catalog No. 68-67395.

36. Endo, Y., S. Saito, and E. Hirota. Journal of Chemical Physics. Vol. 81, p. 122, 1984.

37. Yarkony, D. R., H. F. Schaefer III, and S. Rothenberg. Journal of the American Chemical Society. Vol. 96, p. 656, 1974.

38. Adams, G. F., G. D. Bent, G. D. Purvis, and R. J. Bartlett. Chemical Physics Letters. Vol. 81, p. 461, 1981.

39. Jackels, C. F. Journal of Chemical Physics. Vol. 76, p. 505, 1982.

40. Saebo, S., L. Radom, and H. F. Schaefer III. Journal of Chemical Physics. Vol. 78, p. 845, 1983.

41. Herzberg, G. Molecular Spectra and Molecular Structure: I. Spectra of Diatomic Molecules. New York: Van Nostrand Reinhold Company, NY, 1950.

42. Miller, W. H., and T. F. George. Journal of Chemical Physics. Vol. 56, p. 5668, 1972.

43. Metropolis, N., A. W. Rosenbluth, M. N. Rosenbluth, A. H. Teller, and E. Teller. Journal of Chemical Physics. Vol. 21, p. 1087, 1953.

44. Raff, L. M., and D. L. Thompson. Theory of Chemical Reaction Dynamics. Edited by M. Baer, Chemical Rubber, Boca Raton, FL, 1985.

45. Rice, B. M., L. M. Raff, and D. L. Thompson. Journal of Chemical Physics. Vol. 85, p. 4392, 1986; L. M. Raff, R. Viswanathan, and D. L. Thompson. Journal of Chemical Physics. Vol. 80, p. 6141, 1984; and R. Viswanathan, D. L. Thompson, and L. M. Raff. Journal of Chemical Physics. Vol. 80, p. 4230, 1984.

No of
Copies Organization

2   Administrator
    Defense Technical Info Center
    ATTN: DTIC-DDA
    Cameron Station
    Alexandria, VA 22304-6145

1   HQDA (SARD-TR)
    WASH DC 20310-0001

1   Commander
    US Army Materiel Command
    ATTN: AMCDRA-ST
    5001 Eisenhower Avenue
    Alexandria, VA 22333-0001

1   Commander
    US Army Laboratory Command
    ATTN: AMSLC-DL
    Adelphi, MD 20783-1145

2   Commander
    US Army, ARDEC
    ATTN: SMCAR-IMI-I
    Picatinny Arsenal, NJ 07806-5000

2   Commander
    US Army, ARDEC
    ATTN: SMCAR-TDC
    Picatinny Arsenal, NJ 07806-5000

1   Director
    Benet Weapons Laboratory
    US Army, ARDEC
    ATTN: SMCAR-CCB-TL
    Watervliet, NY 12189-4050

1   Commander
    US Army Armament, Munitions
     and Chemical Command
    ATTN: SMCAR-ESP-L
    Rock Island, IL 61299-5000

1   Director
    US Army Aviation Research
     and Technology Activity
    ATTN: SAVRT-R (Library)
    M/S 219-3
    Ames Research Center
    Moffett Field, CA 94035-1000

No of
Copies Organization

1   Commander
    US Army Missile Command
    ATTN: AMSMI-RD-CS-R (DOC)
    Redstone Arsenal, AL 35898-5010

1   Commander
    US Army Tank-Automotive Command
    ATTN: AMSTA-TSL (Technical Library)
    Warren, MI 48397-5000

1   Director
    US Army TRADOC Analysis Command
    ATTN: ATRC-WSR
    White Sands Missile Range, NM 88002-5502

(Class. only) 1   Commandant
    US Army Infantry School
    ATTN: ATSH-CD (Security Mgr.)
    Fort Benning, GA 31905-5660

(Unclass. only) 1   Commandant
    US Army Infantry School
    ATTN: ATSH-CD-CSO-OR
    Fort Benning, GA 31905-5660

1   Air Force Armament Laboratory
    ATTN: AFATL/DLODL
    Eglin AFB, FL 32542-5000

Aberdeen Proving Ground

2   Dir, USAMSAA
        ATTN: AMXSY-D
             AMXSY-MP, H. Cohen
1   Cdr, USATECOM
        ATTN: AMSTE-TD
3   Cdr, CRDEC, AMCCOM
        ATTN: SMCCR-RSP-A
             SMCCR-MU
             SMCCR-MSI
1   Dir, VLAMO
        ATTN: AMSLC-VL-D

No. of Copies	Organization

4   Commander
        US Army Research Office
        ATTN: R. Ghirardelli
              D. Mann
              R. Singleton
              R. Shaw
        P.O. Box 12211
        Research Triangle Park, NC
         27709-2211

2   Commander
        US Army, ARDEC
        ATTN: SMCAR-AEE-B,
              D. S. Downs
              SMCAR-AEE, J. A. Lannon
        Picatinny Arsenal, NJ 07806-5000

1   Commander
        US Army, ARDEC
        ATTN: SMCAR-AEE-BR, L. Harris
        Picatinny Arsenal, NJ 07806-5000

1   Office of Naval Research
        Department of the Navy
        ATTN: R. S. Miller, Code 432
        800 N. Quincy Street
        Arlington, VA 22217

1   Commander
        Naval Air Systems Command
        ATTN: J. Ramnarace, AIR-54111C
        Washington, DC 20360

1   Commander
        Naval Surface Warfare Center
        ATTN: J. L. East, Jr., G-23
        Dahlgren, VA 22448-5000

2   Commander
        Naval Surface Warfare Center
        ATTN: R. Bernecker, R-13
              G. B. Wilmot, R-16
        Silver Spring, MD 20903-5000

5   Commander
        Naval Research Laboratory
        ATTN: M. C. Lin
              J. McDonald
              E. Oran
              J. Shnur
              R. J. Doyle, Code 6110
        Washington, DC 20375

1   Commanding Officer
        Naval Underwater Systems Center
         Weapons Department
        ATTN: R. S. Lazar/Code 36301
        Newport, RI 02840

2   Commander
        Naval Weapons Center
        ATTN: T. Boggs, Code 388
              T. Parr, Code 3895
        China Lake, CA 93555-6001

1   Superintendent
        Naval Postgraduate School
        Dept. of Aeronautics
        ATTN: D. W. Netzer
        Monterey, CA 93940

3   AL/LSCF
        ATTN: R. Corley
              R. Geisler
              J. Levine
        Edwards AFB, CA 93523-5000

1   AL/MKPB
        ATTN: B. Goshgarian
        Edwards AFB, CA 93523-5000

1   AFOSR
        ATTN: J. M. Tishkoff
        Bolling Air Force Base
        Washington, DC 20332

1   OSD/SDIO/IST
        ATTN: L. Caveny
        Pentagon
        Washington, DC 20301-7100

1   Commandant
        USAFAS
        ATTN: ATSF-TSM-CN
        Fort Sill, OK 73503-5600

1   F.J. Seiler
        ATTN: S. A. Shackleford
        USAF Academy, CO 80840-6528

1   University of Dayton Research
         Institute
        ATTN: D. Campbell
        AL/PAP
        Edwards AFB, CA 93523

91

92

No. of Copies	Organization
1	United Technologies Research Center ATTN: A. C. Eckbreth East Hartford, CT 06108
3	United Technologies Corp. Chemical Systems Division ATTN: R. S. Brown 　　　　 T. D. Myers (2 copies) P.O. Box 49028 San Jose, CA 95161-9028
1	Universal Propulsion Company ATTN: H. J. McSpadden Black Canyon Stage 1 Box 1140 Phoenix, AZ 85029
1	Veritay Technology, Inc. ATTN: E. B. Fisher 4845 Millersport Highway P.O. Box 305 East Amherst, NY 14051-0305
1	Brigham Young University Dept. of Chemical Engineering ATTN: M. W. Beckstead Provo, UT 84058
1	California Institute of Tech. Jet Propulsion Laboratory ATTN: L. Strand/MS 512/102 4800 Oak Grove Drive Pasadena CA, 91109
1	California Institute of Technology ATTN: F. E. C. Culick/MC 301-46 204 Karman Lab. Pasadena, CA 91125
1	University of California Los Alamos Scientific Lab. P.O. Box 1663, Mail Stop B216 Los Alamos, NM 87545
1	University of California, Berkeley Chemistry Department ATTN: C. Bradley Moore 211 Lewis Hall Berkeley, CA 94720
1	University of California, San Diego ATTN: F. A. Williams AMES, B010 La Jolla, CA 92093

No. of Copies	Organization
2	University of California, Santa Barbara Quantum Institute ATTN: K. Schofield 　　　　 M. Steinberg Santa Barbara, CA 93106
1	University of Colorado at Boulder Engineering Center ATTN: J. Daily Campus Box 427 Boulder, CO 80309-0427
2	University of Southern California Dept. of Chemistry ATTN: S. Benson 　　　　 C. Wittig Los Angeles, CA 90007
1	Cornell University Department of Chemistry ATTN: T. A. Cool Baker Laboratory Ithaca, NY 14853
1	University of Delaware ATTN: T. Brill Chemistry Department Newark, DE 19711
1	University of Florida Dept. of Chemistry ATTN: J. Winefordner Gainesville, FL 32611
3	Georgia Institute of Technology School of Aerospace Engineering ATTN: E. Price 　　　　 W. C. Strahle 　　　　 B. T. Zinn Atlanta, GA 30332
1	University of Illinois Dept. of Mech. Eng. ATTN: H. Krier 144MEB, 1206 W. Green Street Urbana, IL 61801

94

USER EVALUATION SHEET/CHANGE OF ADDRESS

This Laboratory undertakes a continuing effort to improve the quality of the reports it publishes. Your comments/answers to the items/questions below will aid us in our efforts.

1. BRL Report Number ___BRL-TR-3197___ Date of Report ___FEBRUARY 1991___

2. Date Report Received _____

3. Does this report satisfy a need? (Comment on purpose, related project, or other area of interest for which the report will be used.) _____
_____
_____

4. Specifically, how is the report being used? (Information source, design data, procedure, source of ideas, etc.) _____
_____
_____

5. Has the information in this report led to any quantitative savings as far as man-hours or dollars saved, operating costs avoided, or efficiencies achieved, etc? If so, please elaborate. _____
_____
_____

6. General Comments. What do you think should be changed to improve future reports? (Indicate changes to organization, technical content, format, etc.) _____
_____
_____
_____

	_____
	Name
CURRENT	_____
ADDRESS	Organization
	_____
	Address
	_____
	City, State, Zip Code

7. If indicating a Change of Address or Address Correction, please provide the New or Correct Address in Block 6 above and the Old or Incorrect address below.

	_____
	Name
OLD	_____
ADDRESS	Organization
	_____
	Address
	_____
	City, State, Zip Code

(Remove this sheet, fold as indicated, staple or tape closed, and mail.)

--FOLD HERE--

DEPARTMENT OF THE ARMY

Director
U.S. Army Ballistic Research Laboratory
ATTN: SLCBR-DD-T
Aberdeen Proving Ground, MD 210 -5066
   OFFICIAL BUSINESS

```
BUSINESS REPLY MAIL
FIRST CLASS PERMIT No 0001, APG, MD
```

POSTAGE WILL BE PAID BY ADDRESSEE

Director
U.S. Army Ballistic Research Laboratory
ATTN: SLCBR-DD-T
Aberdeen Proving Ground, MD 21005-9989

NO POSTAGE
NECESSARY
IF MAILED
IN THE
UNITED STATES

--FOLD HERE--